Tampere University

TERO ILVESMÄKI

Quantitative Diffusion Tensor Image Analysis

A Clinical Approach to Central Nervous System Injuries

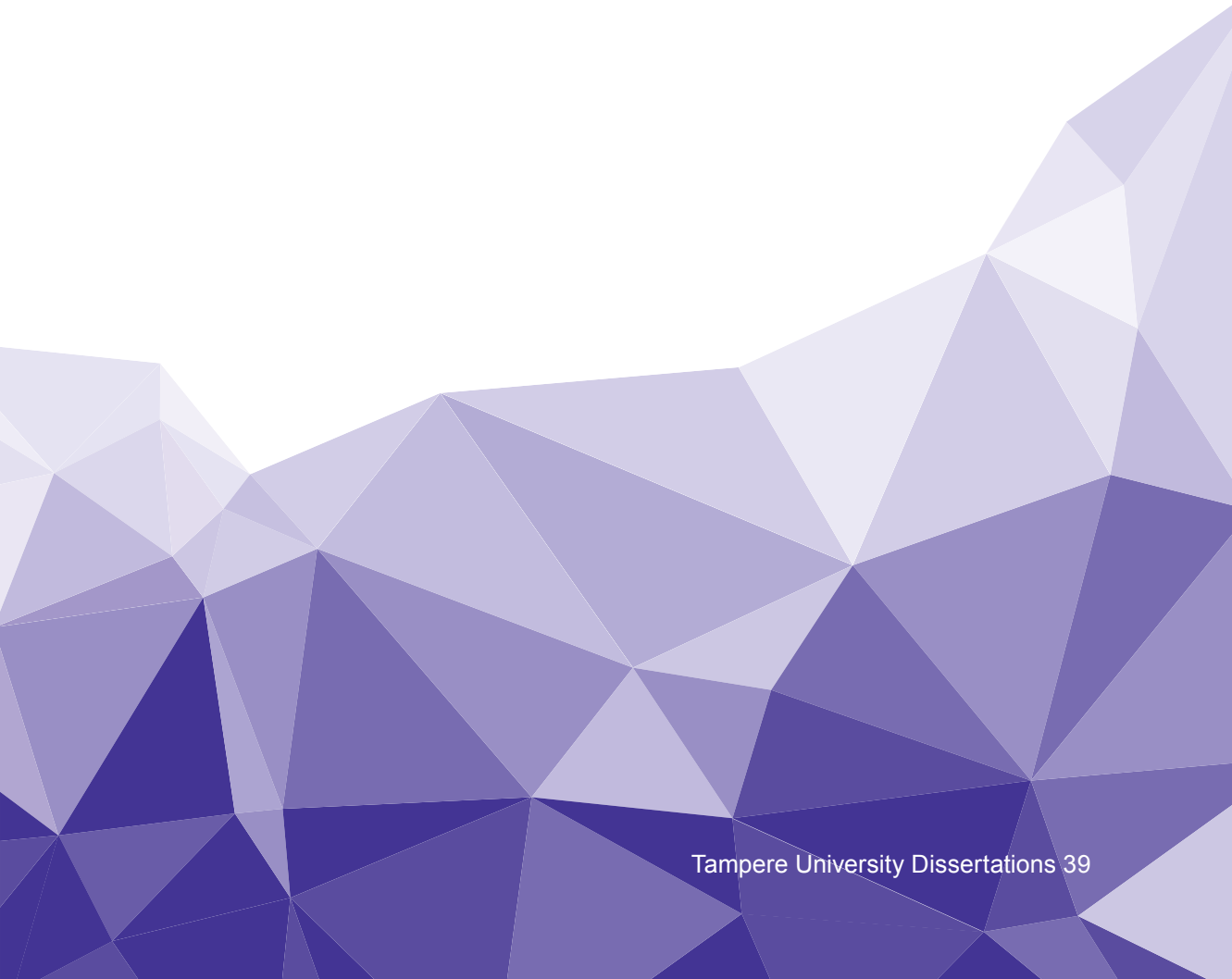

Tampere University Dissertations 39

Tampere University Dissertations 39

TERO ILVESMÄKI

Quantitative Diffusion Tensor Image Analysis

A Clinical Approach to Central Nervous System Injuries

ACADEMIC DISSERTATION
To be presented, with the permission of
the Faculty Council of the Faculty of Medicine and Health Technology
of Tampere University,
for public discussion in the auditorium RG202
of the Rakennustalo building, Korkeakoulunkatu 5, Tampere,
on 29 March 2019, at 12 o'clock.

ACADEMIC DISSERTATION
Tampere University, Faculty of Medicine and Health Technology
Finland

Responsible supervisor and Custos	Professor Hannu Eskola Tampere University Finland	
Supervisor	Adjunct professor Teemu Luoto Tampere University Finland	
Pre-examiners	Professor Ritva Vanninen University of Eastern Finland Finland	Docent Outi Sipilä University of Helsinki Finland
Opponent	Professor Olli Gröhn University of Eastern Finland Finland	

The originality of this thesis has been checked using the Turnitin OriginalityCheck service.

Cover design: Roihu Inc.

ISBN 978-952-03-1014-1 (print)
ISBN 978-952-03-1015-8 (pdf)
ISSN 2489-9860 (print)
ISSN 2490-0028 (pdf)
http://urn.fi/URN:ISBN:978-952-03-1015-8

PunaMusta Oy – Yliopistopaino
Tampere 2019

ACKNOWLEDGEMENTS

I started my post-graduate studies in 2014 after I had finished my MSc degree at Tampere University of Technology. The thesis process, and the whole academic journey have been something remarkably unique, and I am truly grateful to have been given the opportunity to embark on this journey. The work presented in this thesis is the outcome of productive collaboration between the BioMediTech Institute and the Faculty of Biomedical Sciences and Engineering of Tampere University of Technology and Tampere University Hospital. The purpose of the conducted research was to study current quantitative diffusion tensor image analysis methods and to apply the methods to societally and scientifically interesting practical medical problems. The research was funded by personal grants from the Emil Aaltonen Foundation, the Finnish Cultural Foundation and the Orion Research Foundation, and by preparation funding for post-graduate students from Tampere University of Technology. The received funding had a significant role in enabling the completion of this thesis and is greatly appreciated.

I would like to express my sincere gratitude and appreciation to my supervisor, Professor Hannu Eskola, who took me under his wing and guided me throughout my studies and the whole thesis process. I am grateful for Hannu's continuous confidence in my skills, which kept me going onwards. Next, I would like to offer my sincere thanks to my instructor, Adjunct Professor Teemu Luoto, for the vast amount of help provided, especially in the early stages of my research. Teemu introduced me to the current intriguing situation concerning mild traumatic brain injuries, and he has had an inspiring effect on my research.

I would like to thank the co-authors of the original publications included in the thesis, Teemu Luoto, Ullamari Hakulinen, Juha Öhman, Hannu Eskola, Antti Brander, Grant Iverson, Eerika Koskinen, Pertti Ryymin, William Panenka and Douglas Terry. Their collaboration and contribution to the research has been a major component in the completion of this thesis. I would like to give special thanks to Juha Öhman, Teemu Luoto, and Eerika Koskinen from the Tampere University Hospital for providing the research material for my research. I would also like to

thank my past and present colleagues and co-workers in Tampere, Pori and Turku who have been really understanding and encouraging towards me during the journey.

I would like to express my appreciation to my pre-examiners, Professor Ritva Vanninen and Docent Outi Sipilä, for the evaluation of my thesis and their valuable feedback during the pre-examination process. I would also like to express my appreciation to Peter Heath, MA, for the proficient proofreading and language revision of my thesis.

My thanks go to my friends for their encouraging words and their eccentric sense of humour. I would also like to thank my close relatives who supported me throughout this long process.

I am especially grateful to my loving parents for continuously encouraging me to study and for always maintaining their faith in me, even when mine faltered. Finally, a special thank you to my beloved partner Kati, who can light up the room with her positive energy, and can brighten even the darkest of my days. Thank you for standing by me for these years.

Pori, March 2019

Tero Ilvesmäki

ABSTRACT

Since the introduction of magnetic resonance imaging (MRI), the full extent of its possibilities has been extensively studied. Diffusion weighted imaging is a specific MRI protocol that enables the quantitative study of water diffusion in tissue. More recently, diffusion imaging has been extended to diffusion tensor imaging (DTI), which can extract detailed information of tissue microstructure. Overall, the most popular clinical application of DTI is the assessment of human brain white matter (WM). DTI can reveal changes in the brain WM microstructure that are not visible by other means of medical imaging. This microstructural resolution allows DTI to be used for the detection of several neuropathologies affecting the brain's neural network, such as traumatic brain injuries and various types of neurodegenerative disorders.

Mild traumatic brain injury (mTBI) can be defined as a traumatically induced brain function disruption which, in most cases, is not detectable by conventional medical imaging. mTBIs are grievous ailments due to high occurrence and a lack of distinct quantitative diagnostic tools and biomarkers. This signifies that the diagnosis of mTBI is based on subjective clinical measures. Extensive research has been carried out in order to find a clear correlation between DTI derived quantitative metrics and the post-mTBI brain WM. No uniform evidence of absolute conditions of pathology or association with post-injury prognosis has yet been found. However, many previous studies report different correlations between DTI metrics and post-injury brain WM. Unfortunately, the observed changes vary between studies, and final conclusions on the effects of mTBI on brain WM have yet to be made. One source of variation is the incoherency of the analysis methods used in the assessment of mTBI patients. Additionally, the heterogeneity of the studied patient cohorts hinders the chances of drawing a generalisable clinical conclusion.

Our work aims to overcome the issues in quantitative mTBI analysis methods by introducing a simple yet robust automated analysis method for human brain WM analysis. Our research began by applying a novel third-party group level analysis method, tract-based spatial statistics (TBSS), to an mTBI patient sample. We tested the whole sample and several subgroups for abnormal WM, but the results were negative. It was also noted during the study that TBSS would not be a suitable tool

for clinical mTBI diagnostic purposes as the method is not fully modifiable for the assessment of individual patients and involves an excessive amount of complex image data manipulation. An additional study of traumatic spinal cord injury (SCI) patients was successfully performed applying TBSS. We found widespread neurodegenerative changes in the post-SCI cerebral WM, but also signs of possible neuroplasticity. The results further confirmed the method's applicability to neuropathologic conditions with homogeneous effects on the brain WM microstructure.

Based on our findings, we began to create an automated analysis method using a region of interest (ROI) approach. We utilised human brain atlas-based ROIs in the analysis, which were automatically registered to the analysed subjects. The procedure ensures that the subjects' images are not heavily processed. This in turn minimises the bias caused by image manipulation. The patients were compared against a normal population DTI reference value model created from our control subjects. The preliminary normal population DTI model created for the purpose was a successful quantitative model of DTI reference values. The normal population model could be used in a variety of clinical applications if a large enough number of control subjects were introduced to the model. The normal model would be especially useful in support of mTBI diagnosis methods.

In summary, this thesis has three conclusions. First, we found no DTI measurable associations between WM integrity and acute mTBI when applying TBSS. Second, we found extensive WM changes in the post-SCI brain, which imply an ongoing neuroplastic process in addition to the initial SCI-induced changes. These cerebral WM changes were far more extensive than previously reported. Third, an automated quantitative DTI brain analysis method with prospective clinical applications was introduced. The sensitivity and specificity of the automated method is at an acceptable level when used in conjunction with our preliminary control population set. For clinical applicability, the method requires minor refinements to its usability. More importantly, the normal population model needs to be updated to clinical standards by increasing its statistical power. A large enough normal population data pool could be achieved through an MRI data collection scheme resembling that of a biobank data collection method. In addition, machine learning could be applied in future to create better statistical models for the analysis with more accurate model predicted DTI scalar values.

TIIVISTELMÄ

Jo magneettikuvantamisen (MK) alkuajoista lähtien kyseinen kuvantamismodaliteetti on herättänyt runsasta mielenkiintoa sen laajojen mahdollisuuksien ansiosta. MK:ta käytetään laajalti sekä rutinoidusti potilastutkimuksissa että edistyksellisissä tutkimuksissa. Diffuusiopainotteisella kuvantamisella voidaan arvioida kudoksen mikroskooppista rakennetta veden diffuusiota mittaamalla. Myöhemmässä vaiheessa diffuusiokuvauksen rinnalle saapui tarkempi tapa määrittää kudoksen rakennetta: diffuusiotensorikuvantaminen (DTI). DTI:n avulla voidaan tutkia aivojen hienorakennetta sekä mikroskooppisia rakenteenmuutoksia, joita ei voida havaita muilla kuvantamismenetelmillä. DTI on mahdollistanut useiden neuropatologisten sairauksien kvantifioinnin lääketieteellisen kuvantamisen avulla, ja varsinkin hermoston rappeumasairauksia voidaan evaluoida DTI:llä.

Lievä aivovamma on ulkoisen voiman aiheuttama aivotoiminnan häiriö tai rakenteellinen vaurio, jota usein ei pystytä havaitsemaan kuvantamisen avulla. Suuren ilmaantuvuutensa, yhteisöllisten kustannusten sekä haastavan diagnostiikan takia lievien aivovammojen ennaltaehkäisy on tärkeää. Lievien aivovammojen diagnostiikka perustuu kliinisen arviointiin, jota perinteiset kuvantamistutkimukset (tietokonetomografia ja MK) täydentävät. Perinteisten aivokuvantamistutkimusten ollessa useimmiten löydöksettömiä vammamuutosten suhteen, diagnostiikka jää virhealttiin kliinisen arvioinnin varaan. Objektiivisille diagnostisille menetelmille olisi huutava tarve. DTI-menetelmää on tutkittu pitkään mahdollisena objektiivisena diagnostisena työkaluna. Paljon tutkimusta on tehty DTI skalaarien ja lievien aivovammojen välisen yhteyden löytämiseksi. Nykyisten tutkimustulosten valossa ei voida vielä todeta yksiselitteisen DTI indikaattorin olemassaoloa. DTI:llä nähtävien aivojen valkean aineen muutoksien on kuitenkin tutkimuksissa todettu olevan kytköksissä lievien aivovammojen patologiaan. Valitettavasti tutkimustulokset ovat osittain ristiriitaisia, joten lopullista johtopäätöstä ei vielä voida kirjallisuuden perusteella tehdä. Ristiriitaisten tulosten mahdollinen selitys tosin lienee huomattavasti vaihtelevat tutkimukselliset metodit sekä aineistot.

Tutkimuksellamme pyrimme yhtenäistämään aivojen kvantitatiivisen kuva-analyysin menetelmiä tuomalla kehittelemämme automatisoidun menetelmän kliiniseen ympäristöön. Analyysimme on tehty mahdollisimman yksinkertaiseksi,

jotta menetelmä olisi läpinäkyvä, toistettava ja käytäntöön implementoitava. Tutkimuksemme alussa sovelsimme hiljattain julkaistua analyysimenetelmää, Tract-based spatial statisticsia (TBSS) potilaisiin, joilla on todettu lievä aivovamma. Vertasimme aivovammapotilaita verrokkeihin eri tutkimusasetelmissa, mutta emme löytäneet eroa ryhmien välillä. Negatiivisten tulosten valossa päädyimme johtopäätökseen, että TBSS ei ole sopiva menetelmä lievien aivovammojen analyysiin. Vertasimme seuraavaksi selkäydinvammapotilaiden aivojen valkeaa ainetta verrokkien valkeaan aineeseen hyödyntäen muutamaa eri tutkimusasetelmaa. Tutkimuksemme paljasti laaja-alaisia degeneratiivisia sekä mahdollisia aivojen muuntautumiskykyä indikoivia muutoksia selkärankavammapotilaiden aivoissa. Tulokset myös varmistivat TBSS:n soveltuvuuden kollektiivisia valkean aineen muutoksia aiheuttavien neurodegeneratiivisten sairauksien analyysiin.

Saatujen kliinisten tulosten perusteella lähdimme kehittämään uutta analyysimenetelmää, joka olisi sovellettavissa lievien aivovammojen lisäksi myös muihin erityyppisiin neurologisiin sairauksiin. Päädyimme mielenkiintoalueisiin (region of interest, ROI) perustuvaan analyysiin, jota voidaan käyttää yksittäisten potilaiden analyysiin. ROI:na käytämme valmiita rakenteellisia aivokartastoja, joiden ROIt rekisteröidään lineaarisesti sekä epälineaarisesti kohteiden DTI kuviin. Tämä lähtökohtaisesti auttaa vähentämään kuvankäsittelyn aiheuttamaa virhettä kvantitatiivisiin arvoihin, sillä kuvattua dataa ei käsitellä. Potilaiden DTI-kuvien kvantitatiivisia arvoja vertaillaan verrokkiaineiston avulla luotuun referenssiarvomalliin. Muodostimme alustavan normaalipopulaatioon perustuvan DTI mallin verrokkidatamme avulla, ja testasimme mallin herkkyyttä ja tarkkuutta, jotka molemmat olivat tyydyttävällä tasolla. Jatkossa riittävän isolla verrokkiaineistolla voitaisiin luoda tarkempi malli normaalipopulaatiosta, jolla voitaisiin mallintaa aivojen DTI-arvoja iän funktiona. Eritoten tämä olisi hyödyllistä lievien aivovammojen tunnistamisessa.

Väitöskirjan yhteenveto voidaan jakaa kolmeen johtopäätökseen. Ensiksi; emme löytäneet TBSS:n avulla eroja lievän aivovamman saaneiden potilaiden ja verrokkiaineistomme valkean aineen mikrorakenteessa. Toiseksi; löytämämme poikkeamat selkäydinvammapotilaiden aivojen valkeassa aineessa ovat huomattavasti laajemmat kuin on aiemmin raportoitu. Laaja-alaiset muutokset viittasivat vamman jälkeen esiintyvän neuroplastisiteetin jatkuvan vielä pitkään akuutin trauman jälkeen. Kolmanneksi; esittelemämme automatisoitu DTI-analyysimenetelmä on monikäyttöinen työkalu, jonka kliinistä käyttökelpoisuutta voidaan parantaa lisäämällä verrokkiaineiston kokoa sekä parantelemalla yleistä käytettävyyttä. Riittävän verrokkiaineiston keruu voitaisiin taata esimerkiksi

biopankkityylisellä DTI-datankeruujärjestelmällä. Lisäksi tarkempaa tilastollista mallia varten voitaisiin soveltaa tekoälyä koneoppimisen muodossa, jolloin myös DTI skalaarien ennustearvot tarkentuisivat verrokkiaineiston kasvamisen myötä.

CONTENTS

ABBREVIATIONS

ABA	Atlas-Based Analysis
AD	Axial Diffusivity
ADC	Apparent Diffusion Coefficient
ANCOVA	Analysis of Covariance
CST	Corticospinal Tract
CT	Computed Tomography
DICOM	Digital Imaging and Communications in Medicine
DTI	Diffusion Tensor Imaging
DWI	Diffusion Weighted Imaging
EPI	Echo-Planar Imaging
FA	Fractional Anisotropy
FLIRT	FMRIB's Linear Image Registration Tool
FMRIB	Oxford Centre for Functional MRI of the Brain
FNIRT	FMRIB's Nonlinear Image Registration Tool
FSL	FMRIB Software Library
GCS	Glasgow Coma Scale
GLM	General Linear Model
HARDI	High Angular Resolution Diffusion Imaging
ICBM	International Consortium for Brain Mapping
IFOF	Inferior Fronto-Occipital Fasciculus
IIT	Illinois Institute of Technology
JHU	Johns Hopkins University
MD	Mean Diffusivity
MNI	Montreal Neurological Institute
MRI	Magnetic Resonance Imaging
mTBI	Mild Traumatic Brain Injury
Nifti	Neuroimaging Informatics Technology Initiative
NMR	Nuclear Magnetic Resonance
NMV	Net Magnetic Moment Vector
RD	Radial Diffusivity

RF	Radiofrequency
RMSE	Root-Mean-Square Error
ROI	Region of Interest
SCI	Spinal Cord Injury
SCISSORS	Spinal Cord Injury Series of Tampere – Retrospective Study
SNR	Signal to Noise Ratio
TBI	Traumatic Brain Injury
TBSS	Tract-Based Spatial Statistics
TE	Echo Time
TheBrainS	Tampere Traumatic Head and Brain Injury Study
TR	Repetition Time
UF	Uncinate Fasciculus
WM	White Matter

ORIGINAL PUBLICATIONS

This thesis is based on the following three original publications and an unpublished manuscript which are referred to in the text as Publication I-IV. The publications are reproduced with kind permissions from the publishers.

Publication I Ilvesmäki T, Luoto TM, Hakulinen U, Brander A, Ryymin P, Eskola H, Iverson GL, Öhman J. Acute mild traumatic brain injury is not associated with white matter change on diffusion tensor imaging. Brain 2014;137:1876–82. doi:10.1093/brain/awu095.

Publication II Ilvesmäki T, Koskinen E, Brander A, Luoto T, Öhman J, Eskola H. Spinal Cord Injury Induces Widespread Chronic Changes in Cerebral White Matter. Hum Brain Mapp 2017;38:3637–47. doi:10.1002/hbm.23619.

Publication III Ilvesmäki T, Hakulinen U, Eskola H. Automated pipeline for brain ROI analysis with results comparable to previous freehand measures in clinical settings. In: Eskola H, Väisänen O, Viik J, Hyttinen J, editors. IFMBE Proc., vol. 65, Springer, Singapore; 2018, p. 635–8. doi:10.1007/978-981-10-5122-7_159.

UNPUBLISHED MANUSCRIPT

Publication IV Ilvesmäki T, Luoto TM, Hakulinen U, Panenka WJ, Terry DP, Iverson GL, Brander A, Eskola H. A Robust Quantitative Diffusion Tensor Analysis Method: Application to Ageing and Mild Traumatic Brain Injury. Unpublished (12/2018)

AUTHORS' CONTRIBUTION

The authors' contributions to the publications were as follows.

Publication I. T.I. was mainly responsible for data processing and analysis and primary drafting of the manuscript. T.L and J.Ö. were responsible for the study and methodological design and collection of the original data. U.H. and T.L. contributed to the data analysis and drafting of the manuscript. A.B., P.R., H.E. and G.I. contributed significantly to the drafting of the manuscript and presentation of the data.

Publication II. T.I. was responsible for co-design of the study, implementation of the analyses and primary drafting of the manuscript. E.K. contributed significantly to the study design, data analysis and presentation, and drafting of the manuscript. E.K., T.L. and J.Ö. were responsible for the collection of the original data. A.B., T.L., J.Ö. and H.E. contributed significantly to the drafting of the manuscript and presentation of the data.

Publication III. T.I. was mainly responsible for study design, methodological testing and drafting of the manuscript. U.H. contributed significantly to the data analysis and drafting of the manuscript. H.E. contributed significantly to study design and drafting of the manuscript.

Publication IV. T.I. was primarily responsible for study design, methodological design, implementation and drafting of the manuscript. Data collection was mainly performed by T.L. U.H. contributed significantly to the data analysis and drafting of the manuscript. T.L. and H.E. contributed to the study design, drafting of the manuscript and presentation of the data. W.P., D.T., G.I. and A.B. contributed significantly to the drafting of the manuscript and presentation of the data.

1 INTRODUCTION

The human brain has been extensively studied through various measures for an extensive period of time. In addition to the structure and functional anatomy of the brain itself, various distinct changes in the cerebral microstructure and the causalities of these changes have been of great interest to the medical research community for centuries (Finger, 2001; Gross, 1987). While the macroscopic structure and basic functions of the brain are well known, the detailed microstructural properties and their associations with functional qualities are still largely undefined. Different types of pathologies can alter the microstructure of the cerebrum, and these changes are a potential biomarker for the disease and its possible progression.

Brain structure and function can be studied using various methods. The study of brain structure, for example, is mostly associated with X-ray computed tomography (CT) or magnetic resonance imaging (MRI), while, in addition to functional imaging, brain activity can be assessed using encephalography measurements. At present, the most reliable manner to study white matter histopathologies is to study the brain post mortem (Benes, 1994; Peter R., 1979). Recently, however, diffusion tensor imaging (DTI) has enabled the accurate study of the human brain white matter (WM) microstructure in vivo.

DTI can be used to estimate the microscopic movement of water in the human body. The measured water diffusion is hypothesised to directly reflect the underlying microstructure of the tissue. This type of information is of value, especially in tissues with organised microscopic structures, such as white matter and muscle tissue. Thus, DTI is most frequently used in the field of neuroscience. DTI data can be analysed by various means, with the most popular ones being region of interest (ROI), voxel-wise, histogram and tractography-based methods, each of which has its own advantages and disadvantages. The aim of this thesis was to evaluate the possible applicability of a voxel-wise analysis and an applied ROI analysis method in the context of neurotrauma. An additional objective was to improve the current clinical diagnostic methodology in quantitative DTI brain analysis.

1.1 Motivation

Traumatic brain injuries (TBI) are woefully common in Europe, with an incidence rate of approximately 260 per 100 000, the majority of which are under 25 years of age (Brazinova et al., 2016; Peeters et al., 2015). While some of the TBIs are severe and may even cause death (prevalence approximately 1 to 8 per 100 000), a notable majority of trauma-based head injuries are mild traumatic brain injuries (mTBI) (Peeters et al., 2015). In Finland, the rate may be slightly lower (S. Koskinen & Alaranta, 2008; Puljula, Mäkinen, Cygnel, Kortelainen, & Hillbom, 2013), but the financial effects of mTBI can still be considered significant (Humphreys, Wood, Phillips, & Macey, 2013). To tackle the unnecessary financial strain, a reliable diagnostic method for the successful classification of the severity of TBI is required. Appropriate diagnostics and adequately focused follow-up procedures lead to efficient rehabilitative measures and substantial savings at a societal level (Humphreys et al., 2013). In addition, suitable rehabilitation will have a significant impact on the patients' quality of life.

In addition to conventional imaging modalities, DTI is used in some specific circumstances as an adjunct measure for detecting white matter damage in mTBI. The lack of proper baseline values and the arduous quantitative DTI analysis process can, however, hinder the overall effectivity and value of this method. The lack of agreement on normal values and the pathological limit of the DTI scalars mean that the interpretation is often made based on qualitative measures. Qualitative interpretations are observer-dependent, and thus subject to error. In the quantitative freehand ROI method, the subjectivity is introduced during the ROI drawing phase. These issues signify that the interpretations of DTI findings are based on subjective methodology. It is this subjectivity that this thesis aims to overcome by introducing a clinically relevant, robust and automated DTI brain analysis method.

Our studies were part of two larger prospective studies carried out at Tampere University Hospital: Tampere Traumatic Head and Brain Injury Study (TheBrainS) and Spinal Cord Injury Series of Tampere – Retrospective Study (SCISSORS). The research questions of the studies were elaborate and well-structured, and with the good quantity of valuable patient and control data, our research proved to be highly interesting. Additionally, the increased scientific attention towards a novel voxel-wise analysis method, tract-based spatial statistics (TBSS), made it an interesting choice for the assessment of mTBIs. The method had received attention due to its different approach to the registration problem in voxel-wise analysis techniques.

1.2 Aims and Objectives

This thesis aims to answer the question: "Can quantitative DTI analysis be used for clinical mTBI interpretation?". The overall agenda can be divided into three primary objectives:

1. To study the possibility to evaluate human brain WM changes in acute mTBI by diffusion tensor imaging.

2. To quantitatively study the comprehensive effect of spinal cord injuries on the human cerebral WM, and to evaluate the applicability of TBSS to spinal cord injuries.

3. To create a clinically viable individually applicable DTI analysis method by using a ROI-based approach and reference values obtained via modelling of normal population diffusion metrics.

2 BACKGROUND

2.1 Magnetic Resonance Imaging

Magnetic resonance imaging (MRI) is one of the latest additions to field of medical imaging and the most technically advanced imaging modality to date. Its origins date back to the early 1970's, and the MRI's triumphant journey has continued ever since (Damadian, 1971; Lauterbur, 1989). MRI is one of the safer imaging methods because it is based on non-ionizing electromagnetic radiation. Several physical and physiological factors affect image formation in MRI, but the main physical phenomenon behind MRI is nuclear magnetic resonance (NMR). In this chapter, some of the basic principles of NMR and MR image formation will be discussed, after which the focus will be on diffusion imaging.

2.1.1 Nuclear Magnetic Resonance

The concept of NMR is based on quantum spins and their interaction with external electromagnetic radiation in a static magnetic field. Disturbing nuclei with a nonzero spin magnetic moment in a constant magnetic field with photons of a certain energy causes the nucleus to absorb the photons' energy, and later to release the absorbed energy to its near surroundings (Meyers & Myers, 1997). This phenomenon was originally discovered in the 1930's by several researchers, but the one usually credited with its invention, due to successful experiments with a molecular beam in a magnetic field, is Nobel prize winning physicist Isidor Rabi (Rabi, 1937; Rabi, Zacharias, Millman, & Kusch, 1938). Although it was only slightly later when NMR was applied to liquid and solid matter instead of to a beam of particles (Bloch, Hansen, & Packard, 1946; Purcell, Torrey, & Pound, 1946).

Elementary particles, such as electrons, protons and neutrons, have a spin angular momentum. Atomic nuclei have a spin that equals the vector sum of the spins of the elementary particles in the nucleus. Nuclei that have an even number of protons and neutrons have no net spin, and thus cannot experience NMR interactions. According to the Zeeman effect, when a nucleus with a spin is placed in a constant external

magnetic field B_0, its energy states become quantised with a limited number of possible values when measured. These energy states are observable in the presence of an external magnetic field:

$$E = -m\gamma\hbar B_0, \tag{1}$$

where E is the energy level corresponding to the energy state, m is the magnetic quantum number, γ is the gyromagnetic ratio, $\hbar$ is the reduced Planck constant and B_0 is the external magnetic field flux density (Suetens, 2009).

The hydrogen nucleus is mainly used in MRI applications. While other nuclei may have several spin states, the hydrogen nucleus has only two, and thus only two possible energy values. The states of spin up and down correspond to states where the proton's magnetic vector moment is either parallel or antiparallel (respectively) to the magnetic field. When observing a proton in a constant external magnetic field, the preferred and most probable state will be the spin up state, which corresponds to the state of lowest energy. For a proton, the values of m for the possible energy levels up and down are $m_u = \frac{1}{2}$ and $m_d = -\frac{1}{2}$, and the energy difference is:

$$E_d - E_u = \gamma\hbar B_0, \tag{2}$$

where E_u and E_d are the energies of spin up and down states, respectively. A photon with the energy equal to the difference of the two energy levels can switch the proton from the lower energy state to the higher (see Figure 1). However, the energy states described by the equation (1) are in fact the maximum and minimum values that the spins can have, and the spin energies reside between these states, defined by the probability density of the wave function. Due to thermal energy, all the spins do not reside in the lower energy state, as would be intuitive. Instead, the distribution of spins follow the Boltzmann distribution (Boltzmann, 1877). As per quantum theory, it is only when the spins are individually measured that their wavefunction will collapse to one of the eigenstates. Indeed, in NMR, the magnetisation of a single spin is never measured. Instead, we measure the total magnetisation of many nuclei (Hanson, 2008). Because further quantum mechanics are not necessary to explain NMR and MRI phenomena, classical mechanics will be used in the following description of NMR, and the spinor property of protons will be simplified as vectors.

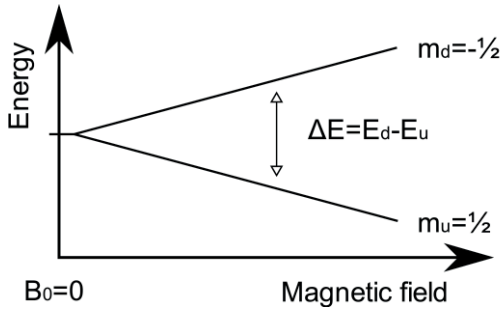

Figure 1. Hydrogen nucleus (spin quantum number ½) spin energy level splitting in an external magnetic field B_0 according to the Zeeman effect. The energy level difference ΔE is directly related to the external field strength B_0.

The spins will precess around the external magnetic field's axis, due to the resulting torque caused by interaction between the external magnetic field and the intrinsic magnetic moment of the proton. The precession rate (frequency) depends on the Larmor frequency of the nucleus and is proportional to the strength of the external magnetic field. The Larmor equation gives us the precession frequency:

$$\omega = \gamma \hbar B_0, \tag{3}$$

where ω is the angular frequency of the precession. This is the frequency that corresponds to the photons that can be used in NMR to disturb the protons and cause the resonance effect. The required frequencies can be calculated with the known values of gyromagnetic ratios for each nucleus. For the proton, the gyromagnetic ratio is 42.58 MHz/T (Hanson, 2008; Hendee & Ritenour, 2003; Larmor, 1897).

In the absence of an external magnetic field B_0, the sum of multiple proton magnetic moments, the net magnetic moment vector (NMV) is a null vector. However, the NMV in the B_0 will be a rotating vector pointing in the direction of the B_0. Due to the incoherence of the precessing spins, the sum vector itself will not precess, but the rotation rate, or angular frequency of the vector, is 42.58 MHz in an external field of 1 T. By exciting the protons with the appropriate resonance radiofrequency (RF) radiation, the NMV is rotated around the RF field vector (see Figure 2). It is this interaction of RF energy with the nuclei that forms the basis of nuclear magnetic resonance applications.

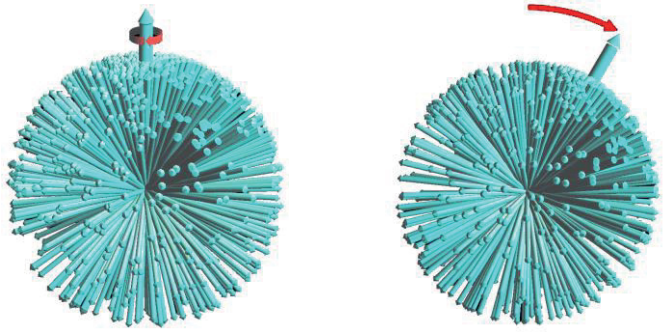

Figure 2. Visualisation of spin distributions in an external magnetic field. The graphic on the left represents the rotation of the NMV in the direction of the B_0 (up), where the orientation of the spins is slightly skewed in the direction of the B_0. The graphic on the right shows the effect of a resonant RF field on the NMV, which rotates toward the transverse plane while precessing about the B_0 vector. The RF field vector in this case is pointed towards the reader. Reprinted with permission from John Wiley & Sons (Hanson, 2008).

2.1.2 MR Image Formation

Credit for the original theory behind the NMV and relaxation times is given to Felix Bloch (Bloch, 1946). The Bloch equations are the basis of MRI and its imaging sequences which take advantage of the various relaxation times of the NMV in different types of tissues. When the spins are excited with an RF pulse and the NMV has a transverse component in relation to the B_0, the NMV will precess around the B_0 and induce a signal in MRI receiver coils. The absorbed energy is released to the close environment of the proton and the magnetic moment vector begins to relax to its original longitudinal plane (Bloch, 1946; Hendee & Ritenour, 2003; Suetens, 2009).

The resonance phenomenon in MRI refers to the absorption of Larmor frequency RF energy by the proton nucleus, while the application of the Larmor frequency pulse is called excitation. The flip angle refers to the angle between the B_0 field and the excited NMV (see Figure 3). The NMV can be flipped to various angles, but the signal is originated from the transverse plane, i.e., the larger the portion of NMV in the transverse plane, the larger the receivable signal (Westbrook, Roth, & Talbot, 2011).

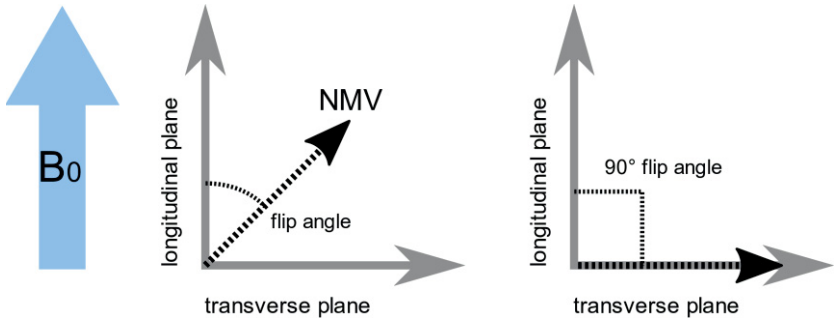

Figure 3. Different flip angles with different amounts of longitudinal and transverse magnetisation. On the left, the flip angle is between zero and 90 degrees, and the NMV is precessing around the B_0 likely causing some signal in the receiver coils. On the right, the NMV is fully flipped (90°) to the transverse plane and will create a maximal signal in the receiver coils.

When the NMV is flipped to the transverse plane either partly or completely, the vector will precess in the transversal plane. This precession can be measured by MR receiver coils that are positioned perpendicular to the B_0 (in the transverse plane). NMV relaxation is caused by thermal energy transfer from the spins to the close environment (T1) and by interactions between spins and local magnetic fields (T2). Another way of describing the relaxations is by their effect on the NMV: T1 relaxation refers to the growth (returning) of the longitudinal component of the NMV after excitation, and T2 relaxation refers to the decay of the transverse component. In general, any process causing T1 relaxation causes T2 relaxation (Hanson, 2008; Westbrook et al., 2011). Tissues have varying, complex microstructures that influence the relaxation times, and, as such, enable their differentiation in MRI. By applying different excitation pulses in a pulse train, the NMV can be manipulated in a preferable way to induce the required signal to the receiver coil.

Spatial encoding of the MRI signal is performed by using gradient fields. These gradient fields change the static magnetic field slightly in the imaging plane. Frequency encoding gradients cause a slight static spatial variation to the field strength in the imaging plane that allows spatial separation of the acquired signal. Frequency encoding can be used for slice selection or spatial encoding in an image slice and are on during signal acquisition. Phase encoding gradients, on the other hand, are turned on temporarily before signal acquisition, and they induce a spatial phase shift in the orthogonal direction of the frequency encoding gradient. These small differences in the signal's frequency and phase can be used to map the acquired signals to the correct spatial locations. (Hendee & Ritenour, 2003; Westbrook et al.,

2011) Because the acquisition is based on frequency and phase encoding, the acquired image is originally in k-space. Hence, instead of spatial coordinates referring to a distinct physical cartesian coordinate location, the signal intensity information is stored in a matrix with frequency and phase coordinates (Hendee & Ritenour, 2003; Suetens, 2009). To obtain the "normal" MRI image, a Fourier transform needs to be applied to the acquired k-space image.

Because the time scale of Brownian motion of water, the basis of diffusion imaging, is extremely short compared with the physical and physiological motion of a living subject, the MRI sequence utilised in diffusion imaging needs to be significantly shorter than sequences used in common structural MR imaging. Extremely short acquisition times (approximately 20 ms to 100 ms) can be achieved through a special MRI imaging technique called echo-planar imaging (EPI) (Poustchi-Amin, Mirowitz, Brown, McKinstry, & Li, 2001; Stehling, Turner, & Mansfield, 1991). EPI was first described by Sir Peter Mansfield in 1977 (Mansfield, 1977). However, due to hardware restrictions, EPI acquisition was not possible at the time. EPI allows for the collection of multiple k-space lines during a single repetition time (TR), and it can be utilised in both spin echo and gradient echo imaging. Instead of merely collecting multiple k-space lines of an image slice within a TR (multi shot EPI), the frequency and phase encoding gradients can also be fluctuated in such a manner that the entire k-space is filled in a single excitation (single shot EPI) (Poustchi-Amin et al., 2001). An EPI sequence without a diffusion gradient is shown in Figure 4.

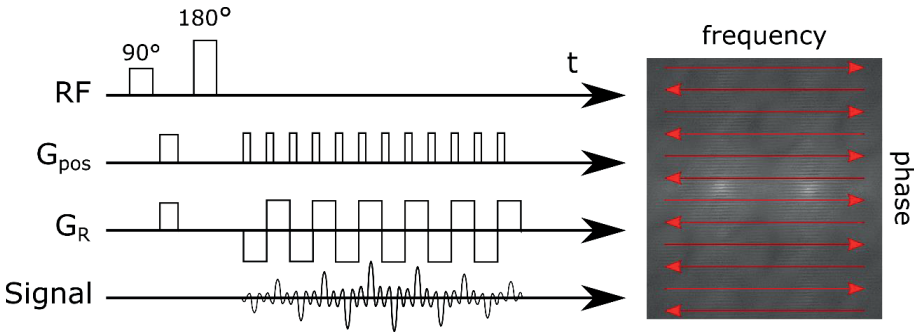

Figure 4. A schematic presentation of a single TR of a spin echo EPI sequence. RF indicates the 90° and 180° excitation pulses, G_{pos} shows the repeated phase encoding gradient, and G_R the oscillated frequency encoding gradient that is applied during signal acquisition. Slice selection gradient is not visible in the diagram. The sequence shown is "blibbed", where the phase encoding gradient is repetitively turned on and off while the frequency encoding gradient oscillates. The k-space image to the right illustrates how the k-space is filled in a zigzag pattern.

2.1.3 Brain Diffusion Tensor Imaging

DTI is an imaging method based on a special MRI pulse sequence. DTI is, in principle, an extension of diffusion weighted imaging (DWI), which is performed by applying a diffusion-sensitising imaging sequence. Diffusion imaging can be used to quantify the microscopic diffusion of hydrogen nuclei originating from Brownian motion of water molecules (P.J. Basser, Mattiello, & LeBihan, 1994; D Le Bihan et al., 1986). The modern diffusion weighted sequence was first introduced by Tanner and Stejskal in the 1960's, when they described a pulsed gradient spin echo sequence using diffusion sensitising gradients (Stejskal & Tanner, 1965; Sugawara & Nikaido, 2014). These gradients act in a way that alters the signal obtained from moving spins compared with stationary ones in a manner that is similar to magnetic resonance angiography, only on a microscopic scale. It was not until the early 1990's that the first "real" diffusion images were created (Filler et al., 1993; Howe, Filler, Bell, & Griffiths, 1992).

In general, DWI uses two paired pulsed (diffusion) gradients in a T2* imaging sequence between a 180° RF pulse before signal acquisition. This type of arrangement causes diffusing spins to phase out (spin precessions move out of phase resulting in a smaller transverse NMV) in a degree dependent on the strength of diffusion, while the effect is cancelled for stationary spins that retain their signal strength (Dietrich, Biffar, Baur-Melnyk, & Reiser, 2010; Hagmann et al., 2006; Stejskal & Tanner, 1965). An extremely simplified visualisation of a diffusion sequence is shown in Figure 5. For diffusion weighted images, at least three (orthogonal) diffusion gradient images are required to obtain isotropic diffusion images. Another important factor in the creation of diffusion images is the b-value, which is proportional to the gradient field strength and time between the gradients (Dietrich et al., 2010; Hagmann et al., 2006). In practice, the b-value defines the amount of diffusion weighting in the acquired image. With zero diffusion weighting (b_0), the diffusion sequence will produce a T2* image, and with small diffusion weighting (b-value) the images will suffer from T2 shine-through, i.e., the contrast on the image will be mainly due to T2 effects. Different direction diffusion gradient images are combined to create trace diffusion images or apparent diffusion coefficient (ADC) images. ADC images are "pure" diffusion images that are further mathematically enhanced to get rid of the possible T2 effects. ADC images require

a b_0 image and at least three diffusion gradient directions to accurately reflect the mean diffusion (Hagmann et al., 2006). Examples of the different image types obtainable through diffusion imaging are shown in Figure 6.

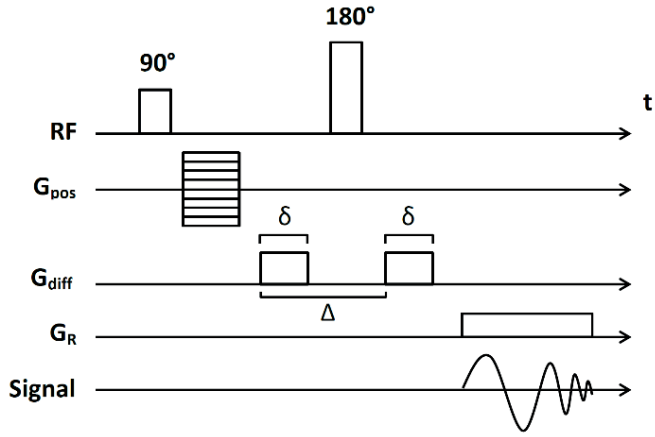

Figure 5. Simplified schematic of a diffusion sensitised pulsed gradient spin echo sequence. RF indicates the 90° and 180° excitation pulses, G_{pos} is the phase encoding gradient, G_{diff} shows the diffusion gradients with an interval Δ, amplitude G and duration δ and G_R the frequency encoding gradient applied during signal acquisition. Slice selection gradient is not visible in the diagram. Diffusion sequences use EPI in practice and resemble the sequence shown in Figure 4.

Diffusion coefficient, D, describes the diffusion of molecules in a liquid or gas, and is described by the Einstein equation (Einstein, 1905):

$$D = \frac{d^2}{6t}, \tag{4}$$

where d is the mean displacement of the molecules and t is the diffusion time. As an example, the diffusion coefficient of water at room temperature is approximately 0.002 mm²/s. The diffusion signal in an isotropic medium is defined by the Stejskal-Tanner equation, by b_0 image signal, S_0, b-value, b, and the diffusion coefficient, D (Stejskal & Tanner, 1965):

$$S(D, b) = S_0 e^{-bD}. \tag{5}$$

The b-value is defined by the amplitude, G, duration, δ, and interval between the opposite diffusion gradient pulses, Δ:

$$b = (\gamma G \delta)^2 (\Delta - \frac{\delta}{3}), \tag{6}$$

where γ is the gyromagnetic ratio of the hydrogen spins. B-values have units of s/mm^2, and a typical value for diffusion imaging is about 1000 s/mm^2 (Dietrich et al., 2010). However, b-values in the range of several thousand can be used for more complex diffusion imaging, e.g., high angular resolution diffusion imaging.

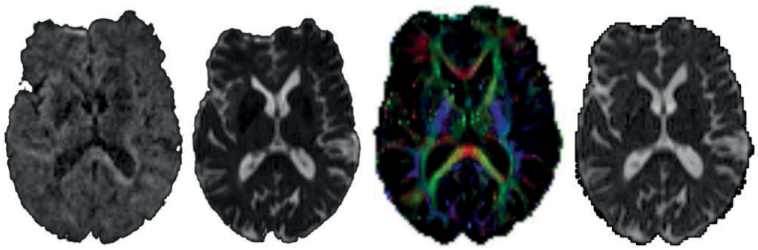

Figure 6. Different types of diffusion images taken from the same subject. From left to right: gradient image, b_0 image, coloured FA map, MD map.

DTI is an advanced form of DWI, and it can be used to visualise the anisotropic diffusion caused by different tissue microstructures. For DTI images, a b_0 image and at least six acquisitions with different diffusion gradient directions are required to calculate the diffusion tensor. The diffusion tensor $\boldsymbol{D}$ can be described as a 3×3 matrix with six degrees of freedom (P.J. Basser et al., 1994; Peter J. Basser & Pierpaoli, 1996):

$$\boldsymbol{D} = \begin{bmatrix} D_{xx} & D_{xy} & D_{xz} \\ D_{xy} & D_{yy} & D_{yz} \\ D_{xz} & D_{yz} & D_{zz} \end{bmatrix}, \tag{7}$$

where the elements D_{xx}, D_{yy} and D_{zz} represent diagonal elements of the diffusion and equal to the diffusion eigenvalues λ_1, λ_2, and λ_3, respectively. Using diffusion ellipsoid to describe diffusion in a frame of reference independent of the scanners will simplify the diffusion tensor by causing all the non-diagonal elements to be zero. Basically, this means defining the three-dimensional diffusion with a vector basis of orthogonal eigenvectors, one of which points in the direction of the highest rate of diffusion. In this way, the diffusion can be defined by the eigenvalues λ_1, λ_2 and λ_3 (for which $\lambda_1 > \lambda_2 > \lambda_3$) and their corresponding eigenvectors (see Figure 7 for

visual details). The anisotropic property of diffusion will make only minor changes to equations (5) and (6), due to the vector notation of the gradient amplitude.

In addition to the axial diffusivity (AD, λ_1) and radial diffusivity [RD, $(\lambda_2 + \lambda_3/2)$], several scalars of interest can be derived from the diffusion tensor. The most important are mean diffusivity (MD) and fractional anisotropy (FA) (Peter J. Basser & Pierpaoli, 1996):

$$MD = \frac{\lambda_1+\lambda_2+\lambda_3}{3} = \frac{D_{xx}+D_{yy}+D_{zz}}{3} = \frac{Trace}{3}, \text{ and} \quad (8)$$

$$FA = \sqrt{\frac{(\lambda_1-\lambda_2)^2+(\lambda_2-\lambda_3)^2+(\lambda_3-\lambda_1)^2}{2\sqrt{\lambda_1{}^2+\lambda_2{}^2+\lambda_3{}^2}}}. \quad (9)$$

FA and MD are the most used scalars in quantitative DTI analysis (Hulkower, Poliak, Rosenbaum, Zimmerman, & Lipton, 2013), but RD and AD are also often used today. In addition, some novel scalar metrics, e.g., kurtosis imaging or neurite orientation dispersion and density imaging (Cox et al., 2016; Nørhøj Jespersen, 2018; Tuch et al., 2002; Wu & Alexander, 2007) are derived from the diffusion tensor but have not yet gained the popularity of the FA, MD, RD and AD scalars.

Axial and radial diffusivities indicate the amount of diffusion in the direction of the first eigenvector and the mean diffusion in the direction of the second and third eigenvectors, respectively. See Figure 7 for a demonstrative visualisation of the diffusion ellipsoid. Mean diffusivity is the average of the eigenvalues, indicating overall magnitude of diffusion. FA, however, is a slightly more complex scalar, representing the degree of anisotropy and overall directionality of the diffusion: the larger the FA value, the more anisotropic the diffusion. The overall strength of diffusion does not affect FA, since it is a measure of the degree of directionality. FA is higher in orderly structured tissues, such as muscle or nervous tissue, and it can be used to track neural pathways.

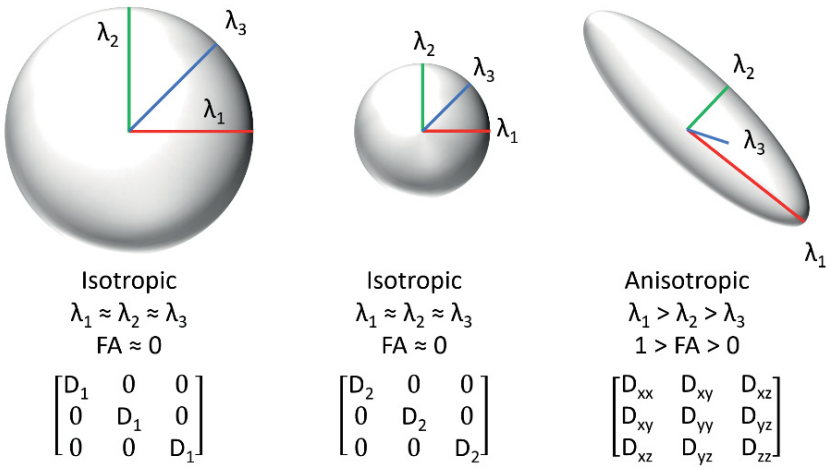

Figure 7. Diffusion ellipsoids, eigenvalues, FA approximations and diffusion tensors of three different types of diffusion. Left: unrestricted diffusion, diffusion is equal in each direction and each eigenvalue is equal. Middle: diffusion equally restricted in each direction, like the case on the left, with the exception $D_1 > D_2$. Right: anisotropic tissue, e.g., in neural tracts running in the direction of λ_1. Note that here FA is closer to one than zero. The diffusion tensor in the anisotropic diffusion is defined in the scanner frame of reference and can be reduced to a diagonal matrix by change of the vector basis.

The diffusion scalars have the following clinical interpretations in brain tissue. Diffusion anisotropy, particularly FA, is one of the most used properties and is thought to be correlated with neural tract properties, such as axonal density, axonal myelination, axon diameter and the packing density of neuroglial cells (P.J. Basser et al., 1994; Minati & Węglarz, 2007; C Pierpaoli, Jezzard, Basser, Barnett, & Di Chiro, 1996). Changes in FA is a possible sign of neuropathologies causing inflammation, demyelination, oedema or damage to the axons themselves (Alexander, Lee, Lazar, & Field, 2007). Higher FA suggests a more structured geometry, and thus most likely a healthy axonal structure, whereas a drop in FA may suggest degenerative changes in the neural tracts (Carlo Pierpaoli et al., 2001). FA is often used due to its high sensitivity to microstructures and neuropathologies. Its specificity, however, is less than ideal and additional information is required to draw conclusions on possible pathologic findings. FA is generally considered to be a marker of white matter integrity (Alexander et al., 2007).

MD is a measure of the overall diffusion strength and will reflect changes in the level of water diffusion restriction. Increased MD has been associated with neural tract degeneration and pathologies, and it can be a sign of inflammation, oedema or tissue necrosis (Alexander et al., 2007; Beaulieu, 2002). The change in MD is highly

susceptible to the time of imaging, and the direction of change can be either negative or positive depending on whether the subject was imaged in the acute or chronic stage (possibly also applicable to other DTI metrics). In general, MD can be considered to be a marker of neural fibre density and/or white matter health, and it can also be used to help specify different pathologic events in WM when used in conjunction with FA (Lebel, Walker, Leemans, Phillips, & Beaulieu, 2008; Carlo Pierpaoli et al., 2001).

The eigenvalues of the diffusion tensor, along with AD and RD, are less utilised than FA and MD. AD and RD are more specific diffusion scalars, and they can be used to further specify the cause of changes to FA or MD (C Pierpaoli et al., 1996). Looking at the eigenvalues alone can give an accurate description of diffusion, but it is slightly more challenging to interpret compared with FA and MD (C Pierpaoli et al., 1996). RD is considered to reflect demyelination, whereas AD is slightly controversial and harder to interpret per se (Song et al., 2002). The use of AD and RD can increase specificity, but it is important to observe the situation in its entirety. While the DTI metrics give a good insight into the WM microstructure of the brain, it is important to understand that the scalars do not reflect the direction of the eigenvectors, and thus the direction of the anisotropic diffusion (Song et al., 2002; Wheeler-Kingshott & Cercignani, 2009). It is therefore crucial to take note of multiple different measures instead of concentrating on only a single scalar.

2.2 Quantitative Diffusion Image Data Analysis

Common DTI analysis methods currently in use are ROI, voxel-wise, histogram and tractography-based methods (Hulkower et al., 2013; Jorge et al., 2012; Lange, Iverson, Brubacher, Mädler, & Heran, 2012; Levin et al., 2010; M. E. Shenton et al., 2012; Toth et al., 2013; Wilde et al., 2012). While each of the analysis methods have their uses, tractography (fibre tracking) is not recommended for quantitative analysis. Due to several limitations, e.g., crossing fibres and seed point inter-observer repeatability, tractography will, in most cases, result in unstandardised and unrepeatable tract volumes of interest, which makes it unreliable as a quantitative analysis method (Jones, 2010). Histogram analysis has its uses, but it is either highly unspecific or requires accurate ROIs to give detailed and meaningful results. We will concentrate more on a special case of voxel-wise analysis, TBSS and on ROI-based methods in the following chapters.

Studies generally concentrate on using a single DTI analysis technique, predominantly ROI. However, studies using multiple parallel techniques have been published (Jorge et al., 2012). DTI parameters are extremely susceptible to different distorting factors, and particular care should be taken to control the effects of age in statistical analyses (Stadlbauer, Salomonowitz, Strunk, Hammen, & Ganslandt, 2008; Yoon, Shim, Lee, Shon, & Yang, 2008). In addition, gender (Chou, Cheng, Chen, Lin, & Chu, 2011; Kanaan et al., 2012), intracranial procedures and neurological disorders, e.g., Alzheimer's disease (Pitel, Chanraud, Sullivan, & Pfefferbaum, 2010) can affect white matter microstructure. Even attention-deficit hyperactivity disorder (Lawrence et al., 2013), dyslexia (Vandermosten et al., 2012), depression (de Diego-Adeliño et al., 2014), alcoholism (Pitel et al., 2010), drug abuse (Bora et al., 2012) and online gaming addiction (Weng et al., 2013) are associated with white matter changes detectable with DTI. However, as previously mentioned, the single most important factor to consider is age. Accounting for the effects of ageing in statistical brain analyses is often an adequate way to suppress a main source of bias.

2.2.1 Tract-Based Spatial Statistics

Tract-based spatial statistics (TBSS) is a newer method for whole brain DTI analysis developed by the Oxford Centre for Functional MRI of the Brain (FMRIB) analysis group (Smith et al., 2006). TBSS is a part of the FMRIB Software Library (FSL) (Mark Jenkinson, Beckmann, Behrens, Woolrich, & Smith, 2012; Smith et al., 2004), which includes several image processing and mathematical analysis tools for structural MRI, functional MRI and DTI brain data. FSL is Linux based, but it can be run on modern Windows computers via a virtual machine.

One of the benefits of using a whole brain approach is that a priori information is not required in the analysis; in contrast to ROI analysis, the whole white matter is examined. TBSS analysis, however, differs substantially from other voxel-wise analyses by its registration and skeletonisation stages. TBSS aims to solve problems in subject-wise registrations by using nonlinear registration and a unique skeletonisation stage that effectively reduces the need for perfect alignment in the registration process. The subject-wise statistical comparisons are made between the generated WM skeleton images rather than all the voxels in the brain images.

The skeletonisation stage creates a wire model of the brain's WM tracts, and uses only the thin skeleton area for voxel-wise comparisons. The skeleton is created by finding the voxels in the middle of the WM neural tract structures. For each subject,

the voxels with the highest FA values are then searched in a perpendicular direction from the middle points of the obtained tract. An example of the skeleton created from our control subject data is shown in Figure 8. The voxels with the highest values are then projected to the skeleton and used in the analysis.

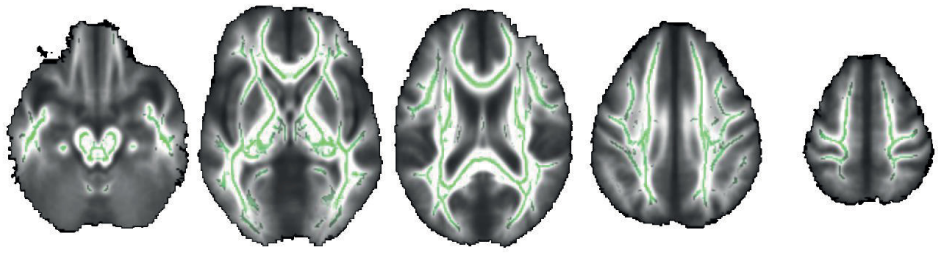

Figure 8. Mean FA map and its FA skeleton created from our control subject data. The FA skeleton is shown as green and represents the tract centres.

The analysis itself is based on nonparametric permutation tests utilising general linear model (GLM) design for statistics. The GLM can be defined as $\boldsymbol{Y} = \boldsymbol{X}\boldsymbol{\beta}$ with a null hypothesis $H_0: \boldsymbol{c}\boldsymbol{\beta} = 0$, where $\boldsymbol{Y}$ is the original data to be tested, $\boldsymbol{X}$ is the design matrix (regressors), $\boldsymbol{\beta}$ is the model parameters and $\boldsymbol{c}$ is defined depending on the research question one wants to answer with the analysis. For example, when testing two groups (A and B) for differences with TBSS, one would need two different randomisation tests with $\boldsymbol{c} = [1 \quad -1]$ and $\boldsymbol{c} = [1 \quad -1]$. The two tests correspond to situations where group A > B and B < A.

2.2.2 Region of Interest Based Analysis

ROI-based methods use the scalar values inside predefined regions in single subject or group comparisons. The regions of interest are actually volumes of interest, and even the freehand ROIs drawn on a single image slice have a volume equal to the area of the ROI times the slice thickness. The term ROI is associated here with these volumes, regardless of their three-dimensional nature. There are multiple ways to define the ROIs, the freehand method being just one of many. Other methods to determine the ROIs include circular or spherical ROIs (Hakulinen et al., 2012), the use of fibre tracking to determine individualised ROIs (Farquharson et al., 2013) and structural and functional anatomic ROIs based on relevant brain atlases (Oishi et al., 2009, 2008; Peng et al., 2009). The use of atlases requires warping of the subject

image to the standard space of the atlas, or vice versa. Different types of analyses can be applied to the defined regions, including mean value comparison (Froeling, Pullens, & Leemans, 2016), different types of statistical analyses or histogram analyses (Young, Babb, Law, Pollack, & Johnson, 2007).

A limitation of most ROI methods is the need for a priori data for the placement of the ROIs. The placement can be done according to structural or functional information, according to prior knowledge of the assumed location of pathology, according to prior voxel-wise analysis results or by using an anatomical atlas. Apart from the use of atlases, each method requires a certain type of a priori knowledge. Furthermore, manually defined ROIs will always include a significant inter-observer variability and a mediocre intra-observer variability (Hakulinen et al., 2012), which affect the repeatability of the method. With a standardised use of atlases together with a robust registration process, the variability of the ROI method can be minimised and potentially reduced to zero.

2.2.3 Age Association

Several studies (Cox et al., 2016; Kodiweera, Alexander, Harezlak, McAllister, & Wu, 2016; Madden et al., 2012; Moseley, 2002; Rathee, Rallabandi, & Roy, 2016; Westlye et al., 2010) have shown a statistically significant correlation between ageing and various diffusion parameters in the majority of the brain volume. Age is the most prominent factor affecting the DTI metrics of a healthy brain, although its impact on the DTI metrics is neither linear nor unidirectional throughout the human lifespan. The correlation between age and FA, MD and RD can be considered quadratic (U-shaped), especially when dealing with a younger population (Lebel & Beaulieu, 2011; Westlye et al., 2010). Due to their still maturing brains, the younger population will experience WM development, seen as an increase in FA and a decrease in MD, up until about the age of 25 (Lebel & Beaulieu, 2011). For adult populations, with subjects aged over twenty years, a linear approximation of the age effect is sufficient (Westlye et al., 2010).

For more accurate clinical results, the age association should be further acknowledged in analyses. By applying an appropriate method to model the normal values of human white matter in terms of age and other possible confounding factors, accurate reference values may be derived.

2.3 Mild Traumatic Brain Injury

In 2010, an expert group formed by the Demographics and Clinical Assessment Working Group of the International and Interagency Initiative toward Common Data Elements for Research on Traumatic Brain Injury and Psychological Health proposed the following definition of TBI: "TBI is defined as an alteration in brain function, or other evidence of brain pathology, caused by an external force" (Menon, Schwab, Wright, & Maas, 2010). While slightly vague, the definition is superior to the earlier consensus where concussion was considered to be a completely reversible disorder (Peerless & Rewcastle, 1967).

Currently, the diagnosis of TBI is based on subjective clinical signs and conventional neuroimaging. The clinical signs include any period of loss of or a decreased level of consciousness, any loss of memory for events immediately before (retrograde amnesia) or after the injury (post-traumatic amnesia), neurologic deficits (e.g., weakness, loss of balance, change in vision, dyspraxia paresis/plegia [paralysis], sensory loss, aphasia, etc.) and any alteration in mental state at the time of the injury (confusion, disorientation, slowed thinking, etc.). Clinical signs are accompanied by acute traumatic lesions on brain imaging (CT and MRI) (Menon et al., 2010).

Cerebral microhaemorrhages (see Figure 9) are often associated with TBI and can be identified by susceptibility weighted MRI (SWI). However, microhaemorrhages are often absent in mTBI (Trifan, Gattu, Haacke, Kou, & Benson, 2017). The lesion type mainly associated with mTBIs is diffuse axonal injury (DAI), which cannot be reliably identified through conventional medical imaging (M. E. Shenton et al., 2012). DTI is being utilised for research purposes in an attempt to objectively differentiate DAIs and to obtain evidence of mTBIs through medical imaging.

Since the first DTI studies of TBI (Benson et al., 2007; Werring et al., 1998), the research community has considered DTI to be a promising and valuable tool for the detection of post traumatic WM injury (Hulkower et al., 2013; Wallace, Mathias, & Ward, 2018). Most publications have reported a decrease in FA and an increase in MD values following TBI (Hulkower et al., 2013; M. E. Shenton et al., 2012; Wallace et al., 2018), while a notable number of publications have reported opposite behaviour in WM DTI (Hulkower et al., 2013). In addition, altogether negative findings have been published (Jorge et al., 2012; Lange et al., 2012; Levin et al., 2010). In the recent literature, more emphasis has been given to the chronological nature of the findings, since DTI metrics have been shown to vary considerably depending on the time of imaging (Hasan et al., 2014; Lancaster et al., 2016). It is therefore crucial to understand the complex effect of TBI on the DTI metrics, and to always

consider the TBI stage (acute, sub-acute, and chronic) at the time of imaging. The time of imaging is an even more essential factor in mTBI where the changes in WM are even more subtle.

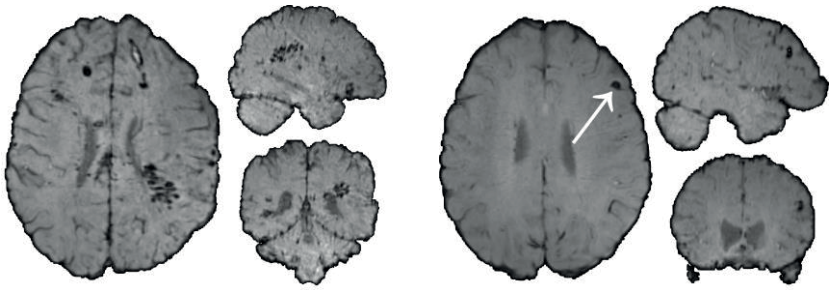

Figure 9. Two examples of susceptibility weighted MR images taken from TBI patients. The black dots seen in the images (arrow in the right subject image) are signal voids caused by TBI induced microbleeds.

Numerous studies have established a relation between symptomatic mTBI and abnormal diffusion metrics (Aoki, Inokuchi, Gunshin, Yahagi, & Suwa, 2012). Within and between samples, heterogeneity is a possible explanation for the inconsistent DTI results, while another possible cause for the incoherency are the various unstandardised analysis methods. With different subject inclusion and exclusion criteria, different image processing methods and varying statistical analyses, the inconsistency between mTBI DTI analysis results is to be expected.

2.4 Traumatic Spinal Cord Injury

Traumatic spinal cord injury (SCI) refers to damage caused by an external force to the vertebrae-shielded neural tracts of the central nervous system. SCIs can be of different severity. For example, the neural tracts may be completely damaged at the site of trauma or the damage may only be partial (Kakulas, 1987). In addition to the immediate damage to the trauma site, secondary degeneration of WM tracts often commences in both anterograde and retrograde directions from the primary injury site (Beirowski et al., 2005; Buss, 2004). This degenerative process can take years, causing slow progressive demyelination leading to gliosis (Buss, 2004). The secondary degeneration may also extend to the cerebrum, especially to the motor and sensory pathways, such as the corticospinal tract (Freund et al., 2011;

Henderson, Gustin, Macey, Wrigley, & Siddall, 2011; Yamamoto, Yamasaki, & Imai, 1989).

After a SCI, remedial mechanisms are initiated in the brain and parts of the whole central nervous system. This repair mechanism is called neuroplasticity, and it is similar to the constructive process that occurs in normal brain development and during learning processes (Keyvani & Schallert, 2002; Zatorre, Fields, & Johansen-Berg, 2012). Neuroplasticity remodels the neural structure of the brain and spinal cord so that functional parts of the central nervous system can take over at least parts of the disabled regions (Nudo, Plautz, & Frost, 2001). This regenerative process should, in theory, be observable by DTI.

Spinal cord DTI has been shown to be sensitive to SCI-induced neural damage to the spine near the site of injury, but also further away from the trauma site (Chang, Jung, Yoo, & Hyun, 2010; E. Koskinen et al., 2013). This suggests that DTI is also sensitive to the secondary Wallerian degeneration caused by the primary lesion. While there have been a few DTI studies of SCI, most have only focused on the corticospinal tract (Gustin, Wrigley, Siddall, & Henderson, 2010; E. A. Koskinen et al., 2014; Wei et al., 2008). In a study by Wrigley et al. (2009), however, DTI changes were found outside the corticospinal tract, suggesting the more widespread effects of SCIs on the cerebral WM. The study by Wrigley et al. served as inspiration for our SCI study.

3 IMAGE DATA AND ANALYSIS METHODS

For the research, we used two different patient groups with different central nervous system injuries (MTBI and SCI), and a total of 70 control participants. All subjects provided written informed consent according to the Declaration of Helsinki. The subject material will be discussed in detail in the following sections, and demographical information of all the clinical subject groups is presented in Table 1. In addition, a brief overview on the human brain atlases used in the research will be given. After the imaging material, the different analysis methods are reviewed.

Table 1. Demographics of the different subject groups used in the study.

	Publication I Controls (n = 40)	Publication II & IV Controls (n = 70)	Publication I mTBI Patients (n = 75)	Publication II SCI Patients (n = 32)
Age, years mean ± SD (range)	40.6 ± 12.2 (20 – 59)	39.5 ± 11.8 (18 – 60)	37.2 ± 12.0 (18 – 60)	56.5 ± 14.2 (24 – 75)
Gender, male / female	20 / 20	29 / 41	45 / 30	25 / 7

3.1 Clinical Subject Data

3.1.1 Imaging

All the subjects were imaged with an identical image protocol at Tampere University Hospital. Brain MRI was performed with a 3 Tesla MRI scanner (Siemens Trio) using a 12-channel head matrix coil. The protocol included the following sequences: sagittal T1-weighted 3D inversion recovery prepared gradient echo, axial T2 turbo spin echo, conventional axial and high-resolution sagittal FLAIR, axial T2*, axial susceptibility-weighted imaging and diffusion-weighted imaging series. In addition, the DTI image data were collected by a single-shot, spin echo-based and diffusion-weighted EPI sequence. The parameters for the DTI sequence were TR 5144 ms, echo time (TE) 92 ms, field of view 230 mm, matrix 128 × 128, 3 averages, slice/gap

3.0/0.9 mm, and voxel dimension of 1.8 mm × 1.8 mm × 3.0 mm. Two diffusion weighting b-values were used, 0 and 1000 s/mm², with 20 diffusion gradient orientations.

The image data were natively in Digital Imaging and Communications in Medicine (DICOM) format but were converted into Neuroimaging Informatics Technology Initiative (Nifti) for image processing purposes. All conversions were performed using MRIConvert (developed at the Lewis Center for Neuroimaging at the University of Oregon). All post-conversion image manipulations were executed with tools included in the FSL software package, including diffusion tensor fitting to derive DTI scalars, eddy current correction and all the registrations. The overall mean signal-to-noise ratio (SNR) of our data was approximately 25, which can generally be considered to be good and sufficient for reliable quantitative analysis (Hakulinen et al., 2012). The SNR was calculated from the b_0 images according to the National Electrical Manufacturers Association (NEMA) standards 1-2008, defining SNR by the following equation:

$$SNR = \frac{S}{N} = \frac{S}{SD/0.66}, \tag{10}$$

where S is mean signal measured from in vivo freehand ROIs, and N is noise measured from separate background ROIs.

3.1.2 Patient Material

3.1.2.1 Mild Traumatic Brain Injury Subjects

The mTBI patients in our study (used in **Publications I** and **IV**) were prospectively enrolled from the emergency department of Tampere University Hospital between August 2010 and July 2012 for the TheBrainS study. All consecutive patients with head CT due to acute head trauma (n = 3023) formed the initial population of the study. The population was carefully screened to obtain a sample of working-aged adults without pre-injury medical or mental health problems. The aim was to examine 'pure' mTBI patients who could probably be reached for an outcome visit. The final sample included 75 patients. Of the 75 patients, 45 (60%) were men and 30 (40%) were women, and the mean age was 37.2 years (SD = 12.0, median = 36.0).

The enrolment protocol for the mTBI patients is described in detail in previous publications (Isokuortti et al., 2016; Luoto et al., 2013).

For **Publication IV**, ten of the mTBI patients, including five complicated and five uncomplicated cases, were handpicked to represent the mTBI subject pool. Complicated MTBI refers to patients with traumatic lesions on conventional brain MRI. This cohort was chosen to test the applicability of the method described in our study.

3.1.2.2 Spinal Cord Injury Subjects

The SCI patients used in **Publication II** were collected from all patients with a chronic traumatic cervical spine injury at Tampere University Hospital for the SCISSORS study. The primary SCIs were sustained between 1989 and 2010 (n = 88). The patients were contacted about participation in the study in 2011. The final population used in our study comprised 32 SCI patients. Of the 32 patients, 25 (78%) were men and 7 (22%) were women, and the mean age was 56.5 years (SD = 14.2, median = 60.6). Further details on the collection of the SCI data is presented in the publication of Koskinen et al. (2014).

3.1.3 Control Subjects

The control group in **Publication I** comprised the original 40 subjects enrolled for the TheBrainS study in Tampere. The subjects were orthopaedically injured patients evaluated in the emergency department of Tampere University Hospital. Patients with ankle injury (n = 609) were screened for inclusion in the study as controls. The subjects were enrolled in an age and gender stratified manner, resulting in four age groups: 18 – 30, 31 – 40, 41 – 50 and 51 – 60 years, with five women and five men in each group. Of the 40 control subjects, 20 (50%) were men and 20 (50%) were women. The mean age for the control subjects was 40.6 years (SD = 12.2, median = 41.7).

For **Publications II** and **IV**, the control subject pool was increased by 30 to a total of 70 subjects. The additional subjects comprised previously imaged healthy volunteers from members of Tampere University Hospital staff. Of the 30 control subjects, 9 (30%) were men and 21 (70%) were women. The mean age for the control subjects was 37.8 years (SD = 11.2, median = 34.5). For the total 70 controls, the corresponding figures were: 29 (41%) men, 41 (59%) female, mean age 39.5 (SD = 11.8, median = 39). All the control subjects' head MRI's were interpreted as normal.

3.2 Human Brain Atlases

Human brain white matter atlases were used in **Publications II**, **III** and **IV**. The atlases were used to differentiate the brain regions with WM anomalies and in a complementary atlas-based analysis approach in **Publication II**. In **Publications III** and **IV**, the use of atlases in the analysis was the basis of our research, and therefore played an important role.

We used the following atlas image data in our research: the International Consortium for Brain Mapping (ICBM) DTI-81 WM labels atlas (Mori, Wakana, Nagae-Poetscher, & Van Zijl, 2005; Oishi et al., 2008), FA map of the Johns Hopkins University (JHU), Montreal Neurological Institute, Single Subject (MNI-SS) atlas (Oishi et al., 2009), JHU WM probabilistic tractography atlas (Hua et al., 2008) and the Illinois Institute of Technology (IIT) Human Brain atlas v. 4.1 with its probabilistic tractography maps (Zhang & Arfanakis, 2018). All the atlases used in our research have an isotropic voxel size of 1 mm^3. The atlas ROIs are listed in Table 2, and the atlases are visualised in Figure 10.

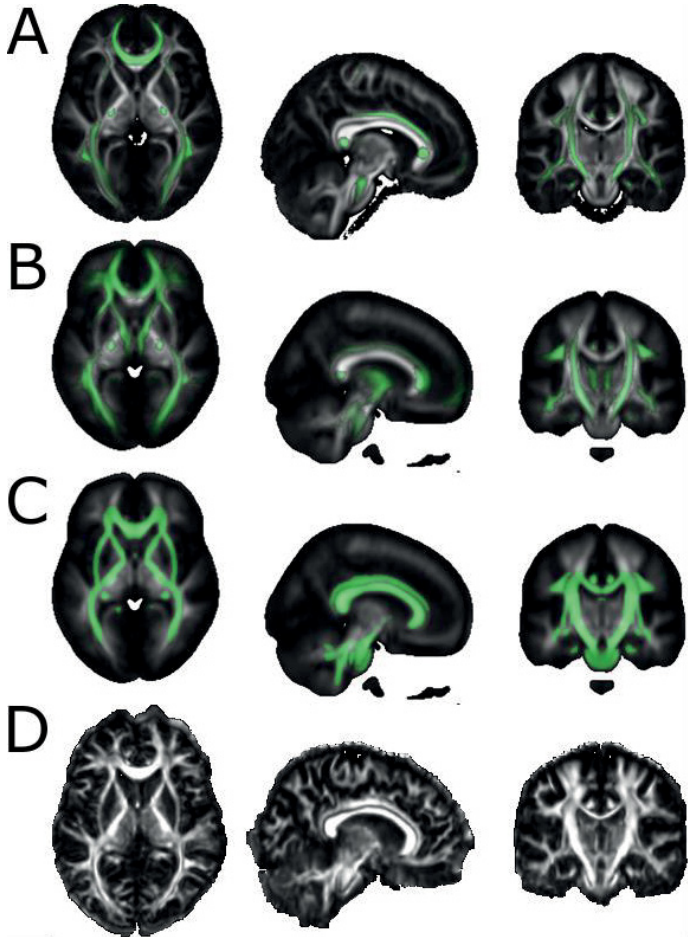

Figure 10. Different atlases used in the study. A) IIT Human Brain atlas with its major fibre bundles overlaid on top, B) ICBM DTI-81 mean FA map and the JHU WM probabilistic atlas, C) ICBM DTI-81 mean FA map and the ICBM DTI-81 WM labels atlas on top, D) JHU-MNI-SS FA map.

Table 2. Human brain white matter structures included in the applied standard brain atlases.

	ICBM DTI-81	JHU probabilistic	IIT Atlas
Anterior corona radiata	x		
Anterior thalamic radiation		X	
Anterior limb of internal capsule	x		
Body of corpus callosum	x		
Cerebral Peduncle	x		
Cingulum (cingulate gyrus)	x	X	x
Hippocampal Cingulum	x	X	x
Corticospinal tract (CST)	x	X	x
External capsule	x		
Forceps major (F major)		X	x
Forceps minor (F minor)		X	x
Fornix (column and body of fornix)	x		x
Fornix (cres) / Stria terminalis	x		
Genu of corpus callosum	x		
Inferior cerebellar peduncle	x		
inferior fronto-occipital fasciculus (IFOF)		X	x
inferior longitudinal fasciculus		X	x
Medial lemniscus	x		
Middle cerebellar peduncle	x		
Pontine crossing tract	x		
Posterior corona radiata	x		
Posterior limb of internal capsule	x		
Posterior thalamic radiation	x		
Retrolenticular part of internal capsule	x		
Sagittal stratum	x		
Splenium of corpus callosum	x		
Superior cerebellar peduncle	x		
Superior corona radiata	x		
Superior fronto−occipital fasciculus	x	X	
Superior longitudinal fasciculus	x	X	x
Tapetum	x		
Uncinate fasciculus (UF)	x	X	x

3.3 Application of Tract-Based Spatial Statistics

The application of TBSS was done in a standardised way in **Publications I and II**, using the steps recommended by the Oxford Analysis Group in the analysis. These steps include data pre-processing, preparing data for the analysis and linear and nonlinear registrations. After the registrations, the data are skeletonised and fed to the provided statistical program (randomise) for GLM modelling and significance testing. These results can be presented visually, and they can be further refined into quantitative measures. The p-value limit for statistical significance in the TBSS analyses was chosen at $p < 0.01$ due to multiple comparisons.

3.3.1 Normal Ageing

In addition to patient tests, we performed a secondary age effect analysis for the control group in **Publication I** for future purposes. We used TBSS to compare the three older age groups against the youngest age group. The age effect was determined by direct comparison of the age groups, with no confounding factors used as covariates. This was due to the age and gender stratification of the control group. The comparison for an age group pair was done by using two one-sided GLM tests with null hypothesis of no differences between the groups. The test was done twice in order to test the difference both ways, i.e., younger groups minus older, and vice versa.

3.3.2 Mild Traumatic Brain Injury

To test whether mTBI patients would have congruent WM structural properties in comparison with healthy subjects, several group comparisons between the mTBI patients and the healthy controls were performed in **Publication I**. First, the entire patient group (n = 75) was compared against the controls (n = 40), by controlling for age and gender effects. Then, the comparison was done by age- and gender matching the groups (n = 40). The patient group was also divided into subgroups with varying mTBI severity indexes, and the subgroups were compared against matched controls. The patients were divided into subgroups based on loss of consciousness (n = 7), post-traumatic amnesia (n = 25), conventional imaging findings (n = 15), Glasgow Coma Scale (GCS) (n = 6) and combinations of the previous criteria (n = 29, 20, 12). All the comparisons were done for FA, MD, RD

and AD diffusion measures, and by either age and gender matching or using age and gender as covariates. The one-sided GLM tests were repeated to test the differences both ways.

3.3.3 Traumatic Spinal Cord Injury

In **Publication II** we studied SCI and its collective effect on the brain by comparing the group of 32 SCI patients and a subgroup of ten patients with more severe SCI (American Spinal Injury Association Impairment Scale, grade A), against the control group of 70 healthy subjects. In addition, we performed partial regression analyses for several SCI related clinical variables. Partial correlation analyses were performed between DTI metrics and total motor score, upper and lower extremities motor score, total sensory score and time between injury and MRI. Each analysis was performed for FA, MD, RD and AD diffusion measures. Group comparisons were performed by two one-sided GLM tests, and correlation was assessed by testing linear regression both ways. All the analyses were done by controlling for age and gender effects in the GLM design.

3.4 Minimising Bias in Brain Analysis

To counter some sources of bias, the manipulation of the original subject image data was kept at a minimum for the created analysis pipeline in **Publications III and IV**. To achieve this, we did not use smoothing, resizing, registration or any other image manipulation methods on the subject DTI data. Instead, we operated on the template images and atlases. The subject data underwent pre-processing similar to the TBSS method; eddy current correction, head movement correction, brain masking and tensor fitting.

3.4.1 Atlases and Templates

We included a complimentary atlas-based analysis (ABA) in **Publication II** in addition to the TBSS analysis. In the ABA, the TBSS skeleton was divided into anatomical WM ROIs based on the ICBM DTI-81 WM labels atlas regions. The derived regions' DTI metrics were compared by analysis of covariance (ANCOVA), and the correlations were assessed by linear regression analysis with JASP (JASP

Team, 2016, version 0.8). This type of complementary analysis increased the overall sensitivity of the study. The atlas was also used to localise the findings. In **Publications III** and **IV,** the atlases were the core of the research, and the analyses were performed exclusively using the atlas-based approach. We did not use the atlases in a conventional way, i.e., register subject data to a standard template. Instead, we registered the atlases to each subject resulting in the WM atlas regions in the patients' standard space.

3.4.2 The Automated Analysis Process

All the registrations in the research were executed with the inherent tools of the FSL software package. In **Publications I and II**, the TBSS analysis used inbuilt sections which ran linear and nonlinear registration programs of the software package. For the automated ABA in **Publications III and IV**, we included the same linear and nonlinear registration subprograms that were used in the TBSS pipeline. The linear registration tool FLIRT (FMRIB's Linear Image Registration Tool) (M Jenkinson & Smith, 2001; Mark Jenkinson, Bannister, Brady, & Smith, 2002) was applied for affine registrations, and the nonlinear tool FNIRT (FMRIB's Linear Image Registration Tool) (Mark Jenkinson et al., 2012) for the warp field applications.

The process described in **Publication III** begins with an affine registration (12 degrees of freedom, trilinear interpolation and correlation-ratio-based cost function) of the high-resolution standard template to each of the subjects. The linear transformation matrices are saved in the process. Next, the linearly transformed template is nonlinearly (cubic b-spline, trilinear interpolation, 10 mm warp base resolution, 2 mm Gaussian smoothing) registered to the subject, and the warp field is saved. Then, the ROIs included in the template's atlas are transformed one by one to the subject's space by first applying the affine transformation to the ROI, and then applying the warp field to the linearly transformed ROI. Nearest neighbour interpolation is used to preserve the probabilistic nature of the ROI. After the registrations, the ROIs are in the native subject space, and are ready to be used in statistical analyses. The registration process is visualised as a flowchart in Figure 11. Automation of the whole analysis process is crucial for its usability and repeatability. Therefore, the registration phase is compiled in a way that requires no user input. Applying the pipeline to the same subject using the same atlas regions and the same DTI template in the registration will result in the exact same results each time. Registrations can be done by running a single pipeline which includes the pre-

processing and registrations of the ROIs. Currently, the choice of statistical analysis method and software is not fully integrated to the process, and the user may choose different statistical software.

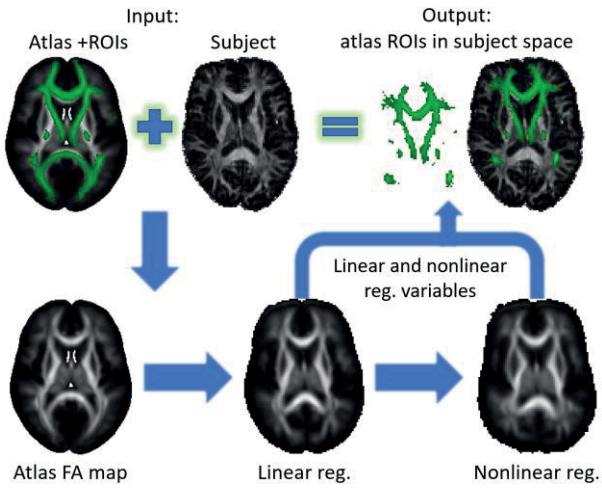

Figure 11. Flow chart of the registrations used in the automated pipeline.

In **Publication III,** we tested whether the registration method could be successfully and reliably applied to freehand ROIs, and whether the results would be directly comparable with previously executed freehand measurements. A set of nine freehand ROIs was drawn to the JHU-MNI-SS atlas in an exact manner as previous DTI freehand measurements made at Tampere University Hospital. Each of the ROIs lay only on a single slice, which can be seen in Figure 12. The binary ROIs were registered to the normal subjects linearly and nonlinearly, using linear interpolation, and the ROIs were transformed back to binary masks after the registrations by discarding voxels with values less than 0.15. Within subject ROIs, means were compared from manually drawn regions and the ROIs automatically registered to the subject.

In **Publication IV**, the use of freehand ROIs was discarded, and the focus was shifted mainly to anatomical brain atlases with probabilistic 3D ROIs: the JHU WM probabilistic atlas and the IIT Human Brain atlas. Probabilistic ROIs were chosen for the creation of a normal population model because they can be considered to be slightly more forgiving of the registration accuracy. Probabilistic ROIs give more weight to the voxels that are more likely to be inside a neural tract and less weight to voxels in the peripheral regions. This is a significant advantage of the probabilistic ROIs. The use of different interpolation methods based on the type of the input

ROIs would unnecessarily complicate the pipeline and lead to the use of nearest neighbour interpolation. Registering binary ROIs to lower resolution using the nearest neighbour interpolation instead of trilinear interpolation results in the possibility that a voxel outside the WM is included inside the ROI. However, the choice of utilising the nearest neighbour as the interpolation method allows for the use of both probabilistic and binary ROIs in the analysis without modifications to the pipeline.

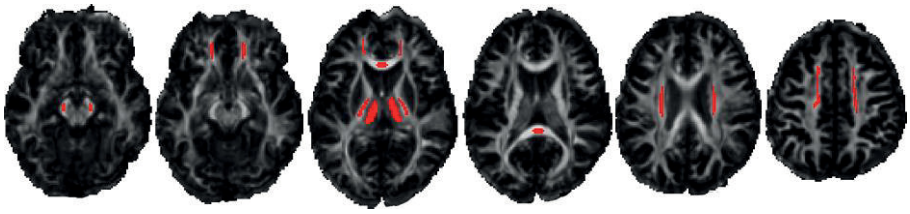

Figure 12. Manually drawn freehand ROIs used in **Publication III**. The ROIs are shown in red on top of the JHU-MNI-SS FA map.

3.4.3 DTI Reference Value Analysis

In order to obtain reference values using normal population modelling in **Publication IV**, the registrations were performed on the whole control subject pool (n = 70), and the mean values of the ROIs were stored in a spreadsheet. Using statistical software (JASP), the regions' association with age was examined, and simple linear regression functions (of the form $y = ax + b$) were formed for each region. For increased accuracy, multiple linear regression with additional covariates should be used with a larger subject pool. The model essentially predicts age-dependent mean DTI scalar values for each ROI, with a variability calculated as the root-mean-square error (RMSE). RMSE can be used to assess an individual subject's fit to the model by treating it as a Z-score:

$$Z_r = \frac{M_s - M_m}{RMSE_{ROI}}, \tag{10}$$

where Z_r is the RMSE associated standard score, M_s is the subject's ROI mean, M_m is the model's predicted ROI mean, adjusted for age, and $RMSE_{ROI}$ is the ROI dependent RMSE of the model. In addition, the statistical significance of the model is predicted as a p-value.

The normal model was tested for specificity by dividing the subject pool into a training set (n = 65) and a test set (n = 5). Only those ROIs with statistically significant linear regression functions were considered in the specificity test. The training set subjects' ROI means were compared with the values predicted by the model, and a limit of acceptance for the specificity analysis was chosen at $|Z_r| < 1.645$. For further validation of the normal model, we did a small-scale comparison with the results obtained by Cox et al. (2016).

The control population derived data were also used to analyse ten mTBI patients in **Publication IV**. This was done by comparing the mTBI patients' data against the normal population (n = 70) model's predicted ROI DTI values. The model predicted values were compared with the patient ROI means using a limit for pathologic finding of $|Z_r| \geq 2$. The analysis process is shown as a flowchart in Figure 13. To evaluate the sensitivity of the method to DTI metric changes induced by mTBI, we performed standard freehand ROI measurements for the same ten mTBI patients and compared the findings between the two methods. The freehand ROI analysis included 14 ROIs: the genu and splenium of the corpus callosum, thalamus, forceps minor, uncinate fasciculus, centrum semiovale, posterior corona radiata and posterior limb of the internal capsule. Left and right hemispheric regions were measured separately, except for the corpus callosum. The freehand ROI comparison was made against 40 control subjects instead of 70, due to limitations in the commercial software. Because the ROIs and the methodology differ slightly between the two methods, the comparison was not straightforward. However, the possible diffuse axonal injuries, if present, should be distinguishable with various types of ROIs. Comparing the number and extent of the findings should be enough to effectively compare the success rates of the current standard method of brain DTI analysis method and our automated analysis method.

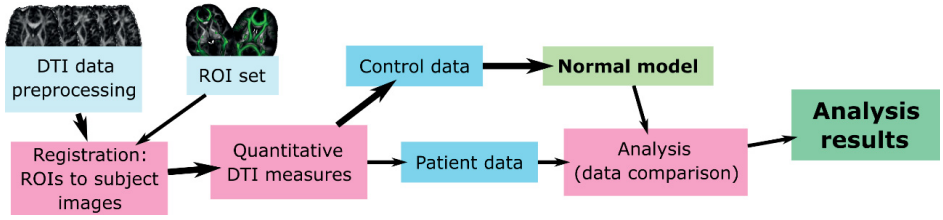

Figure 13. The quantitative brain analysis process as a flow chart. Following the bolded arrows, the statistical power and accuracy of the normal population model can be improved by adding control subjects. Blue rectangles present data, pink rectangles present work phases and green indicates results (adapted from **Publication IV**).

4 RESULTS

Microstructural changes in the brain were studied in patient groups with two fundamentally different central nervous system injuries, as well as in a normal aging population. Pathological changes were assessed at a group level to understand the possible common behaviour of the neuropathology, and by a single subject approach for a better clinical utilisation. Changes associated with normal aging were studied in a between-group design comparison and by continuous correlation analysis. The results of the group analyses are presented below. In addition, we present results from our automated single subject brain analysis application to mTBI subjects, including normal population model testing.

4.1 Tract-Based Spatial Statistics

In **Publication I**, our first application of TBSS was to test the effect of age on the normal human brain. The analysis was carried out with a between-group design in which the youngest age group (age 18–30) was used as a baseline for comparison against the older age groups (31–40, 41–50, 51–60). The comparisons against the age group 18–30 yielded statistically significant ($p < 0.01$) lower FA values in the age groups 41–50 and 51–60, higher MD values in the age group 51–60, and lower AD values and higher RD values in the age groups 41–50 and 51–60. The mean whole brain skeleton DTI metrics are plotted against subject age in Figure 14, which gives a good indication of how age affects the whole brain volume's DTI scalars in a healthy population. The effect can be considered linear throughout the age interval of our control population. The main objective in **Publication I** was, however, to study our mTBI patient pool with TBSS. In the study, we found no statistically significant ($p < 0.01$) differences between the control group and the mTBI patient group, independent of the age correction method (age matching or covariate control). In addition, none of the patient subgroup analyses reached statistical significance.

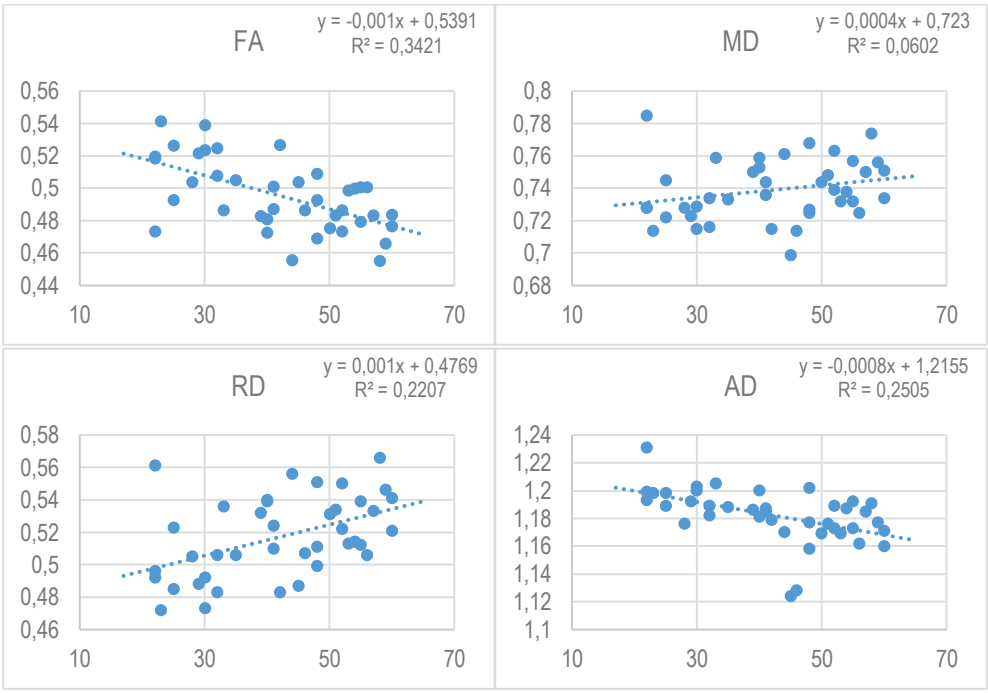

Figure 14. Whole brain DTI metric data of the 40 control subjects calculated from the skeleton mean. A linear fit is made to the graph points, and its equation and R-squared value is given in the upper right corner of each graph. The horizontal axis in the graphs represents age, while the vertical axis is dimensionless for FA and of units 10^{-3} mm^2/s for MD, RD and AD.

Performing TBSS analyses on SCI patients in **Publication II** resulted in a completely different outcome to what we saw with mTBI patients. Comparing the SCI patients (n = 32) against the controls (n = 70) resulted in vast areas with significant differences ($p < 0.01$) in FA, MD, RD and AD. FA was significantly lower and MD, RD and AD were higher in SCI patients compared with controls. For FA, MD and RD, one third of the examined volume was significantly different from the controls, whereas AD was increased in only 13% of the examined WM volume. The whole-brain skeleton means of the patients and controls are presented in Figure 15. Significant changes in the patient group with more severe SCI were also found in FA, MD and RD, though the results were spatially more restricted. The sensory and motor scores of the SCI patients did not correlate with DTI metrics in our study. However, time since injury had a statistically significant positive correlation with FA, and a negative correlation with MD, RD and AD measurable with TBSS.

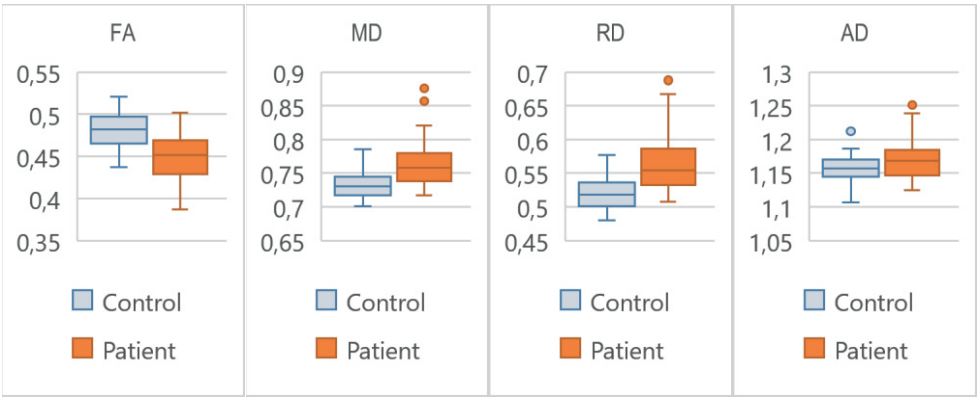

Figure 15. Whisker plots created from whole brain skeleton mean data for the 70 control subjects and 32 SCI patients. The vertical axis is dimensionless for FA and of units 10^{-3} mm^2/s for MD, RD and AD.

4.2 Atlas-Based Approach

4.2.1 Spinal Cord Injury Group Comparison

The use of atlases was integrated in the analysis for the first time in **Publication II**, where we complemented the TBSS analysis by using DTI metrics derived from atlas ROIs. The ABA applied to the SCI population was a group-wise comparison that used the TBSS's heavily modified skeleton data. In the complimentary ABA of the SCI patients, we found 36 atlas regions, from a total of 48, that had significant differences ($p < 0.01$) compared with normal subjects. The differences were analogous to the TBSS results in FA, MD and RD. However, both higher and lower AD values were found in the regions of the SCI patients. Also, similar to the TBSS correlation results, time since injury was associated with DTI metrics in several atlas regions, and FA showed positive correlation and MD, RD and AD negative correlation. In contrast to the TBSS results, the sensory and motor scores of the SCI patients correlated in a few regions in the ABA. Positive correlation was found between FA and upper extremities motor score, total motor score and total sensory score. Negative correlations were found between MD and upper extremities motor score and total sensory score, and between RD and upper extremities motor score.

4.2.2 Single Subject Application

Publication III was the first to concentrate on the single subject ABA, and mainly focused on describing the registration process. At the time of the third publication, trilinear interpolation was used in the registrations instead of the nearest neighbour interpolation used in **Publication IV**. However, the obtained results were considered acceptable at the time. To verify the success of the registration, we compared the scalar values inside the ROIs with each other. The registered freehand ROIs were mainly within 10% of the original drawn freehand ROIs, and only a few differed over 20%. While the approach resulted in fair quantitative results, the similarity of the ROIs should have been measured by their region overlap instead. The registrations were also executed on the ICBM WM labels atlas, which seemed to have an overall higher deviation in scalar values compared with the freehand ROIs.

In **Publication IV**, we concentrated primarily on the atlas regions. The registered anatomical ROIs were visually assessed by healthcare professionals, and their accuracy was deemed sufficient for the purpose. After setting up the registration process, we could feed the ROIs quantitative data to any statistical software for analysis.

4.3 Normal Population Modelling

In **Publication IV**, we created a normal population model using the pool of 70 control subjects with two different probabilistic atlases. Of the two atlases, the JHU atlas had better success with the linear regression. All the JHU atlas ROIs had statistically significant ($p < 0.05$) regression models for FA, and most of the ROIs had significant regression models for MD and RD. Only eight of the ROIs had significant regression functions for AD. While FA, MD and RD correlation were logical in the sense of degrading neural tracts with age, AD correlations were less coherent with positive and negative correlations. The IIT atlas had consistently fewer significant ROIs for each DTI metric, which was why we chose the JHU probabilistic WM atlas for further applications. Linear regression models of the forceps major and minor and the corticospinal tract for the DTI metrics are shown in Table 3, including p-values and the RMSE of the regression models. Additionally, some of the FA and MD regressions are visualised in Figure 16 for the JHU probabilistic atlas.

Our results from Publication IV were quite similar to those of Cox et al. The correlation directions were equal in both studies, although some differences arose in AD correlation. Furthermore, while we had both positive and negative correlations between age and AD in different ROIs, Cox et al. reported only a positive correlation. For the comparison, we combined our right and left hemispheric regions to achieve identical areas in both studies.

Table 3. Examples of the normal value model linear regression functions obtained for both JHU and IIT atlases. Statistical significance and root-mean-square error is also given in the table for the ROIs. The level of significance was $p < 0.05$.

	JHU probabilistic atlas				IIT Human Brain atlas			
	CST L	**CST R**	**F major**	**F minor**	**CST L**	**CST R**	**F major**	**F minor**
FA	0.56731 -0.00102 ×age	0.55445 -0.00098 ×age	0.52563 -0.00092 ×age	0.49042 -0.00138 ×age	0.63411 -0.00155 ×age	0.62543 -0.00143 ×age	0.72740 -0.00108 ×age	0.65173 -0.00193 ×age
P	<0.001	<0.001	0.001882	<0.001	<0.001	<0.001	<0.001	<0.001
E	0.02022	0.02050	0.02808	0.02265	0.02430	0.02518	0.02863	0.02848
MD	0.78061 +0.00013 ×age	0.77839 +0.00052 ×age	0.88413 +0.00028 ×age	0.76858 +0.00105 ×age	0.73175 +0.00015 ×age	0.73833 +0.00032 ×age	0.77335 +0.00082 ×age	0.73059 +0.00061 ×age
P	0.60033	0.05821	0.59285	<0.001	0.56722	0.26913	0.01888	0.01715
E	0.02449	0.02654	0.05074	0.02509	0.02523	0.02789	0.03352	0.02472
RD	0.50642 +0.00084 ×age	0.51172 +0.00109 ×age	0.60020 +0.00089 ×age	0.53344 +0.00177 ×age	0.41955 +0.00120 ×age	0.42984 +0.00122 ×age	0.36638 +0.00152 ×age	0.40233 +0.00171 ×age
P	0.00502	<0.001	0.09153	<0.001	<0.001	<0.001	<0.001	<0.001
E	0.02861	0.02955	0.05093	0.03069	0.02898	0.03171	0.0413	0.03095
AD	1.32901 -0.00130 ×age	1.31166 -0.00061 ×age	1.45201 -0.00094 ×age	1.23887 -0.00039 ×age	1.35616 -0.00195 ×age	1.35533 -0.00148 ×age	1.58729 -0.00057 ×age	1.38710 -0.00158 ×age
P	<0.001	0.049677	0.188967	0.178079	<0.001	<0.001	0.268619	<0.001
E	0.02846	0.03021	0.06977	0.02803	0.03795	0.03788	0.05014	0.04026

FA = fractional anisotropy (dimensionless), MD/RD/AD = mean/radial/axial diffusivity (10^{-3} mm^2/s), E = root-mean-square error, F major/minor = forceps major/minor, CST = corticospinal tract, L/R = left/right.

The specificity of our normal model was tested by creating a separate training set (n = 65) and a test set (n = 5). The linear regression functions were highly similar in the training set when compared with the functions obtained from the whole population (Table 3), and the deviation between the training set and the full (n = 70) model was

always less than 2%. Only ROIs with statistically significant ($p < 0.05$) training models were considered in the specificity testing. Factoring in all the significant ROIs from all the test set subjects, with the acceptance limit of $|Z_r| < 1.645$, the specificity of the DTI metrics for the JHU atlas regions were: FA 78.9%, MD 95%, RD 89.5% and AD 91.1%. For the IIT atlas, the corresponding figures were 78.3%, 90%, 83.3% and 100% for FA, MD, RD and AD, respectively. However, the number of ROIs with significant linear regression was considerably lower for the IIT atlas than for the JHU atlas.

Figure 16. JHU atlas regressions of the forceps major and minor for FA and MD. The model is plotted as a dashed line with ± 1.645 RMSE values as dotted lines. The horizontal axis represents age and the vertical axis is dimensionless for FA and of units 10^{-3} mm²/s for MD (adapted from **Publication IV**).

†) Not a statistically significant regression model.

4.3.1 Brain Injury Analysis Applying the Normal Model

For the mTBI analysis in **Publication IV**, only regions that had a statistically significant ($p < 0.05$) linear model were considered. The limit for abnormal findings

in the diffusion metrics was twice the model's RMSE of the region in question. The IIT atlas had considerably fewer ROIs with a statistically significant linear model and is disregarded here. Several JHU atlas areas had differences in more than one DTI metric in the same region. Results of both freehand and JHU normal model analysis are presented in Table 4 on a per-subject basis, while a more detailed, region-based review of the results can be seen in Table 5. Regions with abnormal findings for patients 4 and 5 are shown in Figure 17.

Table 4. Results from both freehand ROI and our automated normal model (JHU atlas) comparison analyses of the mTBI patients. X indicates abnormal DTI metric value ($|Z_r| > 2$ for automated analysis and $|Z| > 2$ for freehand ROI) in comparison with the normal population (automated analysis n = 70, freehand n = 40).

	Automated analysis				Freehand ROI			
	FA	**MD**	**RD**	**AD**	**FA**	**MD**	**RD**	**AD**
Patient 1				x				
Patient 2	X	X			x		x	x
Patient 3	X		X		x			x
Patient 4	X	X	X		x		x	
Patient 5	X	X	X			x		x
Patient 6		X	X	x		x		x
Patient 7	X	X	X					
Patient 8								
Patient 9								
Patient 10					x		x	x

FA = fractional anisotropy, MD/RD/AD = mean/radial/axial diffusivity.

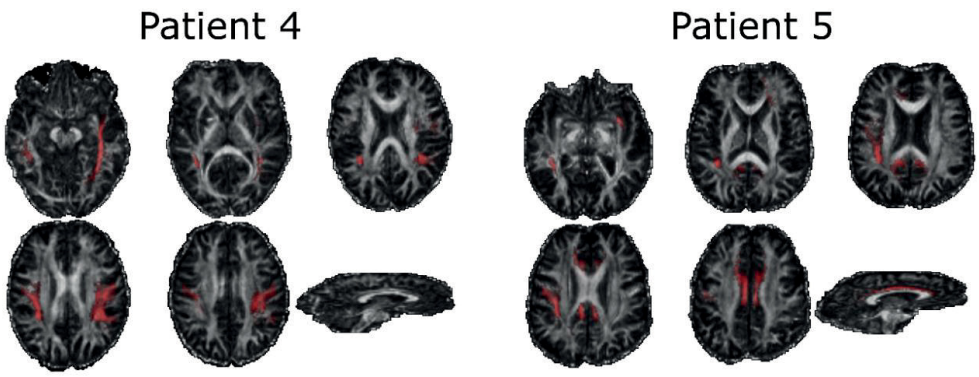

Figure 17. Regions with abnormal DTI metrics (± 2 RMSE) when compared with the normal model for patients 4 and 5. The regions are shown in red on top of the patients' FA maps. The analysis was done using the JHU atlas.

Table 5. Normal value model analysis (JHU atlas) results of the 10 mTBI patients. Table values are presented as Z_r, i.e., difference from the model predicted value as multiples of the model's root-mean-square error. The difference was considered significant if $|Z_r| > 2$.

Region	FA	MD	RD	AD
Cingulate gyrus L	Pat 5†: -2.175			
Cingulate gyrus R	Pat 5†: -2.416	Pat 5†: +2.623 Pat 6: -2.139	Pat 5†: +2.758	
Hippocampal portion of the cingulum R		Pat 2†: +2.031		
CST R	Pat 3†: +2.064		Pat 3†: -2.177 Pat 6: -3.178	Pat 6: -4.205
Forceps minor	Pat 2†: +2.198			
IFOF R		Pat 4†: +2.081		
Temporal part of the SLF L	Pat 4†: -2.086 Pat 5†: -2.353	Pat 5†: +2.099	Pat 5†: +2.306	
Temporal part of the SLF R		Pat 4†: +2.222	Pat 4†: +2.282	
SLF R		Pat 4†: +2.078	Pat 4†: +2.185	
UF L	Pat 7: -2.911	Pat 7: +3.074	Pat 7: +3.385	Pat 1†: +2.449
UF R	Pat 5†: -2.258			

FA = fractional anisotropy, MD/RD/AD = mean/radial/axial diffusivity, CST = corticospinal tract, IFOF = inferior fronto-occipital fasciculus, SLF = superior longitudinal fasciculus, UF = uncinate fasciculus, L = left, R = right.

†) Patients with complicated mild traumatic brain injury.

The freehand ROI measurements included in **Publication IV** also revealed regions with abnormal DTI metrics for most of the patients (see Table 4). The freehand method found abnormal FA values in four patients and the automated analysis in five patients. The number of abnormal ROIs for freehand and automated analysis for MD was two and five, for RD it was three and five and for AD it was five and two. Apart from AD, the automated analysis was able to identify a larger number of patients with abnormal DTI metrics. Patient 10 was an exception with abnormalities found in FA, RD and AD in the freehand measurement, but none in the automated analysis.

5 DISCUSSION

5.1 Tract-Based Spatial Statistics

We had objectives associated with TBSS that were addressed in **Publications I** and **II**. **Publication I** focused on revealing the effects of mTBI on the cerebral WM, while also validating the effects of ageing on the healthy human brain. Our group-wise TBSS analysis implied prominent DTI detectible ageing-related abnormalities in the human brain WM especially from age 40 onwards, which is in line with previous studies with similar objectives (Bennett, Madden, Vaidya, Howard, & Howard, 2009; Cox et al., 2016; Lebel & Beaulieu, 2011). Ageing generally contributes negatively to FA and AD and positively to MD and RD, an effect which was evident in our results. Due to the strong correlation between age and DTI metrics, it was crucial to mitigate the effect in our mTBI analysis to allow the study of the mTBI effect exclusively. The effects of ageing were considered by age-matching the patient and control groups or by including age as a covariate in the GLM.

We adopted a strict criterion of statistical significance in our first study ($p < 0.01$) to correct for multiple comparisons. Even with the strict methodological control and a highly homogeneous patient sample, we could not associate acute mTBI with collective microstructural changes in the brain WM by DTI. Perhaps partly due to the strict p-value, no abnormalities were found with TBSS. With a more liberal p-value ($p < 0.05$) some of the mTBI subgroup analyses would have indeed reached significance in a pattern similar to some previous studies (Hulkower et al., 2013; Wallace et al., 2018). As a conclusion of the results of **Publication I**, we inferred that even though the results were nearly significant, TBSS is not the preferred tool for mTBI analysis.

The heterogeneous study methodologies may be a significant explanatory variable for the highly variant results of previous mTBI studies. For the quantitative DTI study of mTBI, a different approach should be considered, and the focus should be on individual differences in brain WM caused by mTBI. Due to the variability in trauma mechanisms, the region and extent of the induced changes will differ considerably from patient to patient. Therefore, using group comparison may cause

these individual abnormalities to average out and cause the witnessed negative findings in brains that are evidently pathologic. Finally, age is a considerable confounding factor to be accounted for in DTI WM analyses.

In **publication II**, we continued to utilise TBSS, but instead of brain trauma we assessed traumatic spinal cord injuries. While previous publications had mainly concentrated on the motor and sensory pathways of the brain and the spinal cord itself, we wanted to focus on the whole volume of the brain to fully examine the extent of SCI induced WM abnormalities. In addition to the TBSS analysis, an ancillary ABA was included in the study to compliment the results and to increase sensitivity. The results were extensive and revealed WM changes commonly associated with neural tract degeneration (Guleria et al., 2008) in the majority of the brain. In addition to the degeneration related findings, increased AD was found in parts of the brain. This indicates a possible increase of neural connections, suggesting post SCI neuroplasticity (Keyvani & Schallert, 2002; Nudo et al., 2001; Schallert, Leasure, & Kolb, 2000). Furthermore, the regenerative changes were associated with time since injury, implying a possible continuous neuroplastic process. Hence, positive correlation with FA and negative with MD and RD may be a sign of axonal regeneration or synaptogenesis (Keller & Just, 2016; Sagi et al., 2012). These findings suggest that after the initial Wallerian type degeneration (Carlo Pierpaoli et al., 2001), cerebral neuroplastic changes may occur continuously even in the late chronic stages after SCI.

With the successful application of TBSS to SCI patients in **Publication II**, we concluded that methodologically TBSS was best used in pathologies that are not brain trauma related and have minimal inter-subject variability in the neuropathological process. In addition, TBSS cannot generally be considered as a viable option for clinical single subject analysis, and a different approach was needed.

5.2 Atlas-Based Analysis

Atlas regions were used in **Publication II** as a complimentary method for the TBSS analysis. The ABA findings mostly confirmed the TBSS results for FA, MD and RD, while AD results were unclear with regions of higher and of lower values compared with controls. This inconsistency may be attributed to possible regional differences in the post-SCI brain. Some regions exhibit low AD due to tract degeneration while some exhibit higher AD due to neuroplastic effects (Freund et al., 2012; Nudo et al., 2001). Further studies on the effects of SCI on the brain WM may reveal possible

biomarkers for patient outcome and can potentially aid in the decision of different rehabilitative measures. However, chronological studies would be required to increase the understanding of the possible ongoing degenerative and neuroplastic mechanisms in the post-SCI brain WM.

After the results from both of our initial publications, we came to a conclusion on the applicability of TBSS and similar group-wise analysis methods. In order to continue the study of mTBI, we needed to re-evaluate the fundamentals of the analysis method. After some consideration and a few trial and error iterations, we chose a ROI-based method as the basis for our automated DTI analysis. We tested different ways to use ROIs and tried to incorporate the skeletonisation from TBSS in the analysis. For increased accuracy and robustness, the analysis stages were minimised and TBSS was omitted from our method.

Subjects are often registered to a template in analysis pipelines, but we decided to register the template to subjects instead. Because registration of the subject image data distorts the image data and creates additional smoothing and further partial volume artefacts, we wanted to minimise the subject image data processing and work with the template and atlas ROIs instead. A similar approach has been successfully introduced by Radoeva et al. (2012). Registering the high-resolution standard FA templates to the subjects' lower resolution FA maps is a robust procedure that includes both linear and nonlinear registrations. Any type of ROI can be used in the registration process, as long as the underlying standard FA map is included.

Initially, in **Publication III**, we attempted to use freehand ROIs in the analysis pipeline in a manner that would allow direct comparison between previously conducted freehand ROI analyses and the automated analysis method results. While the quantitative DTI metric results seemed very promising, qualitatively the registration results would not be fully comparable to freehand ROIs. This is because freehand ROIs are drawn to a single image slice, whereas the registrations transform the ROIs into volumes that cross over several slices. Because of this difference, the freehand ROIs drawn by an operator and the freehand ROIs registered to a subject are not comparable.

For **Publication IV**, we discarded the possibility of using freehand ROIs in the analysis due to a lack of any additional benefits. Instead, we focused on existing well-known human brain atlases and their included anatomical ROIs. We used the created pipeline to analyse a selected group of ten mTBI patients and compared the results in a semi-quantitative way against results obtained from a freehand ROI comparison. Our analysis found more regions with abnormal DTI metrics, reflecting higher sensitivity compared with the freehand ROI measurement. Application of our

automated analysis to mTBI patients successfully identified regions with WM abnormalities, leading to a highly positive outlook for the method. The possibility to use different ROIs in the analysis makes the method versatile enough to be a prospective clinical tool in the near future. In conclusion, a versatile automated quantitative DTI brain analysis pipeline was created.

5.3 Normal Population Model

An intriguing aspect of our study was the creation of a normal population model in **Publication IV**. Accurate reference values for human brain DTI would allow direct evaluation of a subject's WM integrity, independent of the studied pathology. Normal values would be especially sought after in mTBI-related DTI assessment, due to the lack of distinct visual cues of brain WM trauma. In practice, none of the patients who have suffered mTBI have prior medical images to compare to, and having a quantitative reference database to compare the acquired DTI data would therefore significantly improve the accuracy of DTI assessment of mTBI.

Our normal population DTI model was highly successful for the JHU atlas, especially for the relevant FA model. Results for AD were mostly non-significant and heterogeneous in the JHU atlas. This finding is, however, in line with previous studies (Bennett et al., 2009; Burzynska et al., 2010). In contrast, almost half of the IIT atlas ROIs did not reach significance, which makes the IIT atlas unrecommendable to be used in the pipeline. The low success rate of the IIT atlas model may have been due to the smaller ROIs compared with the JHU atlas, or simply due to the difference in the anatomical locations of the ROIs. The smaller ROIs of the IIT atlas may render it more suitable for specific analyses, but its usefulness may be hindered by low statistical power due to the small control population. Based on our findings, we discarded the IIT atlas and concentrated on the use of the JHU atlas. We tested the specificity of our normal population-based method by creating separate training and test sets. The specificity of our method was sufficiently high for all DTI metrics in the JHU atlas, with false positive rates of 21%, 5%, 11% and 9% for FA, MD, RD and AD, respectively. Specificity should increase when applying a multiple regression model. Sensitivity would be more important for a supportive analysis method, which was the original agenda for our automated analysis. The sensitivity can be increased with relative ease by adding more control subjects to the normal population pool.

Cox et al. had notably larger subject material in their study from which they derived age association plots and age- and gender-based DTI models. With the larger pool of subjects, Cox et al. were able to use multiple regression in their models with increased statistical power. In addition, they used more novel neurite orientation dispersion and density imaging measures, including estimates of neurite density, extracellular water diffusion and tract complexity. We compared our results to Cox et al.'s where applicable.

Comparing our normal model with the results obtained by Cox et al. (2016) revealed identical results when accounting for the ROIs' direction of correlation with DTI metrics. Only AD differed from the trend. Our correlations were partly positive and partly negative, while Cox et al. observed only positive correlation between age and AD. This difference may be characterised by the differences in the control population age distributions and sample sizes or by the difference in the definition of statistical significance (Cox et al. used a limit of $p < 0.001$). While the comparison was not exhaustive, we concluded that the linear regression model was mostly equivalent to what was achieved by Cox et al.

5.4 Limitations

TBSS uses statistical methods to compare groups of subjects and can thus identify common features of WM microstructure inside a group of subjects. This is likely a confounding factor in the analysis of mTBI, where the patients have been subjects of different blunt head traumas. Generally, these head traumas are inherently varying (not controlled) in nature, and thus the variation in the trauma mechanics is a factor to be considered in patient grouping. Pooling together patients with different trauma mechanics may distort the results and even average out the findings in an inhomogeneous patient group (Kenzie et al., 2017). Because some WM regions, e.g., the corpus callosum (Aoki et al., 2012), are more prone to the effects of mTBI, it is possible TBSS can detect the abnormalities in these areas, but cannot distinguish individual differences dependent on trauma mechanisms and patient characteristics. Thus, analysing mTBI patients with TBSS may lead to a loss of sensitivity by averaging out possible focal abnormalities in different anatomical regions.

An important factor in the study of mTBI is the time of imaging, which can cause confusion and heterogeneity between mTBI study results. The heterogeneity in the reported mTBI study results can at least be partly explained by the variation in the time of imaging of the patients. The effect of mTBI on the WM is not linear through

time, and DTI metrics can fluctuate between high and low depending on the time since injury (Hasan et al., 2014; Lancaster et al., 2016). Our results are thus valid only for mTBI patients imaged in the acute stage.

Our subject data were limited in numbers, which creates limitations to the statistical power of the analyses and can directly impact the quality of inferences drawn from the results. While our patient pools are reasonably large, for more reliable results, the number of control subjects should be larger. In some cases, age- and gender matching can alleviate the deficiency, but overall the analyses would benefit from a larger control pool. In general, the same limitations apply to our SCI study as were noted for the mTBI TBSS study. In addition to these limitations, the possibility of a concomitant mTBI cannot be ruled out when dealing with traumatic spinal injuries (Wei et al., 2008). In defence of our study, the abnormal findings in the post-SCI brain WM were located in regions less frequently associated with TBIs (Hulkower et al., 2013). The time of imaging in our sample was not an optimal one, and for more clinically relevant results the imaging should be done in the acute phase of the injury.

The limited control subject data used to create our normal model led to a few prior conclusions concerning the modelling process. First, instead of more advanced nonlinear or piecewise regression models, we felt compelled to use linear regression in the age-dependency model, which, nevertheless, has been postulated to be a sufficient predictor of age-dependency (Kodiweera et al., 2016; Salat et al., 2005; Sullivan, Rohlfing, & Pfefferbaum, 2010). Second, the only demographical parameter taken into account in the model was age, while variables, such as gender and education, may have a significant effect on DTI metrics (Hsu et al., 2008; Kanaan et al., 2012; Noble, Korgaonkar, Grieve, & Brickman, 2013). A considerably larger control pool would be needed to create a prospective normal population model. In their study, Knofczynski and Mundfrom (2007) concluded that a minimum sample size of approximately 300 subjects is required for a good prediction level in multiple regression analysis. Collecting a control sample of this magnitude is, however, too expensive and time-consuming.

Additionally, there are multiple universal limitations in DTI that need to be taken into account when considering the results of any type of quantitative DTI analysis. The first and one of the most important restriction is the imaging process. While the acquisition of DTI data using EPI minimises motion artefacts, the collected data suffers from low spatial resolution and a medium to low signal-to-noise ratio due to current hardware limitations (Tournier, Mori, & Leemans, 2011). The use of low spatial resolution in an application where the objective is to examine microstructural

qualities is, in my opinion, a sort of paradox. The DWI EPI sequence is also highly susceptible to several imaging artefacts, such as magnetic field inhomogeneity induced geometric distortions, eddy current artefacts, chemical shift artefacts, T2 shine-through artefact and point spread function artefacts (Jones & Cercignani, 2010; Denis Le Bihan, Poupon, Amadon, & Lethimonnier, 2006; Soares, Marques, Alves, & Sousa, 2013; Tournier et al., 2011). If the image artefacts cannot be avoided, or if dealing with retrospective data, a possible solution is to exclude the affected volume from the analysis (Soares et al., 2013). The applied imaging parameters will affect the accuracy and quality of the collected diffusion data, some of the most important of which are the number of diffusion gradient directions, applied diffusion weighting (b-value), physical size of the imaging matrix (field of view, acquisition matrix) and the used TE and TR (Soares et al., 2013). In addition, the acquisition parameters need to be identical for the images to be comparable, for a slight change in any of the parameters will cause a deviation in the quantitative DTI scalars. Diffusion data obtained with identical parameters from different scanners are also not comparable.

In addition to the standard image quality control steps, there is also a number of things to account for in the DTI image processing stage. The first real issue with the image processing is that no consensus has yet been reached for a standardized DTI processing pipeline. This is an issue similar to the variation in imaging parameters, and in practice leads to the fact that most current studies are not directly comparable with each other. Possible sources of bias in the results include different diffusion tensor estimation algorithms, varying pre-processing methods, various registration-based differences and distortions, and the possible spatial and quantitative distortion caused by lesions (Jones & Cercignani, 2010). A significant source of bias specific to DTI are crossing fibres, which are partly countered by acquiring diffusion data with a high diffusion gradient direction count (HARDI, high angular resolution diffusion imaging), and by using an appropriate q-ball imaging reconstruction (Tuch, 2004). Crossing fibres are neural pathways that cross inside an image voxel, causing the diffusion to seem isotropic inside the voxel. Crossing fibres are a notable source of error, especially in tractography where they can potentially cause disconnections in the visualised tracts (Denis Le Bihan et al., 2006; Soares et al., 2013).

While TBSS claims to solve some of the registration-based issues in DTI analysis, it also adds some specific issues to the analysis process. One of the issues with TBSS is that it includes a vast number of image processing and mathematical calculation steps, which should be understood before interpreting the results. While the skeletonisation step reduces registration bias, it is only a coarse simplification of the

fibre bundle it represents and, due to its wireframe model property, the majority of diffusion information in thick fibre bundles is ignored by the analysis (Bach et al., 2014). Brain lesions may produce invalid FA skeleton geometry or give rise to false low FA values in the skeleton (Jones & Cercignani, 2010). For more detailed information on possible diffusion MRI analysis pitfalls, I suggest the reader takes a look at the publications by Jones and Cercigani (2010), Le Bihan et al. (2006), Soares et al. (2013), and Bach et al. (2014).

The diffusion data used in this thesis may be considered dated. For example, the spatial resolution and the number of diffusion-encoding gradient directions are lower than in current state-of-the-art studies. The slice thickness of 3 mm can be considered to be one of the main issues with the data. The slice thickness also means that the voxels are non-isotropic. In addition, the slices include a small 0.9 mm gap, which would cause possible issues with tractography (Soares et al., 2013). The use of non-isotropic voxels has benefits in terms of higher SNR and lower imaging time, but can also lead to issues with partial volume averaging and the possible orientation dependence of FA values (Jones, Knösche, & Turner, 2013; Oouchi et al., 2007). The quality of the diffusion data is a potential limitation and a possible source of error that likely resulted in a loss of sensitivity in the analyses.

5.5 Further Aspects

Additional research on both mTBI and SCI would be warranted, and the single most important aspect to consider is chronologicity, i.e., changes in DTI metrics with regards to the time between injury and imaging. While the DTI observable changes in brain WM induced by mTBI have a complex pattern of alteration dependent on the time of imaging, SCI is likely to have a more straightforward pattern. In both cases, it would be important to examine the chronological post-injury brain WM alteration patterns to be able to understand the microstructural pathologic process and to associate changes possibly linked to clinical recovery. Additionally, the whole brain should be targeted in SCI DTI studies instead of concentrating only on the somatosensory tracts.

In its current state, the analysis pipeline is missing a reliable, clinical-grade reference value model. Also, if young subjects are to be analysed with the pipeline, a piecewise linear or a parabolic model should be applied. This is because the young brain is still developing into early adulthood, and an appropriate break point for a

piecewise solution would be at the age of about 25 (Lebel & Beaulieu, 2011; Westlye et al., 2010). Because the normal population model presented in our study was a preliminary one, an important future research prospect is to complete the control subject pool by adding to the number of control subjects. With a larger control subject pool, a more advanced regression model can also be applied. However, due to high costs of recruiting a massive volunteer control pool, an inexpensive and conveniently executable alternative for the control population gathering must be presented. A possible alternative could be the use of any clinical subjects whose brain MRI are interpreted as normal, and who have not suffered previous brain trauma nor have neurodegenerative disease. The collection method should seamlessly fit the standard clinical MRI procedure in the current golden age of biobanks. However, the applicability of clinical subjects as a control sample is highly questionable, and the mandatory exclusion criteria may render the method unusable.

A highly intriguing aspect would be to include artificial intelligence (AI) in the pipeline. Possible areas where machine learning could be utilised are the registration step and regression analysis. AI could be used to increase the registration accuracy by teaching a deformable image registration framework based on deep learning algorithms (Wang, Kim, Wu, & Shen, 2017). This type of approach has the potential to continuously increase the registration accuracy with practically minimal human interaction required. The second use for AI is in the core of our analysis. Accurate correlations between subject demographics and DTI metrics could be effortlessly and more accurately determined with deep learning algorithms. Even the whole foundation of the analysis could be based on AI (Vieira, Pinaya, & Mechelli, 2017), but that is far beyond the scope of our current research. However, the addition of AI aspects to parts of the pipeline is something that should be considered in the near future.

An important clinical aspect that should also be dealt with in the future is mTBI litigation and the use of DTI-based evidence in jurisprudence. In the few past years in Finland, there has been an increasing interest in the use of DTI as a method for differentiating brain injury from the healthy brain. Quantitative DTI values have been utilised to some extent in the discrimination of possible brain injury in brain trauma cases. This type of approach may sometimes be used by insurance companies to determine the possibility of a trauma induced brain injury. Due to this, medical experts are being asked for reports based on DTI imaging for evidence in mTBI litigation. The use of quantitative DTI values as evidence of mTBI causes a problem due to the various pitfalls of diffusion imaging that were explained in the previous chapter. In addition to the issues concerning the DTI data in general, a common

misinterpretation of previous mTBI studies is that the group-wise analysis results could be applied directly to individual level diagnostics. According to Wortzel et al. (2011), objective DTI based evidence of mTBI in the past literature is mainly achieved in cases where other types of evidence of mTBI are already present and observable. Additionally, they advise against using DTI as evidence of mTBI until the acquisition and analysis processes are standardised. Another study on the subject by Shenton et al. (2018) concluded with similar views concerning the use of DTI in the courtroom. While DTI seems promising in the detection of mTBIs, the methodology is not yet standardised or even matured to the point where the obtained quantitative data could be unambiguously interpreted.

Due to the findings of the aforementioned studies and based on the experience obtained in the course of this thesis, I would conclude that the use of an objective means of assessing brain injuries is more than advisable. However, DTI analysis as an instrument for individual level mTBI assessment requires further research and standardisation to reach a level of unambiguousness suitable for mTBI litigation. It is plausible that diffusion imaging will continue to bring forth an increasing amount of important quantitative information on mTBI, and further enhance the objectivity and robustness of clinical mTBI assessment. In order for the method to become a universally accepted diagnostic tool, however, advances in the imaging techniques and analyses are required. The reliability of DTI or even HARDI is currently not quite at the level it should be, but the future does seem promising for quantitative diffusion imaging as an assessment tool for central nervous system integrity.

6 CONCLUSIONS

We evaluated the applicability of existing DTI analysis methods through different stages of the thesis and achieved important results and inferences in the process. We obtained intriguing new information on the microstructural effects of mTBI and SCI on the human brain and created a potentially clinically relevant automated quantitative DTI analysis method. The main outcomes of the thesis can be summarised as follows:

1. The effects of mTBI on the human brain WM cannot be reliably assessed by TBSS even in a strictly controlled dataset. However, with a methodological consensus and further research, the utilisation of DTI in clinical mTBI assessment is plausible in the near future.

2. Traumatic SCIs cause extensive changes in the cerebral WM detectable by DTI. The observed changes suggest wider degenerative and neuroplastic changes in the post-SCI brain than previously reported.

3. An automated quantitative DTI analysis pipeline was created with clinical versatility via the possibility of arbitrary choice of ROIs. The analysis uses reference values derived from a normal population DTI metric model for delineation of pathologies.

REFERENCES

Alexander, A. L., Lee, J. E., Lazar, M., & Field, A. S. (2007). Diffusion tensor imaging of the brain. *Neurotherapeutics*, *4*(3), 316–329. https://doi.org/10.1016/j.nurt.2007.05.011

Aoki, Y., Inokuchi, R., Gunshin, M., Yahagi, N., & Suwa, H. (2012). Diffusion tensor imaging studies of mild traumatic brain injury: a meta-analysis. *Journal of Neurology, Neurosurgery & Psychiatry*, *83*(9), 870–876. https://doi.org/10.1136/jnnp-2012-302742

Bach, M., Laun, F. B., Leemans, A., Tax, C. M. W., Biessels, G. J., Stieltjes, B., & Maier-Hein, K. H. (2014). Methodological considerations on tract-based spatial statistics (TBSS). *NeuroImage*, *100*, 358–369. https://doi.org/10.1016/j.neuroimage.2014.06.021

Basser, P. J., Mattiello, J., & LeBihan, D. (1994). MR diffusion tensor spectroscopy and imaging. *Biophysical Journal*, *66*(1), 259–267. https://doi.org/10.1016/S0006-3495(94)80775-1

Basser, P. J., & Pierpaoli, C. (1996). Microstructural and Physiological Features of Tissues Elucidated by Quantitative-Diffusion-Tensor MRI. *Journal of Magnetic Resonance, Series B*, *111*(3), 209–219. https://doi.org/10.1006/jmrb.1996.0086

Beaulieu, C. (2002). The basis of anisotropic water diffusion in the nervous system - a technical review. *NMR in Biomedicine*, *15*(7–8), 435–455. https://doi.org/10.1002/nbm.782

Beirowski, B., Adalbert, R., Wagner, D., Grumme, D. S., Addicks, K., Ribchester, R. R., & Coleman, M. P. (2005). The progressive nature of Wallerian degeneration in wild-type and slow Wallerian degeneration (WldS) nerves. *BMC Neuroscience*, *6*, 6. https://doi.org/10.1186/1471-2202-6-6

Benes, F. M. (1994). Myelination of a Key Relay Zone in the Hippocampal Formation Occurs in the Human Brain During Childhood, Adolescence, and Adulthood. *Archives of General Psychiatry*, *51*(6), 477–484. https://doi.org/10.1001/archpsyc.1994.03950060041004

Bennett, I. J., Madden, D. J., Vaidya, C. J., Howard, D. V., & Howard, J. H. (2009). Age-related differences in multiple measures of white matter integrity: A diffusion tensor imaging study of healthy aging. *Human Brain Mapping*, *31*(3), 378–390. https://doi.org/10.1002/hbm.20872

Benson, R. R., Meda, S. A., Vasudevan, S., Kou, Z., Govindarajan, K. A., Hanks, R. A., … Haacke, E. M. (2007). Global White Matter Analysis of Diffusion Tensor Images Is Predictive of Injury Severity in Traumatic Brain Injury. *Journal of Neurotrauma*, *24*(3), 446–459. https://doi.org/10.1089/neu.2006.0153

Bloch, F. (1946). Nuclear Induction. *Physical Review*, *70*(7–8), 460–474. https://doi.org/10.1103/PhysRev.70.460

Bloch, F., Hansen, W. W., & Packard, M. (1946). The Nuclear Induction Experiment. *Physical Review*, *70*(7–8), 474–485. https://doi.org/10.1103/PhysRev.70.474

Boltzmann, L. (1877). Über die Beziehung zwischen dem zweiten Hauptsatze des mechanischen Wärmetheorie und der Wahrscheinlichkeitsrechnung, respective den Sätzen über das Wärmegleichgewicht. *Wiener Berichte*, *76*(2), 373–435.

Bora, E., Yücel, M., Fornito, A., Pantelis, C., Harrison, B. J., Cocchi, L., … Lubman, D. I. (2012). White matter microstructure in opiate addiction. *Addiction Biology*, *17*(1), 141–148. https://doi.org/10.1111/j.1369-1600.2010.00266.x

Brazinova, A., Rehorcikova, V., Taylor, M. S., Buckova, V., Majdan, M., Psota, M., … Synnot, A. (2016). Epidemiology of Traumatic Brain Injury in Europe: A Living Systematic Review. *Journal of Neurotrauma*, *30*, neu.2015.4126. https://doi.org/10.1089/neu.2015.4126

Burzynska, A. Z., Preuschhof, C., Bäckman, L., Nyberg, L., Li, S.-C., Lindenberger, U., & Heekeren, H. R. (2010). Age-related differences in white matter microstructure: Region-specific patterns of diffusivity. *NeuroImage*, *49*(3), 2104–2112. https://doi.org/10.1016/j.neuroimage.2009.09.041

Buss, A. (2004). Gradual loss of myelin and formation of an astrocytic scar during Wallerian degeneration in the human spinal cord. *Brain*, *127*(1), 34–44. https://doi.org/10.1093/brain/awh001

Chang, Y., Jung, T.-D., Yoo, D. S., & Hyun, J. K. (2010). Diffusion Tensor Imaging and Fiber Tractography of Patients with Cervical Spinal Cord Injury. *Journal of Neurotrauma*, *27*(11), 2033–2040. https://doi.org/10.1089/neu.2009.1265

Chou, K.-H., Cheng, Y., Chen, I.-Y., Lin, C.-P., & Chu, W.-C. (2011). Sex-linked white matter microstructure of the social and analytic brain. *NeuroImage*, *54*(1), 725–733. https://doi.org/10.1016/j.neuroimage.2010.07.010

Cox, S. R., Ritchie, S. J., Tucker-Drob, E. M., Liewald, D. C., Hagenaars, S. P., Davies, G., … Deary, I. J. (2016). Ageing and brain white matter structure in 3,513 UK Biobank participants. *Nature Communications*, *7*, 13629. https://doi.org/10.1038/ncomms13629

Damadian, R. (1971). Tumor detection by nuclear magnetic resonance. *Science (New York, N.Y.)*, *171*(3976), 1151–1153. https://doi.org/10.1126/science.171.3976.1151

de Diego-Adeliño, J., Pires, P., Gómez-Ansón, B., Serra-Blasco, M., Vives-Gilabert, Y., Puigdemont, D., … Portella, M. J. (2014). Microstructural white-matter abnormalities associated with treatment resistance, severity and duration of illness in major depression. *Psychological Medicine*, *44*(06), 1171–1182. https://doi.org/10.1017/S003329171300158X

Dietrich, O., Biffar, A., Baur-Melnyk, A., & Reiser, M. F. (2010). Technical aspects of MR diffusion imaging of the body. *European Journal of Radiology*, *76*(3), 314–322. https://doi.org/10.1016/j.ejrad.2010.02.018

Einstein, A. (1905). Über die von der molekularkinetischen Theorie der Wärme geforderte Bewegung von in ruhenden Flüssigkeiten suspendierten Teilchen. *Annalen Der Physik*, *322*(8), 549–560. https://doi.org/10.1002/andp.19053220806

Farquharson, S., Tournier, J.-D., Calamante, F., Fabinyi, G., Schneider-Kolsky, M., Jackson, G. D., & Connelly, A. (2013). White matter fiber tractography: why we need to move beyond DTI. *Journal of Neurosurgery*, *118*(6), 1367–1377. https://doi.org/10.3171/2013.2.JNS121294

Filler, A. G., Kliot, M., Winn, H. R., Tsuruda, J. S., Hayes, C. E., Howe, F. A., … Filler, A. G. (1993). Magnetic resonance neurography. *The Lancet*, *341*(8846), 659–661. https://doi.org/10.1016/0140-6736(93)90422-D

Finger, S. (2001). *Origins of Neuroscience: A History of Explorations Into Brain Function*. Oxford University Press. Retrieved from https://books.google.fi/books?id=_GMeW9E1IB4C

Freund, P., Weiskopf, N., Ward, N. S., Hutton, C., Gall, A., Ciccarelli, O., … Thompson, A. J. (2011). Disability, atrophy and cortical reorganization following spinal cord injury. *Brain*, *134*(6), 1610–1622. https://doi.org/10.1093/brain/awr093

Freund, P., Wheeler-Kingshott, C. A., Nagy, Z., Gorgoraptis, N., Weiskopf, N., Friston, K., … Hutton, C. (2012). Axonal integrity predicts cortical reorganisation following cervical injury. *Journal of Neurology, Neurosurgery & Psychiatry*, *83*(6), 629–637. https://doi.org/10.1136/jnnp-2011-301875

Froeling, M., Pullens, P., & Leemans, A. (2016). DTI Analysis Methods: Region of Interest Analysis. In W. Van Hecke, L. Emsell, & S. Sunaert (Eds.), *Diffusion Tensor Imaging* (pp. 175–182). New York, NY: Springer New York. https://doi.org/10.1007/978-1-4939-3118-7_9

Gross, C. G. (1987). Early History of Neuroscience. In *Encyclopedia of Neuroscience* (pp. 843–847). Boston : Birkhäuser.

Guleria, S., Gupta, R. K., Saksena, S., Chandra, A., Srivastava, R. N., Husain, M., … Narayana, P. A. (2008). Retrograde Wallerian degeneration of cranial corticospinal tracts in cervical spinal cord injury patients using diffusion tensor imaging. *Journal of Neuroscience Research*, *86*(10), 2271–2280. https://doi.org/10.1002/jnr.21664

Gustin, S. M., Wrigley, P. J., Siddall, P. J., & Henderson, L. A. (2010). Brain Anatomy Changes Associated with Persistent Neuropathic Pain Following Spinal Cord Injury. *Cerebral Cortex*, *20*(6), 1409–1419. https://doi.org/10.1093/cercor/bhp205

Hagmann, P., Jonasson, L., Maeder, P., Thiran, J.-P., Wedeen, V. J., & Meuli, R. (2006). Understanding Diffusion MR Imaging Techniques: From Scalar Diffusion-weighted Imaging to Diffusion Tensor Imaging and Beyond. *RadioGraphics*, *26*(suppl_1), S205–S223. https://doi.org/10.1148/rg.26si065510

Hakulinen, U., Brander, A., Ryymin, P., Öhman, J., Soimakallio, S., Helminen, M., … Eskola, H. (2012). Repeatability and variation of region-of-interest methods using quantitative diffusion tensor MR imaging of the brain. *BMC Medical Imaging*, *12*(1), 30. https://doi.org/10.1186/1471-2342-12-30

Hanson, L. G. (2008). Is quantum mechanics necessary for understanding magnetic resonance? *Concepts in Magnetic Resonance Part A*, *32A*(5), 329–340. https://doi.org/10.1002/cmr.a.20123

Hasan, K. M., Wilde, E. a, Miller, E. R., Kumar Patel, V., Staewen, T. D., Frisby, M. L., … Narayana, P. a. (2014). Serial Atlas-Based Diffusion Tensor Imaging Study of Uncomplicated Mild Traumatic Brain Injury in Adults. *Journal of Neurotrauma*, *31*(5), 466–475. https://doi.org/10.1089/neu.2013.3085

Hendee, W. R., & Ritenour, E. R. (2003). *Medical Imaging Physics* (4th ed.). Wiley. Retrieved from https://books.google.fi/books?id=55lh1B82SLsC

Henderson, L. A., Gustin, S. M., Macey, P. M., Wrigley, P. J., & Siddall, P. J. (2011). Functional Reorganization of the Brain in Humans Following Spinal Cord Injury: Evidence for Underlying Changes in Cortical Anatomy. *Journal of Neuroscience*, *31*(7), 2630–2637. https://doi.org/10.1523/JNEUROSCI.2717-10.2011

Howe, F. A., Filler, A. G., Bell, B. A., & Griffiths, J. R. (1992). Magnetic Resonance Neurography. *Magnetic Resonance in Medicine*, *28*(2), 328–338. https://doi.org/10.1002/mrm.1910280215

Hsu, J.-L., Leemans, A., Bai, C.-H., Lee, C.-H., Tsai, Y.-F., Chiu, H.-C., & Chen, W.-H. (2008). Gender differences and age-related white matter changes of the human brain:

A diffusion tensor imaging study. *NeuroImage*, *39*(2), 566–577. https://doi.org/10.1016/j.neuroimage.2007.09.017

Hua, K., Zhang, J., Wakana, S., Jiang, H., Li, X., Reich, D. S., … Mori, S. (2008). Tract probability maps in stereotaxic spaces: Analyses of white matter anatomy and tract-specific quantification. *NeuroImage*, *39*(1), 336–347. https://doi.org/10.1016/j.neuroimage.2007.07.053

Hulkower, M. B., Poliak, D. B., Rosenbaum, S. B., Zimmerman, M. E., & Lipton, M. L. (2013). A Decade of DTI in Traumatic Brain Injury: 10 Years and 100 Articles Later. *American Journal of Neuroradiology*, *34*(11), 2064–2074. https://doi.org/10.3174/ajnr.A3395

Humphreys, I., Wood, Phillips, C., & Macey. (2013). The costs of traumatic brain injury: a literature review. *ClinicoEconomics and Outcomes Research*, *5*, 281. https://doi.org/10.2147/CEOR.S44625

Isokuortti, H., Iverson, G. L., Kataja, A., Brander, A., Öhman, J., & Luoto, T. M. (2016). Who Gets Head Trauma or Recruited in Mild Traumatic Brain Injury Research? *Journal of Neurotrauma*, *33*(2), 232–241. https://doi.org/10.1089/neu.2015.3888

Jenkinson, M., Bannister, P., Brady, M., & Smith, S. (2002). Improved optimization for the robust and accurate linear registration and motion correction of brain images. *NeuroImage*, *17*(2), 825–841. Retrieved from http://www.ncbi.nlm.nih.gov/pubmed/12377157

Jenkinson, M., Beckmann, C. F., Behrens, T. E. J., Woolrich, M. W., & Smith, S. M. (2012). FSL. *NeuroImage*, *62*(2), 782–790. https://doi.org/10.1016/j.neuroimage.2011.09.015

Jenkinson, M., & Smith, S. (2001). A global optimisation method for robust affine registration of brain images. *Medical Image Analysis*, *5*(2), 143–156. Retrieved from http://www.ncbi.nlm.nih.gov/pubmed/11516708

Jones, D. K. (2010). Challenges and limitations of quantifying brain connectivity in vivo with diffusion MRI. *Imaging in Medicine*, *2*(3), 341–355. https://doi.org/10.2217/iim.10.21

Jones, D. K., & Cercignani, M. (2010). Twenty-five pitfalls in the analysis of diffusion MRI data. *NMR in Biomedicine*, *23*(7), 803–820. https://doi.org/10.1002/nbm.1543

Jones, D. K., Knösche, T. R., & Turner, R. (2013). White matter integrity, fiber count, and other fallacies: The do's and don'ts of diffusion MRI. *NeuroImage*, *73*, 239–254. https://doi.org/10.1016/j.neuroimage.2012.06.081

Jorge, R. E., Acion, L., White, T., Tordesillas-Gutierrez, D., Pierson, R., Crespo-Facorro, B., & Magnotta, V. A. (2012). White Matter Abnormalities in Veterans With Mild Traumatic Brain Injury. *American Journal of Psychiatry*, *169*(12), 1284–1291. https://doi.org/10.1176/appi.ajp.2012.12050600

Kakulas, B. A. (1987). The clinical neuropathology of spinal cord injury a guide to the future. *Spinal Cord*, *25*(3), 212–216. https://doi.org/10.1038/sc.1987.37

Kanaan, R. A., Allin, M., Picchioni, M., Barker, G. J., Daly, E., Shergill, S. S., … McGuire, P. K. (2012). Gender Differences in White Matter Microstructure. *PLoS ONE*, *7*(6), e38272. https://doi.org/10.1371/journal.pone.0038272

Keller, T. A., & Just, M. A. (2016). Structural and functional neuroplasticity in human learning of spatial routes. *NeuroImage*, *125*, 256–266. https://doi.org/10.1016/j.neuroimage.2015.10.015

Kenzie, E. S., Parks, E. L., Bigler, E. D., Lim, M. M., Chesnutt, J. C., & Wakeland, W. (2017). Concussion As a Multi-Scale Complex System: An Interdisciplinary Synthesis of Current Knowledge. *Frontiers in Neurology*, *8*, 513. https://doi.org/10.3389/fneur.2017.00513

Keyvani, K., & Schallert, T. (2002). Plasticity-associated molecular and structural events in the injured brain. *Journal of Neuropathology and Experimental Neurology*, *61*(10), 831–840. Retrieved from http://www.ncbi.nlm.nih.gov/pubmed/12387449

Knofczynski, G. T., & Mundfrom, D. (2008). Sample Sizes When Using Multiple Linear Regression for Prediction. *Educational and Psychological Measurement*, *68*(3), 431–442. https://doi.org/10.1177/0013164407310131

Kodiweera, C., Alexander, A. L., Harezlak, J., McAllister, T. W., & Wu, Y.-C. (2016). Age effects and sex differences in human brain white matter of young to middle-aged adults: A DTI, NODDI, and q-space study. *NeuroImage*, *128*, 180–192. https://doi.org/10.1016/j.neuroimage.2015.12.033

Koskinen, E. A., Hakulinen, U., Brander, A. E., Luoto, T. M., Ylinen, A., & Öhman, J. E. (2014). Clinical correlates of cerebral diffusion tensor imaging findings in chronic traumatic spinal cord injury. *Spinal Cord*, *52*(3), 202–208. https://doi.org/10.1038/sc.2013.163

Koskinen, E., Brander, A., Hakulinen, U., Luoto, T., Helminen, M., Ylinen, A., & Öhman, J. (2013). Assessing the State of Chronic Spinal Cord Injury Using Diffusion Tensor Imaging. *Journal of Neurotrauma*, *30*(18), 1587–1595. https://doi.org/10.1089/neu.2013.2943

Koskinen, S., & Alaranta, H. (2008). Traumatic brain injury in Finland 1991–2005: A nationwide register study of hospitalized and fatal TBI. *Brain Injury*, *22*(3), 205–214. https://doi.org/10.1080/02699050801938975

Lancaster, M. A., Olson, D. V, McCrea, M. A., Nelson, L. D., LaRoche, A. A., & Muftuler, L. T. (2016). Acute white matter changes following sport-related concussion: A serial diffusion tensor and diffusion kurtosis tensor imaging study. *Human Brain Mapping*, *37*(11), 3821–3834. https://doi.org/10.1002/hbm.23278

Lange, R. T., Iverson, G. L., Brubacher, J. R., Mädler, B., & Heran, M. K. (2012). Diffusion Tensor Imaging Findings Are Not Strongly Associated With Postconcussional Disorder 2 Months Following Mild Traumatic Brain Injury. *Journal of Head Trauma Rehabilitation*, *27*(3), 188–198. https://doi.org/10.1097/HTR.0b013e318217f0ad

Larmor, J. (1897). LXIII. On the theory of the magnetic influence on spectra; and on the radiation from moving ions. *The London, Edinburgh, and Dublin Philosophical Magazine and Journal of Science*, *44*(271), 503–512. https://doi.org/10.1080/14786449708621095

Lauterbur, P. C. (1989). Image formation by induced local interactions. Examples employing nuclear magnetic resonance. 1973. *Clinical Orthopaedics and Related Research*, *242*(244), 3–6. https://doi.org/10.1038/242190a0

Lawrence, K. E., Levitt, J. G., Loo, S. K., Ly, R., Yee, V., O'Neill, J., … Narr, K. L. (2013). White Matter Microstructure in Subjects With Attention-Deficit/Hyperactivity Disorder and Their Siblings. *Journal of the American Academy of Child & Adolescent Psychiatry*, *52*(4), 431–440.e4. https://doi.org/10.1016/j.jaac.2013.01.010

Le Bihan, D., Breton, E., Lallemand, D., Grenier, P., Cabanis, E., & Laval-Jeantet, M. (1986). MR imaging of intravoxel incoherent motions: application to diffusion and perfusion in neurologic disorders. *Radiology*, *161*(2), 401–407. https://doi.org/10.1148/radiology.161.2.3763909

Le Bihan, D., Poupon, C., Amadon, A., & Lethimonnier, F. (2006). Artifacts and pitfalls in diffusion MRI. *Journal of Magnetic Resonance Imaging*, *24*(3), 478–488. https://doi.org/10.1002/jmri.20683

Lebel, C., & Beaulieu, C. (2011). Longitudinal Development of Human Brain Wiring Continues from Childhood into Adulthood. *Journal of Neuroscience*, *31*(30), 10937–10947. https://doi.org/10.1523/JNEUROSCI.5302-10.2011

Lebel, C., Walker, L., Leemans, A., Phillips, L., & Beaulieu, C. (2008). Microstructural maturation of the human brain from childhood to adulthood. *NeuroImage*, *40*(3), 1044–1055. https://doi.org/10.1016/j.neuroimage.2007.12.053

Levin, H. S., Wilde, E., Troyanskaya, M., Petersen, N. J., Scheibel, R., Newsome, M., … Li, X. (2010). Diffusion Tensor Imaging of Mild to Moderate Blast-Related Traumatic Brain Injury and Its Sequelae. *Journal of Neurotrauma*, *27*(4), 683–694. https://doi.org/10.1089/neu.2009.1073

Luoto, T. M., Tenovuo, O., Kataja, A., Brander, A., Öhman, J., & Iverson, G. L. (2013). Who Gets Recruited in Mild Traumatic Brain Injury Research? *Journal of Neurotrauma*, *30*(1), 11–16. https://doi.org/10.1089/neu.2012.2611

Madden, D. J., Bennett, I. J., Burzynska, A., Potter, G. G., Chen, N., & Song, A. W. (2012). Diffusion tensor imaging of cerebral white matter integrity in cognitive aging. *Biochimica et Biophysica Acta (BBA) - Molecular Basis of Disease*, *1822*(3), 386–400. https://doi.org/10.1016/j.bbadis.2011.08.003

Mansfield, P. (1977). Multi-planar image formation using NMR spin echoes. *Journal of Physics C: Solid State Physics*, *10*(3), L55–L58. https://doi.org/10.1088/0022-3719/10/3/004

Menon, D. K., Schwab, K., Wright, D. W., & Maas, A. I. (2010). Position Statement: Definition of Traumatic Brain Injury. *Archives of Physical Medicine and Rehabilitation*, *91*(11), 1637–1640. https://doi.org/10.1016/j.apmr.2010.05.017

Meyers, H. P., & Myers, H. P. (1997). *Introductory Solid State Physics, Second Edition* (2nd ed.). Taylor & Francis. Retrieved from https://books.google.fi/books?id=1IfYRAAACAAJ

Minati, L., & Węglarz, W. P. (2007). Physical foundations, models, and methods of diffusion magnetic resonance imaging of the brain: A review. *Concepts in Magnetic Resonance Part A*, *30A*(5), 278–307. https://doi.org/10.1002/cmr.a.20094

Mori, S., Wakana, S., Nagae-Poetscher, L. M., & Van Zijl, P. C. M. (2005). *MRI Atlas of Human White Matter. Elsevier Science*. Amsterdam: Elsevier. Retrieved from http://books.google.com/books?id=ltwRYlvFNLIC&printsec=frontcover

Moseley, M. (2002). Diffusion tensor imaging and aging - a review. *NMR in Biomedicine*, *15*(7–8), 553–560. https://doi.org/10.1002/nbm.785

Noble, K. G., Korgaonkar, M. S., Grieve, S. M., & Brickman, A. M. (2013). Higher education is an age-independent predictor of white matter integrity and cognitive control in late adolescence. *Developmental Science*, *16*(5), 653–664. https://doi.org/10.1111/desc.12077

Nørhøj Jespersen, S. (2018). White matter biomarkers from diffusion MRI. *Journal of Magnetic Resonance*, *291*, 127–140. https://doi.org/10.1016/j.jmr.2018.03.001

Nudo, R. J., Plautz, E. J., & Frost, S. B. (2001). Role of adaptive plasticity in recovery of function after damage to motor cortex. *Muscle & Nerve*, *24*(8), 1000–1019. Retrieved from http://www.ncbi.nlm.nih.gov/pubmed/11439375

Oishi, K., Faria, A., Jiang, H., Li, X., Akhter, K., Zhang, J., … Mori, S. (2009). Atlas-based whole brain white matter analysis using large deformation diffeomorphic metric mapping: application to normal elderly and Alzheimer's disease participants. *NeuroImage*, *46*(2), 486–499. Retrieved from http://www.ncbi.nlm.nih.gov/pubmed/19385016

Oishi, K., Zilles, K., Amunts, K., Faria, A., Jiang, H., Li, X., … Mori, S. (2008). Human brain white matter atlas: Identification and assignment of common anatomical structures in superficial white matter. *NeuroImage*, *43*(3), 447–457. https://doi.org/10.1016/j.neuroimage.2008.07.009

Oouchi, H., Yamada, K., Sakai, K., Kizu, O., Kubota, T., Ito, H., & Nishimura, T. (2007). Diffusion Anisotropy Measurement of Brain White Matter Is Affected by Voxel Size: Underestimation Occurs in Areas with Crossing Fibers. *American Journal of Neuroradiology*, *28*(6), 1102–1106. https://doi.org/10.3174/ajnr.A0488

Peerless, S. J., & Rewcastle, N. B. (1967). Shear injuries of the brain. *Canadian Medical Association Journal*, *96*(10), 577–582. Retrieved from http://www.ncbi.nlm.nih.gov/pubmed/6020206

Peeters, W., van den Brande, R., Polinder, S., Brazinova, A., Steyerberg, E. W., Lingsma, H. F., & Maas, A. I. R. (2015). Epidemiology of traumatic brain injury in Europe. *Acta Neurochirurgica*, *157*(10), 1683–1696. https://doi.org/10.1007/s00701-015-2512-7

Peng, H., Orlichenko, A., Dawe, R. J., Agam, G., Zhang, S., & Arfanakis, K. (2009). Development of a human brain diffusion tensor template. *NeuroImage*, *46*(4), 967–980. https://doi.org/10.1016/j.neuroimage.2009.03.046

Peter R., H. (1979). Synaptic density in human frontal cortex — Developmental changes and effects of aging. *Brain Research*, *163*(2), 195–205. https://doi.org/10.1016/0006-8993(79)90349-4

Pierpaoli, C., Barnett, A., Pajevic, S., Chen, R., Penix, L., Virta, A., & Basser, P. (2001). Water Diffusion Changes in Wallerian Degeneration and Their Dependence on White Matter Architecture. *NeuroImage*, *13*(6), 1174–1185. https://doi.org/10.1006/nimg.2001.0765

Pierpaoli, C., Jezzard, P., Basser, P. J., Barnett, A., & Di Chiro, G. (1996). Diffusion tensor MR imaging of the human brain. *Radiology*, *201*(3), 637–648. https://doi.org/10.1148/radiology.201.3.8939209

Pitel, A.-L., Chanraud, S., Sullivan, E. V, & Pfefferbaum, A. (2010). Callosal microstructural abnormalities in Alzheimer's disease and alcoholism: same phenotype, different mechanisms. *Psychiatry Research: Neuroimaging*, *184*(1), 49–56. https://doi.org/10.1016/j.pscychresns.2010.07.006

Poustchi-Amin, M., Mirowitz, S. A., Brown, J. J., McKinstry, R. C., & Li, T. (2001). Principles and Applications of Echo-planar Imaging: A Review for the General Radiologist. *RadioGraphics*, *21*(3), 767–779. https://doi.org/10.1148/radiographics.21.3.g01ma23767

Puljula, J., Mäkinen, E., Cygnel, H., Kortelainen, M.-L., & Hillbom, M. (2013). Incidence of moderate-to-severe traumatic brain injuries after reduction in alcohol prices. *Acta Neurologica Scandinavica*, *127*(3), 192–197. https://doi.org/10.1111/j.1600-0404.2012.01697.x

Purcell, E. M., Torrey, H. C., & Pound, R. V. (1946). Resonance Absorption by Nuclear Magnetic Moments in a Solid. *Physical Review*, *69*(1–2), 37–38. https://doi.org/10.1103/PhysRev.69.37

Rabi, I. I. (1937). Space Quantization in a Gyrating Magnetic Field. *Physical Review*, *51*(8), 652–654. https://doi.org/10.1103/PhysRev.51.652

Rabi, I. I., Zacharias, J. R., Millman, S., & Kusch, P. (1938). A New Method of Measuring Nuclear Magnetic Moment. *Physical Review*, *53*(4), 318–318. https://doi.org/10.1103/PhysRev.53.318

Radoeva, P. D., Coman, I. L., Antshel, K. M., Fremont, W., McCarthy, C. S., Kotkar, A., … Kates, W. R. (2012). Atlas-based white matter analysis in individuals with velo-cardio-facial syndrome (22q11.2 deletion syndrome) and unaffected siblings. *Behavioral and Brain Functions*, *8*(1), 38. https://doi.org/10.1186/1744-9081-8-38

Rathee, R., Rallabandi, V. P. S., & Roy, P. K. (2016). Age-related Differences in White Matter Integrity in Healthy Human Brain: Evidence from Structural Mri and Diffusion Tensor Imaging. *Magnetic Resonance Insights*, *9*, MRI.S39666. https://doi.org/10.4137/MRI.S39666

Sagi, Y., Tavor, I., Hofstetter, S., Tzur-Moryosef, S., Blumenfeld-Katzir, T., & Assaf, Y. (2012). Learning in the Fast Lane: New Insights into Neuroplasticity. *Neuron*, *73*(6), 1195–1203. https://doi.org/10.1016/j.neuron.2012.01.025

Salat, D. H., Tuch, D. S., Greve, D. N., van der Kouwe, A. J. W., Hevelone, N. D., Zaleta, A. K., … Dale, A. M. (2005). Age-related alterations in white matter microstructure measured by diffusion tensor imaging. *Neurobiology of Aging*, *26*(8), 1215–1227. https://doi.org/10.1016/j.neurobiolaging.2004.09.017

Schallert, T., Leasure, J. L., & Kolb, B. (2000). Experience-Associated Structural Events, Subependymal Cellular Proliferative Activity, and Functional Recovery After Injury to the Central Nervous System. *Journal of Cerebral Blood Flow & Metabolism*, *20*(11), 1513–1528. https://doi.org/10.1097/00004647-200011000-00001

Shenton, M. E., Hamoda, H. M., Schneiderman, J. S., Bouix, S., Pasternak, O., Rathi, Y., … Zafonte, R. (2012). A review of magnetic resonance imaging and diffusion tensor imaging findings in mild traumatic brain injury. *Brain Imaging and Behavior*, *6*(2), 137–192. https://doi.org/10.1007/s11682-012-9156-5

Shenton, M. E., Price, B. H., Levin, L., & Edersheim, J. G. (2018). Mild traumatic brain injury: Is DTI ready for the courtroom? *International Journal of Law and Psychiatry*, *61*(September), 50–63. https://doi.org/10.1016/j.ijlp.2018.09.002

Smith, S. M., Jenkinson, M., Johansen-Berg, H., Rueckert, D., Nichols, T. E., Mackay, C. E., … Behrens, T. E. J. (2006). Tract-based spatial statistics: Voxelwise analysis of multi-subject diffusion data. *NeuroImage*, *31*(4), 1487–1505. https://doi.org/10.1016/j.neuroimage.2006.02.024

Smith, S. M., Jenkinson, M., Woolrich, M. W., Beckmann, C. F., Behrens, T. E. J., Johansen-Berg, H., … Matthews, P. M. (2004). Advances in functional and structural MR image analysis and implementation as FSL. *NeuroImage*, *23*, S208–S219. https://doi.org/10.1016/j.neuroimage.2004.07.051

Soares, J. M., Marques, P., Alves, V., & Sousa, N. (2013). A hitchhiker's guide to diffusion tensor imaging. *Frontiers in Neuroscience*, *7*, 31. https://doi.org/10.3389/fnins.2013.00031

Song, S.-K., Sun, S.-W., Ramsbottom, M. J., Chang, C., Russell, J., & Cross, A. H. (2002). Dysmyelination Revealed through MRI as Increased Radial (but Unchanged Axial) Diffusion of Water. *NeuroImage*, *17*(3), 1429–1436. https://doi.org/10.1006/nimg.2002.1267

Stadlbauer, A., Salomonowitz, E., Strunk, G., Hammen, T., & Ganslandt, O. (2008). Age-related Degradation in the Central Nervous System: Assessment with Diffusion-Tensor Imaging and Quantitative Fiber Tracking. *Radiology*, *247*(1), 179–188. https://doi.org/10.1148/radiol.2471070707

Stehling, M. K., Turner, R., & Mansfield, P. (1991). Echo-planar imaging: Magnetic resonance imaging in a fraction of a second. *Science*. https://doi.org/10.1126/science.1925560

Stejskal, E. O., & Tanner, J. E. (1965). Spin Diffusion Measurements: Spin Echoes in the Presence of a Time-Dependent Field Gradient. *The Journal of Chemical Physics*, *42*(1), 288–292. https://doi.org/10.1063/1.1695690

Suetens, P. (2009). *Fundamentals of Medical Imaging*. Cambridge University Press.

Sugawara, E., & Nikaido, H. (2014). Properties of AdeABC and AdeIJK efflux systems of Acinetobacter baumannii compared with those of the AcrAB-TolC system of Escherichia coli. *Antimicrobial Agents and Chemotherapy*, *58*(12), 7250–7257. https://doi.org/10.1128/AAC.03728-14

Sullivan, E. V, Rohlfing, T., & Pfefferbaum, A. (2010). Quantitative fiber tracking of lateral and interhemispheric white matter systems in normal aging: Relations to timed performance. *Neurobiology of Aging*, *31*(3), 464–481. https://doi.org/10.1016/j.neurobiolaging.2008.04.007

Toth, A., Kovacs, N., Perlaki, G., Orsi, G., Aradi, M., Komaromy, H., … Schwarcz, A. (2013). Multi-Modal Magnetic Resonance Imaging in the Acute and Sub-Acute Phase of Mild Traumatic Brain Injury: Can We See the Difference? *Journal of Neurotrauma*, *30*(1), 2–10. https://doi.org/10.1089/neu.2012.2486

Tournier, J.-D., Mori, S., & Leemans, A. (2011). Diffusion tensor imaging and beyond. *Magnetic Resonance in Medicine*, *65*(6), 1532–1556. https://doi.org/10.1002/mrm.22924

Trifan, G., Gattu, R., Haacke, E. M., Kou, Z., & Benson, R. R. (2017). MR imaging findings in mild traumatic brain injury with persistent neurological impairment. *Magnetic Resonance Imaging*, *37*, 243–251. https://doi.org/10.1016/j.mri.2016.12.009

Tuch, D. S. (2004). Q-ball imaging. *Magnetic Resonance in Medicine*, *52*(6), 1358–1372. https://doi.org/10.1002/mrm.20279

Tuch, D. S., Reese, T. G., Wiegell, M. R., Makris, N., Belliveau, J. W., & Wedeen, V. J. (2002). High angular resolution diffusion imaging reveals intravoxel white matter fiber heterogeneity. *Magnetic Resonance in Medicine*, *48*(4), 577–582. https://doi.org/10.1002/mrm.10268

Vandermosten, M., Boets, B., Poelmans, H., Sunaert, S., Wouters, J., & Ghesquiere, P. (2012). A tractography study in dyslexia: neuroanatomic correlates of orthographic, phonological and speech processing. *Brain*, *135*(3), 935–948. https://doi.org/10.1093/brain/awr363

Vieira, S., Pinaya, W. H. L., & Mechelli, A. (2017). Using deep learning to investigate the neuroimaging correlates of psychiatric and neurological disorders: Methods and applications. *Neuroscience & Biobehavioral Reviews*, *74*, 58–75. https://doi.org/10.1016/j.neubiorev.2017.01.002

Wallace, E. J., Mathias, J. L., & Ward, L. (2018). Diffusion tensor imaging changes following mild, moderate and severe adult traumatic brain injury: a meta-analysis. *Brain Imaging and Behavior*, *0*(0), 1–15. https://doi.org/10.1007/s11682-018-9823-2

Wang, S., Kim, M., Wu, G., & Shen, D. (2017). Scalable High Performance Image Registration Framework by Unsupervised Deep Feature Representations Learning. In *Deep Learning for Medical Image Analysis* (Vol. 63, pp. 245–269). Elsevier. https://doi.org/10.1016/B978-0-12-810408-8.00015-8

Wei, C. W., Tharmakulasingam, J., Crawley, A., Kideckel, D. M., Mikulis, D. J., Bradbury, C. L., & Green, R. E. (2008). Use of Diffusion-Tensor Imaging in Traumatic Spinal Cord Injury to Identify Concomitant Traumatic Brain Injury. *Archives of Physical Medicine and Rehabilitation*, *89*(12), S85–S91. https://doi.org/10.1016/j.apmr.2008.07.005

Weng, C.-B., Qian, R.-B., Fu, X.-M., Lin, B., Han, X.-P., Niu, C.-S., & Wang, Y.-H. (2013). Gray matter and white matter abnormalities in online game addiction. *European Journal of Radiology*, *82*(8), 1308–1312. https://doi.org/10.1016/j.ejrad.2013.01.031

Werring, D. J., Clark, C. A., Barker, G. J., Miller, D. H., Parker, G. J. M., Brammer, M. J., … Thompson, A. J. (1998). The structural and functional mechanisms of motor recovery: complementary use of diffusion tensor and functional magnetic resonance imaging in a traumatic injury of the internal capsule. *Journal of Neurology, Neurosurgery & Psychiatry*, *65*(6), 863–869. https://doi.org/10.1136/jnnp.65.6.863

Westbrook, C., Roth, C. K., & Talbot, J. (2011). *MRI in Practice*. Wiley. Retrieved from https://books.google.fi/books?id=BAZVxm3j4NcC

Westlye, L. T., Walhovd, K. B., Dale, A. M., Bjornerud, A., Due-Tonnessen, P., Engvig, A., … Fjell, A. M. (2010). Life-Span Changes of the Human Brain White Matter: Diffusion Tensor Imaging (DTI) and Volumetry. *Cerebral Cortex*, *20*(9), 2055–2068. https://doi.org/10.1093/cercor/bhp280

Wheeler-Kingshott, C. A. M., & Cercignani, M. (2009). About "axial" and "radial" diffusivities. *Magnetic Resonance in Medicine*, *61*(5), 1255–1260. https://doi.org/10.1002/mrm.21965

Wilde, E. A., McCauley, S. R., Barnes, A., Wu, T. C., Chu, Z., Hunter, J. V, & Bigler, E. D. (2012). Serial measurement of memory and diffusion tensor imaging changes within the first week following uncomplicated mild traumatic brain injury. *Brain Imaging and Behavior*, *6*(2), 319–328. https://doi.org/10.1007/s11682-012-9174-3

Wortzel, H. S., Kraus, M. F., Filley, C. M., Anderson, C. A., & Arciniegas, D. B. (2011). Diffusion tensor imaging in mild traumatic brain injury litigation. *The Journal of the American Academy of Psychiatry and the Law*, *39*(4), 511–523. https://doi.org/39/4/511

Wrigley, P. J., Gustin, S. M., Macey, P. M., Nash, P. G., Gandevia, S. C., Macefield, V. G., … Henderson, L. A. (2009). Anatomical Changes in Human Motor Cortex and Motor Pathways following Complete Thoracic Spinal Cord Injury. *Cerebral Cortex*, *19*(1), 224–232. https://doi.org/10.1093/cercor/bhn072

Wu, Y.-C., & Alexander, A. L. (2007). Hybrid diffusion imaging. *NeuroImage*, *36*(3), 617–629. https://doi.org/10.1016/j.neuroimage.2007.02.050

Yamamoto, T., Yamasaki, M., & Imai, T. (1989). Retrograde pyramidal tract degeneration in a patient with cervical haematomyelia. *Journal of Neurology, Neurosurgery & Psychiatry*, *52*(3), 382–386. https://doi.org/10.1136/jnnp.52.3.382

Yoon, B., Shim, Y.-S., Lee, K.-S., Shon, Y.-M., & Yang, D.-W. (2008). Region-specific changes of cerebral white matter during normal aging: A diffusion-tensor analysis. *Archives of Gerontology and Geriatrics*, *47*(1), 129–138. https://doi.org/10.1016/j.archger.2007.07.004

Young, R., Babb, J., Law, M., Pollack, E., & Johnson, G. (2007). Comparison of region-of-interest analysis with three different histogram analysis methods in the determination of perfusion metrics in patients with brain gliomas. *Journal of Magnetic Resonance Imaging*, *26*(4), 1053–1063. https://doi.org/10.1002/jmri.21064

Zatorre, R. J., Fields, R. D., & Johansen-Berg, H. (2012). Plasticity in gray and white: neuroimaging changes in brain structure during learning. *Nature Neuroscience*, *15*(4), 528–536. https://doi.org/10.1038/nn.3045

Zhang, S., & Arfanakis, K. (2018). Evaluation of standardized and study-specific diffusion tensor imaging templates of the adult human brain: Template characteristics, spatial normalization accuracy, and detection of small inter-group FA differences. *NeuroImage*, *172*, 40–50. https://doi.org/10.1016/j.neuroimage.2018.01.046

PUBLICATIONS

PUBLICATION I

Acute Mild Traumatic Brain Injury is not Associated with White Matter Change on Diffusion Tensor Imaging

Ilvesmäki T, Luoto TM, Hakulinen U, Brander A, Ryymin P, Eskola H, Iverson GL, Öhman J.

Original publication channel (Brain 137(7), 1876-1882)
Doi: 10.1093/brain/awu095

Brain Advance Access published May 11, 2014

doi:10.1093/brain/awu095 Brain 2014: Page 1 of 7 | 1

BRAIN
A JOURNAL OF NEUROLOGY

REPORT

Acute mild traumatic brain injury is not associated with white matter change on diffusion tensor imaging

Tero Ilvesmäki,[1,2] Teemu M. Luoto,[3] Ullamari Hakulinen,[4,2] Antti Brander,[1] Pertti Ryymin,[4] Hannu Eskola,[1,2] Grant L. Iverson[5] and Juha Öhman[3]

1 Medical Imaging Centre, Department of Radiology, Tampere University Hospital, Tampere, Finland
2 Department of Electronics and Communications Engineering, Tampere University of Technology, Tampere, Finland
3 Department of Neurosciences and Rehabilitation, Tampere University Hospital, Tampere, Finland
4 Medical Imaging Centre, Department of Radiology and Medical Physics, Tampere University Hospital, Tampere, Finland
5 Department of Physical Medicine and Rehabilitation, Harvard Medical School; and Red Sox Foundation and Massachusetts General Hospital Home Base Program, Boston, Massachusetts, USA

Correspondence to: Tero Ilvesmäki,
Medical Imaging Centre, Department of Radiology,
Tampere University Hospital, Tampere,
Finland
E-mail: tero.ilvesmaki@pshp.fi

This study was designed to (i) evaluate the influence of age on diffusion tensor imaging measures of white matter assessed using tract-based spatial statistics; (ii) determine if mild traumatic brain injury is associated with microstructural changes in white matter, in the acute phase following injury, in a large homogenous sample that was carefully screened for pre-injury medical, psychiatric, or neurological problems; and (iii) examine if injury severity is related to white matter changes. Participants were 75 patients with acute mild traumatic brain injury (age = 37.2 ± 12.0 years, 45 males and 30 females) and 40 controls (age = 40.6 ± 12.2 yrs, 20 males and 20 females). Age effects were analysed by comparing control subgroups aged 31–40, 41–50, and 51–60 years against a group of 18–30-year-old control subjects. Widespread statistically significant areas of abnormal diffusion tensor measures were observed in older groups. Patients and controls were compared using age and gender as covariates and in age- and gender-matched subgroups. Subgroups of patients with more severe injuries were compared to age-and gender-matched controls. No significant differences were detected in patient-control or severity analyses (all *P*-value > 0.01). In this large, carefully screened sample, acute mild traumatic brain injury was not associated with diffusion tensor imaging abnormalities detectable with tract-based spatial statistics.

Keywords: concussion; traumatic brain injury; magnetic resonance imaging; diffusion tensor imaging; statistical analysis
Abbreviations: DTI = diffusion tensor imaging; TBI = traumatic brain injury; TBSS = tract-based spatial statistics

Introduction

In mild traumatic brain injury (TBI) research, white matter integrity assessment by diffusion tensor imaging (DTI) has been the centre of attention for the last decade (Hulkower *et al.*, 2013). Many studies have reported white matter changes in patients with a history of mild TBI, recently or remotely, although heterogeneous and inconsistent conclusions have been drawn. This heterogeneity

Received September 16, 2013. Revised February 27, 2014. Accepted February 28, 2014.

Table 1 A brief summary of previous DTI studies that focus on the acute phase of mild TBI

Reference	Time frame*	Magnet	Patients (gender; age)	Control (gender; age)	Analysis	Findings
Arfanakis *et al.*, 2002	< 24 h	1.5 T	5 (3 M, 2 F; 35.6 ± 14.8)	10 (5 M, 5 F; 28.9 ± 7.6)	ROI	Decreased FA
Bazarian *et al.*, 2007	< 72 h	3 T	6 (4 M, 2 F; mean 21.7, range 18–31 years)	6 (4 M, 2 F; mean 21.7, range 18–31 years)	WBA, ROI	WBA: Decreased trace ROI: Increased FA
Chu *et al.*, 2010	Range 1–6 days	3 T	10 (4 M, 6 F; 15.7 ± 1.18)	10 (4 M, 6 F; 15.7 ± 1.83)	WBA, ROI	Increased FA, Decreased RD
Henry *et al.*, 2011	81.9 ± 46.7 h	3 T	16 (16M; 22.1 ± 1.7)	8 (8 M; 22.8 ± 1.5)	WBA	Increased FA and AD, Decreased MD
Lipton *et al.*, 2009	Range 2–14 days	3 T	20 (9 M, 11 F; 33.4 ± 8.3)	20 (9 M, 11 F; 34.2 ± 9.3)	WBA	Decreased FA, Increased MD
Mayer *et al.*, 2010	12 ± 5.7 days	3 T	21 (8 M, 13 F; 27.45 ± 7.39)	21 (8 M, 13 F; 26.81 ± 6.68)	ROI	Increased FA, Decreased RD
Messé *et al.*, 2012	Range 8–21 days	3 T	53 (35 M, 18 F; 35.5 ± 11.0)	40 (28M, 12 F; 36.3 ± 12.5)	TBSS	Decreased FA, Increased MD and RD
Miles *et al.*, 2008	Range 1–10 days	1.5 T	17 (11 M, 6 F; mean 33.44, range 18–58 years)	29 (15 M, 14 F; mean 35, range 18–61 years)	ROI	Decreased FA, Increased MD
Toth *et al.*, 2013	<72 h	3 T	14 (9 M, 5 F; 34.9 ± 18.4)	14 (9 M, 5 F; 35.8 ± 18.5)	TBSS, volumetric	Decreased FA, Increased MD
Yallampalli *et al.*, 2013	Range 1–16 days	3 T	11 (5 M, 6 F; 15.09 ± 1.14)	11 (5 M, 6 F; 15.82 ± 1.78)	ROI (fornix)	Decreased FA, Increased nADC

*Time from injury to imaging. Reported as mean time ± SD, maximum time or time range. ADC = apparent diffusion coefficient; F = female; FA = fractional anisotropy; M = male; MD = mean diffusivity (= apparent diffusion coefficient); ROI = region of interest; WBA = whole brain analysis.

can partly be explained by methodological differences and limitations, such as small sample sizes, failure to control for pre-injury health factors, major differences in time from injury to imaging, diverse patient characteristics, and differing DTI analysis techniques. A brief summary of previous DTI studies that focus on the acute phase of mild TBI are presented in Table 1.

The current study had three objectives: (i) to evaluate the influence of age on DTI measures and axonal integrity assessed by tract-based spatial statistics (TBSS); (ii) to determine if mild TBI is associated with microstructural changes in white matter in the acute phase following injury, in a large homogenous sample that was carefully screened for pre-injury medical, psychiatric, or neurological problems; and finally (iii) to examine if mild TBI severity is related to white matter changes. Through rigorous inclusion and exclusion criteria, the goal was to reduce or eliminate numerous confounding variables to study a relatively 'pure' sample of civilian patients with acute mild TBIs.

Materials and methods

This work is part of the Tampere Traumatic Head and Brain Injury Study. Subjects were enrolled from the emergency department of the Tampere University Hospital between August 2010 and July 2012; all met mild TBI criteria of the World Health Organization's Collaborating Centre for Neurotrauma Task Force (Holm *et al.*, 2005). The enrolment protocol included three inclusion criteria and nine exclusion criteria, as described in our previous publication (Luoto *et al.*, 2013), that resulted in a small percentage of patients with head trauma being enrolled (the majority of eligible adults were excluded due to comorbidities). Ethics approval was obtained from the Ethical Committee of Pirkanmaa Hospital District, Finland. All patients and controls provided written informed consent according to the Declaration of Helsinki.

Subjects

Of the 75 patients with mild TBI, 45 were male and 30 were female. The mean age was 37.2 ± 12.0 years. Of the 40 control subjects, 20 were male and 20 were female. The mean age for the control subjects was 40.6 ± 12.2 years. The mean time interval between injury and acute clinical assessment was 48.1 ± 45.4 h. The clinical characteristics of the mild TBI sample are presented in Table 2. For mild TBI severity analyses, mild TBI subgroups were formed based on clinical markers as follows: (i) loss of consciousness > 5 min, $n = 7$; (ii) post-traumatic amnesia > 3 h, $n = 25$; (iii) acute traumatic lesion on CT and/or MRI (complicated mild TBI), $n = 15$; (iv) Glasgow Coma Scale = 14, $n = 6$; and (v) a group of patients with a combination of any of the previous criteria (definite mild TBI), $n = 29$.

Control subjects were patients evaluated in the emergency department of Tampere University Hospital who suffered ankle injuries. The same study criteria used with the mild TBI sample were applied in the enrolment of the controls when applicable. Control subjects were enrolled in an age and gender stratified manner, with five males and five females in the following age groups: (i) 18–30 years, (ii) 31–40 years, (iii) 41–50 years; and (iv) 51–60 years. All 40 control subjects underwent a head MRI with the same sequences as the mild TBI sample. With controls, all MRI findings were interpreted as normal.

Table 2 Characteristics of classic clinical mild TBI severity markers

	Presence, *n* (%)		Duration			
	Yes	No	Mean	Median	SD	IQR
Loss of consciousness (min)	28 (37.3)	47 (62.7)	0.9	0	2.2	0–1.0
Post-traumatic amnesia (h)	69 (92.0)	6 (8.0)	2.66	1.5	3.4	0.1–4.5
Retrograde amnesia (h)	17 (22.7)	58 (77.3)	0.4	0	1.7	0
Disorientation	53 (70.7)	22 (29.3)				
Focal neurological deficit	17 (22.7)	58 (77.3)				
GCS, 15 points	69 (92.0)	6 (8.0)				
GCS, 14 points	6 (8.0)	69 (92.0)				
Acute traumatic lesion on CT*	7 (9.3)	68 (90.7)				
Acute traumatic lesion on MRI	15 (20.0)	60 (80.0)				
Diffuse axonal injury	7 (9.3)					
Diffuse axonal injury and subdural haemorrhage	1 (1.3)					
Subdural haemorrhage	1 (1.3)					
Subdural effusion	1 (1.3)					
Subarachnoid haemorrhage	1 (1.3)					
Contusion and subdural haemorrhage	2 (2.7)					
Contusion	2 (2.7)					

*All traumatic lesions were also visible on MRI.
GCS = Glasgow Coma Scale; IQR = interquartile range.

Clinical assessment

A broad clinical assessment of the patients in the final sample was performed by T.L. The patients were interviewed regarding past health including diagnosed medical conditions, medication use, head injury history, alcohol consumption according to the Alcohol Use Disorders Identification Test (Saunders *et al.*, 1993), and drug and narcotics abuse history. The presence and duration of retrograde amnesia and post-traumatic amnesia were assessed using the Rivermead Post-Traumatic Amnesia Protocol (King *et al.*, 1997) together with the Galveston Orientation and Amnesia Test (GOAT) (Levin *et al.*, 1979). All patients scored $\geqslant$80 points on the GOAT (normal 76–100). Persistent post-traumatic amnesia was screened using the revised Westmead Post-Traumatic Amnesia Scale (Shores *et al.*, 1986) and all the patients scored a flawless 12 points at the time of assessment. Glasgow Coma Scale (Teasdale and Jennett, 1976) scores were collected from ambulance forms (if applicable) and the emergency department records (the lowest scores were recorded). The clinical assessment included a complete neurological examination. Participants were determined to have met ICD-10 diagnostic criteria for post-concussional syndrome if they endorsed symptoms on the Sports Concussion Assessment Tool (SCAT2) (McCrory *et al.*, 2009) 22-item symptom scale in at least three of the ICD-10 symptom categories. The time duration criterion was not applied to the acute analyses. The SCAT2 was added later in the study, so only a subset of patients were administered the test ($n = 51$ at emergency department, and $n = 50$ at 1 month due to a patient dropping out of the follow-up evaluation).

Neuroimaging

In the emergency department, a non-contrast head CT was performed with a 64-row CT scanner (GE, Lightspeed VCT) for all consecutive patients with head injury. Head MRI was done with a 3 T MRI scanner (Siemens Trio). The MRI protocol included sagittal T_1-weighted 3D inversion recovery prepared gradient echo, axial T_2 turbo spin echo, conventional axial and high resolution sagittal FLAIR, axial T_2*, axial susceptibility weighted, and diffusion weighted imaging series. Head MRIs were done within 14 days after injury (mean 5.8 $\pm$ 2.5 days). All head MRIs were analysed and systematically coded by two neuroradiologists.

The DTI data were collected by a single-shot, spin echo-based and diffusion-weighted echo planar imaging sequence. The parameters for the DTI sequence were repetition time 5144 ms, echo time 92 ms, field of view 230 mm, matrix 128 $\times$ 128, three averages, slice/gap 3.0/0.9 mm, and voxel dimension of 1.8 $\times$ 1.8 $\times$ 3.0 mm. Two b-factors were used, 0 and 1000 s/mm^2 with 20 diffusion gradient orientations. A 12-channel head matrix coil was used. Finally, the signal to noise ratio value was well above the limit of acceptance for diffusion imaging, following the group's previous work (Hakulinen *et al.*, 2012).

Tract-based spatial statistics

Whole brain voxel-wise statistical analysis was carried out using TBSS (Smith *et al.*, 2006), a part of FSL, version 5.0.1 (Smith *et al.*, 2004). A threshold for fractional anisotropy values for the creation of the skeleton was chosen at $\geqslant$0.3 to exclude peripheral areas from the skeleton and to reduce bias in the results. Effects of age and gender were controlled by adding them as covariates of no interest (nuisance variables) to general linear model setup in non-matched group analysis. No covariates were used in the analyses with matched groups.

Statistical analysis

Non-parametric, permutation-based tests were carried out by Randomize (included in FSL) (Nichols and Holmes, 2002) with 5000 permutations and threshold-free cluster enhancement. To reduce experiment-wise type 1 errors associated with multiple comparisons, the threshold for statistical significance was set at $P \leqslant 0.01$, adjusted for multiple comparisons. Two-sided, two-sample Wilcoxon-Mann-Whitney tests were used for each age- and gender-matched analysis to test the groups' ages for significant differences.

Results

Effect of age on diffusion measures

In the control subjects, comparison of fractional anisotropy values among the four age groups yielded significantly ($P \leqslant 0.01$) lower fractional anisotropy values in age groups 41–50 years and 51–60 years in comparison with control subjects aged between 18 and 30 years. The areas with fractional anisotropy deviations extended widely across the whole cerebral white matter (Fig. 1A). Statistically significant ($P \leqslant 0.01$) differences in apparent diffusion coefficient values were obtained only in the oldest of the age groups, 51–60 years. Apparent diffusion coefficient values were elevated in the anterior parts of the right cerebral hemisphere (Fig. 1B).

Axial diffusivity was found to decrease with age. In the second oldest age group, 41–50 years, lower axial diffusivity values extended from the brainstem to the posterior part of the cerebrum. Similar areas of lower axial diffusivity were found in the oldest age group (Fig. 1C). Radial diffusivity values were increased in the two oldest age groups in a widespread manner (Fig. 1D). See Supplementary Table 1 for quantitative information for the age effect analyses.

Group comparison between controls and patients

The age- and gender-covaried TBSS analysis between the patients with mild TBI and controls did not reveal statistically significant differences in fractional anisotropy, apparent diffusion coefficient, axial diffusivity or radial diffusivity. For the age- and gender-matched analyses, 40 patients with mild TBI were carefully matched on age and gender to the 40 control subjects. No statistically significant differences in fractional anisotropy, apparent diffusion coefficient, axial diffusivity, or radial diffusivity were found.

The association between mild traumatic brain injury severity and diffusion measures

Subgroup analyses were conducted based on injury severity characteristics. For patients with a loss of consciousness for >5 min ($n = 7$) compared with matched control subjects, no statistically significant differences were found in fractional anisotropy, apparent diffusion coefficient, axial diffusivity or radial diffusivity. A subgroup of 25 patients with post-traumatic amnesia >3 h was compared with 25 matched control subjects. There were no statistically significant differences in fractional anisotropy, apparent diffusion coefficient, axial diffusivity or radial diffusivity. A subgroup of 15 patients with complicated mild TBIs (i.e. all had a trauma-related structural abnormality on CT and/or MRI) was compared to 15 matched control subjects. There were no statistically significant differences in fractional anisotropy, apparent diffusion coefficient, axial diffusivity or radial diffusivity. Six patients with Glasgow Coma Scale = 14 were compared to six matched control subjects. There were no statistically significant differences in fractional anisotropy, apparent diffusion coefficient, axial

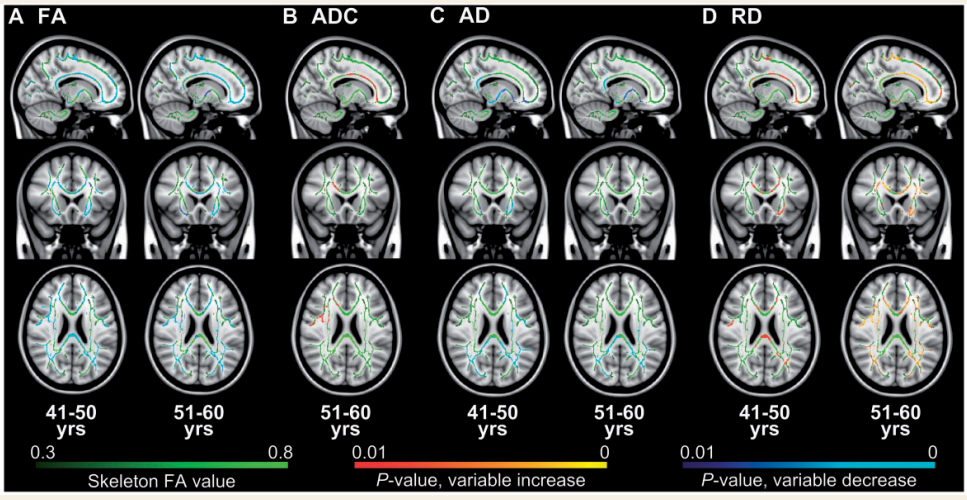

Figure 1 Qualitative results of age effect on DTI measures; the mean fractional anisotropy skeleton is presented in green and laid on top of greyscale MNI152 1 mm T_1 image. Colour coding is used to differentiate whether values on the skeleton increase (red–yellow) or decrease (blue–light blue) in the older age group. The youngest age group (18–30 years) is used as a reference for the other age groups in the analyses. Slice coordinates (MNI152 aligned anatomical) $x = 15$ mm, $y = 20$ mm, $z = 23$ mm. Radiological convention (Left is Right). AD = axial diffusivity; ADC = apparent diffusion coefficient; FA = fractional anisotropy; RD = radial diffusivity.

Table 3 Group sizes, ages and minimum *P*-values of each Mild TBI analysis

	Mild TBI versus covaried controls	Mild TBI versus matched controls	LOC > 5 min versus matched controls	PTA > 3 h versus matched controls	Complicated Mild TBI versus matched controls	GCS = 14 versus matched controls	Definite mild TBI versus matched controls	Mild TBI and PCS versus mild TBI and no PCS: acute	Mild TBI and PCS versus mild TBI and no PCS: 1 month
Sample sizes	75 versus 40	40 versus 40	7 versus 7	25 versus 25	15 versus 15	6 versus 6	29 versus 29	20 versus 20	12 versus 12
Age, patients	37.2 ± 12.0	40.2 ± 11.6	35.9 ± 10.4	37.4 ± 11.6	35.9 ± 10.2	33.0 ± 10.1	38.0 ± 11.2	34.2 ± 10.6	36.3 ± 10.7
Age, controls	40.6 ± 12.2	40.7 ± 12.1	35.9 ± 10.7	38.0 ± 11.4	36.3 ± 10.0	34.5 ± 10.1	40.0 ± 11.7	34.3 ± 10.5	36.2 ± 10.4
Min. *P*-values									
Fractional anisotropy	0.131	0.185	0.158	0.166	0.306	0.212	0.162	0.123	0.320
Apparent diffusion coefficient	0.102	0.118	0.059	0.022	0.186	0.157	0.031	0.102	0.247
Axial diffusivity	0.086	0.189	0.039	0.023	0.021	0.268	0.045	0.220	0.324
Radial diffusivity	0.102	0.118	0.079	0.069	0.330	0.158	0.054	0.070	0.297

All of the analyses, except the final column, suggest an increase in fractional anisotropy values and decrease in apparent diffusion coefficient, axial diffusivity and radial diffusivity values when compared with matched subjects. The post-concussional syndrome (PCS) analysis at 1 month suggested a decrease in fractional anisotropy and increase in apparent diffusion coefficient, axial diffusivity, and radial diffusivity values, although clearly non-significant. GCS = Glasgow coma score; LOC = loss of consciousness; PTA = post-traumatic amnesia.

diffusivity, or radial diffusivity. The final subgroup (definite mild TBI) included patients with a combination of any of the previous criteria. This mild TBI group consisted of 29 patients who were compared to 29 matched controls. There were no statistically significant differences in fractional anisotropy, apparent diffusion coefficient, axial diffusivity or radial diffusivity.

Association between diffusion measures and post-concussional symptoms

TBSS was used to compare the post-concussional syndrome subgroups against age-matched patients who did not meet the ICD-10 symptom criteria for post-concussional syndrome at the acute stage ($n = 20$) or at 1 month post-injury ($n = 12$). Acutely, there were no statistically significant differences between post-concussional syndrome subgroups in fractional anisotropy, apparent diffusion coefficient, axial diffusivity or radial diffusivity. Moreover, there were no statistically significant differences in fractional anisotropy, apparent diffusion coefficient, axial diffusivity, or radial diffusivity in those who had, versus those who did not have post-concussional syndrome, at 1 month after injury.

Discussion

There were three objectives in this study: (i) to illustrate the extensive impact of ageing on brain white matter in adults between the ages of 18 and 60; (ii) to determine whether 'pure' acute mild TBI is associated with white matter changes detectable with TBSS; and (iii) to study the effects of mild TBI severity on DTI measures. No significant ($P < 0.01$) mild TBI-related DTI abnormalities were detectable, even with greater injury severity taken into account. Importantly, none of the DTI measures were significantly associated with post-concussional symptoms acutely or at 1 month after injury. Some of the mild TBI severity analyses resulted in nearly statistically significant results (Table 3). The results of this study would have been different if a liberal criterion for significance, with no consideration of multiple comparisons, was applied (i.e. $P < 0.05$). That is, some of the subgroup analyses would have been considered statistically significant. In contrast, statistically significant age-related axonal degradation was observed in the control group. This is in line with previous reports (Stadlbauer *et al.*, 2008; Yoon *et al.*, 2008) and further establishes that age should be considered carefully in white matter analyses.

In the group comparison between the control subjects and the patients with mild TBI, we used two different methods to manage the effects of age on white matter integrity: (i) covariance correction; and (ii) pair-wise age-matching. Previous studies suggest, in contrast with our results, abnormal DTI findings in acute mild TBI (Hulkower *et al.*, 2013) (Table 1). Differences in the methodology and timing of MRI scanning can partly explain the difference between the present results and previous reports. Pathophysiological alterations after mild TBI are time-dependent, thus rendering chronology a crucial factor in the interpretation of DTI findings (Hulkower *et al.*, 2013; Toth *et al.*, 2013). For the acute stage of mild TBI, multiple publications illustrate an increase or decrease in fractional anisotropy values and decrease in apparent diffusion

coefficient values (Hulkower *et al.*, 2013; Toth *et al.*, 2013). From a neurometabolic view, statistical unification of neuroimaging data obtained acutely (e.g. 2 days) and post-acutely (e.g. 1 month) after injury does not seem justifiable. More research is needed to better understand acute versus post-acute changes in DTI measures after mild TBI.

This study was larger and more tightly methodologically controlled than most previous DTI studies of acute mild TBI. The patients were clinically assessed by the same physician using structured instruments and strict clinical enrolment criteria were applied to both patient and control groups. A specific time interval was used in imaging to reduce the possible effect of diverse neurometabolic stages of mild TBI recovery.

The negative main outcome of this study can be partly caused by the statistical group-wise nature of TBSS. The current result does not rule out individualized patterns of focal white matter changes in different anatomical regions. Moreover, some of the non-significant findings in mild TBI severity subgroups may be explained by the lower statistical power of these analyses. For post-concussional syndrome analyses, patient matching was limited to age-matching due to lack of uniformity in gender distributions. Lack of gender-matching is a methodological limitation in the post-concussional syndrome analysis. Indeed, the heterogeneous nature of brain trauma, combined with methodological differences across studies, likely underlies the fact that the anatomical areas showing DTI differences vary considerably across past mild TBI studies. Therefore, TBSS as a supplement to region of interest analysis could be an appropriate alternative for a comprehensive DTI analysis.

In conclusion, in this large homogeneous, premorbidly healthy sample, acute mild TBI was not associated with obvious DTI abnormalities detectable with TBSS. Clear differences in DTI findings were associated with age, even in healthy subjects in their 40 s. Therefore, age should always be considered a potential confounder in DTI studies.

Acknowledgements

The authors thank research assistants Anne Simi and Marika Suopanki-Ervasti for their contribution in the data collection. A portion of this study was presented at the 10th International Workshop on Computational Systems Biology in June 2013 in Tampere, Finland. The study was also presented at the XXI World Congress of Neurology in September 2013 in Vienna, Austria.

Funding

This work was supported by a grant by the Emil Aaltonen foundation to T.I.

Conflict of interest

Grant Iverson, PhD has been reimbursed by the government, professional scientific bodies, and commercial organizations for discussing or presenting research relating to MTBI and sport-related concussion at meetings, scientific conferences, and symposiums. He has a clinical practice in forensic neuropsychology involving individuals who have sustained MTBIs. He has received honorariums for serving on research panels that provide scientific peer review of programs. The other authors report no competing or conflicts of interest.

Supplementary material

Supplementary material is available at *Brain* online.

References

Arfanakis K, Haughton VM, Carew JD, Rogers BP, Dempsey RJ, Meyerand ME. Diffusion tensor MR imaging in diffuse axonal injury. AJNR Am J Neuroradiol 2002; 23: 794–802.

Bazarian JJ, Zhong J, Blyth B, Zhu T, Kavcic V, Peterson D. Diffusion tensor imaging detects clinically important axonal damage after mild traumatic brain injury: a pilot study. J Neurotrauma 2007; 24: 1447–59.

Chu Z, Wilde EA, Hunter JV, McCauley SR, Bigler ED, Troyanskaya M, et al. Voxel-based analysis of diffusion tensor imaging in mild traumatic brain injury in adolescents. AJNR Am J Neuroradiol 2010; 31: 340–6.

Hakulinen U, Brander A, Ryymin P, Ohman J, Soimakallio S, Helminen M, et al. Repeatability and variation of region-of-interest methods using quantitative diffusion tensor MR imaging of the brain. BMC Med Imaging 2012; 12: 30.

Henry LC, Tremblay J, Tremblay S, Lee A, Brun C, Lepore N, et al. Acute and chronic changes in diffusivity measures after sports concussion. J Neurotrauma 2011; 28: 2049–59.

Holm L, Cassidy JD, Carroll LJ, Borg J. Neurotrauma task force on mild traumatic brain injury of the WHO collaborating centre. Summary of the WHO collaborating centre for neurotrauma task force on mild traumatic brain injury. J Rehabil Med 2005; 37: 137–41.

Hulkower MB, Poliak DB, Rosenbaum SB, Zimmerman ME, Lipton ML. A decade of DTI in traumatic brain injury: 10 years and 100 articles later. AJNR Am J Neuroradiol 2013; 34: 2064–74.

King NS, Crawford S, Wenden FJ, Moss NE, Wade DT, Caldwell FE. Measurement of post-traumatic amnesia: how reliable is it? J Neurol Neurosurg Psychiatry 1997; 62: 38–42.

Levin HS, O'Donnell VM, Grossman RG. The galveston orientation and amnesia test. A practical scale to assess cognition after head injury. J Nerv Ment Dis 1979; 167: 675–84.

Lipton ML, Gulko E, Zimmerman ME, Friedman BW, Kim M, Gellella E, et al. Diffusion-tensor imaging implicates prefrontal axonal injury in executive function impairment following very mild traumatic brain injury. Radiology 2009; 252: 816–24.

Luoto TM, Tenovuo O, Kataja A, Brander A, Ohman J, Iverson GL. Who gets recruited in mild traumatic brain injury research? J Neurotrauma 2013; 30: 11–6.

Mayer AR, Ling J, Mannell MV, Gasparovic C, Phillips JP, Doezema D, et al. A prospective diffusion tensor imaging study in mild traumatic brain injury. Neurology 2010; 74: 643–50.

McCrory P, Meeuwisse W, Johnston K, Dvorak J, Aubry M, Molloy M, et al. Consensus statement on concussion in sport: the 3rd International Conference on Concussion in Sport held in Zurich, November 2008. Br J Sports Med 2009; 43 (Suppl 1): i76–i90.

Messé A, Caplain S, Pelegrini-Issac M, Blancho S, Montreuil M, Levy R, et al. Structural integrity and postconcussion syndrome in mild traumatic brain injury patients. Brain Imaging Behav 2012; 6: 283–92.

Miles L, Grossman RI, Johnson G, Babb JS, Diller L, Inglese M. Short-term DTI predictors of cognitive dysfunction in mild traumatic brain injury. Brain Inj 2008; 22: 115–22.

Nichols TE, Holmes AP. Nonparametric permutation tests for functional neuroimaging: a primer with examples. Hum Brain Mapp 2002; 15: 1–25.

Saunders JB, Aasland OG, Babor TF, de la Fuente JR, Grant M. Development of the alcohol use disorders identification test (AUDIT): WHO collaborative project on early detection of persons with harmful alcohol consumption–II. Addiction 1993; 88: 791–804.

Shores EA, Marosszeky JE, Sandanam J, Batchelor J. Preliminary validation of a clinical scale for measuring the duration of post-traumatic amnesia. Med J Aust 1986; 144: 569–72.

Smith SM, Jenkinson M, Woolrich MW, Beckmann CF, Behrens TE, Johansen-Berg H, et al. Advances in functional and structural MR image analysis and implementation as FSL. Neuroimage 2004; 23 (Suppl 1): S208–19.

Smith SM, Jenkinson M, Johansen-Berg H, Rueckert D, Nichols TE, Mackay CE, et al. Tract-based spatial statistics: voxelwise analysis of multi-subject diffusion data. Neuroimage 2006; 31: 1487–505.

Stadlbauer A, Salomonowitz E, Strunk G, Hammen T, Ganslandt O. Age-related degradation in the central nervous system: assessment with diffusion-tensor imaging and quantitative fiber tracking. Radiology 2008; 247: 179–88.

Teasdale G, Jennett B. Assessment and prognosis of coma after head injury. Acta Neurochir (Wien) 1976; 34: 45–55.

Toth A, Kovacs N, Perlaki G, Orsi G, Aradi M, Komaromy H, et al. Multi-modal magnetic resonance imaging in the acute and sub-acute phase of mild traumatic brain injury: can we see the difference? J Neurotrauma 2013; 30: 2–10.

Yallampalli R, Wilde EA, Bigler ED, McCauley SR, Hanten G, Troyanskaya M, et al. Acute white matter differences in the fornix following mild traumatic brain injury using diffusion tensor imaging. J Neuroimaging 2013; 23: 224–7.

Yoon B, Shim YS, Lee KS, Shon YM, Yang DW. Region-specific changes of cerebral white matter during normal aging: a diffusion-tensor analysis. Arch Gerontol Geriatr 2008; 47: 129–38.

PUBLICATION II

Spinal Cord Injury Induces Widespread Chronic Changes in Cerebral White Matter

Ilvesmäki T, Koskinen E, Brander A, Luoto T, Öhman J, Eskola H.

Original publication channel (Human Brain Mapping 38(7), 3637-3647)
Doi: 10.1002/hbm.23619

◆ Human Brain Mapping 38:3637–3647 (2017) ◆

Spinal Cord Injury Induces Widespread Chronic Changes in Cerebral White Matter

Tero Ilvesmäki,[1,2]* **Eerika Koskinen**,[3] **Antti Brander**,[4] **Teemu Luoto**,[5] **Juha Öhman**,[3] **and Hannu Eskola**[1,4]

[1]*BioMediTech Institute and Faculty of Biomedical Sciences and Engineering, Tampere University of Technology, Tampere, Finland*
[2]*Department of Medical Physics, Turku University Hospital, Turku, Finland*
[3]*Department of Neurosciences and Rehabilitation, Tampere University Hospital, Tampere, Finland*
[4]*Department of Radiology, Medical Imaging Centre of the Pirkanmaa Hospital District, Tampere, Finland*
[5]*Department of Neurosurgery, Tampere University Hospital, Tampere, Finland*

Abstract: Traumatic spinal cord injuries (SCIs) lead to axonal damage at the trauma site, as well as disconnections within the central nervous system. While the exact mechanisms of the long-term pathophysiological consequences of SCIs are not fully understood, it is known that neuronal damage and degeneration are not limited to the direct proximity of the trauma. Instead, the effects can be detected even in the cerebrum. We examined SCI-induced chronic brain changes with a case-control design using 32 patients and 70 control subjects. Whole-brain white matter (WM) tracts were assessed with diffusion tensor imaging (DTI). In addition, we analysed associations between DTI metrics and several clinical SCI variables. Whole-brain analyses were executed by tract-based spatial statistics (TBSS), with an additional complementary atlas-based analysis (ABA). We observed widespread, statistically significant ($P \leq 0.01$) changes similar to neural degeneration in SCI patients, both in the corticospinal tract (CST) and beyond. In addition, associations between DTI metrics and time since injury were found with TBSS and ABA, implying possible long-term post-injury neural regeneration. Using the ABA approach, we observed a correlation between SCI severity and DTI metrics, indicating a decrease in WM integrity along with patient sensory or motor scores. Our results suggest a widespread neurodegenerative effect of SCI within the cerebrum that is not limited to the motor pathways. Furthermore, DTI-measured WM integrity of chronic SCI patients seemed to improve as time elapsed since injury. *Hum Brain Mapp 38:3637–3647, 2017.* © 2017 Wiley Periodicals, Inc.

Key words: diffusion tensor imaging; spinal cord injuries; white matter; humans; cerebrum

Additional Supporting Information may be found in the online version of this article.

Contract grant sponsor: Finnish Cultural Foundation; Contract grant sponsor: Orion Research Foundation.

*Correspondence to: Tero Ilvesmäki, BioMediTech Institute and Faculty of Biomedical Sciences and Engineering, Tampere University of Technology, Tampere, Finland. E-mail: tero.ilvesmaki@student.tut.fi

Received for publication 31 December 2016; Revised 2 April 2017; Accepted 7 April 2017.

DOI: 10.1002/hbm.23619
Published online 21 April 2017 in Wiley Online Library (wileyonlinelibrary.com).

INTRODUCTION

In a traumatic spinal cord injury (SCI), an external force causes immediate damage and death of the neural cells at the injury site, resulting in a secondary neuropathological process that further aggravates neuronal damage. Secondary degeneration of white matter (WM) tracts has been shown to spread in both anterograde and retrograde directions from the injury site over several years after the injury [Beirowski et al., 2005; Buss et al., 2004]. Degeneration includes a slow and progressive demyelination, which eventually leads to gliosis [Buss et al., 2004].

Secondary degeneration of the corticospinal tract (CST) in humans after SCI has been shown histologically to reach cerebral regions. Furthermore, histological evidence supports atrophy of the CST neurons [Yamamoto et al., 1989]. In line with these findings, atrophy-related changes have been detected on volumetric MRI scans in the CST and the sensorimotor cortex in SCI patients [Freund et al., 2011; Wrigley et al., 2009].

After an injury to the central nervous system, complex neuroplastic mechanisms are initiated, similar to those associated with learning processes that occur during normal development of the brain [Keyvani and Schallert, 2002; Zatorre et al., 2013]. Neuroplasticity involves several underlying mechanisms, including changes in myelin structure, axon diameter and packing density changes, axonal sprouting, rerouting, and elimination [Zatorre et al., 2013]. These processes can potentially alter the functional and structural fabric of the brain's neural network to compensate for at least part of the possible damage to the brain [Nudo et al., 2001; Zatorre et al., 2013]. Functional MRI has provided evidence of cortical reorganization that compensates for sensorimotor loss after SCI [Freund et al., 2011; Henderson et al., 2011; Jurkiewicz et al., 2007]. The changes in activation observed by functional MRI after SCI can be explained by both functional and structural alterations in nervous tissue. After experimental SCI structural alterations, the remodelling of synaptic structures and axonal sprouting and the formation of new connections have been demonstrated together with reorganisation in both the cortex and subcortical regions [Florence et al., 1998; Kim et al., 2006; Ramu et al., 2008].

Diffusion tensor imaging (DTI), which measures the diffusion of water molecules in tissues, provides quantitative information on tissue microstructures. In nervous tissue, the orientation of fibre bundles, axonal diameter, density, and myelination affect diffusion metrics [Beaulieu, 2002; Sen and Basser, 2005]. Spinal DTI has been shown to have potential for quantifying the extent of clinical disability following SCI and radiological SCI severity [Chang et al., 2010; Koskinen et al., 2013]. Additionally, DTI could detect diffusion changes at a distance from the macroscopic spinal lesions seen on conventional MRI, suggesting secondary degeneration of WM tracts in the spinal cord [Chang et al., 2010; Cohen-Adad et al., 2011; Koskinen et al., 2013; Petersen et al., 2012]. Degeneration-associated abnormalities in cerebral DTI values after SCI have also been demonstrated in humans, although only in a few studies that were mostly focused on the CST [Freund et al., 2012; Gustin et al., 2010; Koskinen et al., 2014; Wei et al., 2008; Wrigley et al., 2009]. Wrigley et al. [2009] found volumetric and DTI metrics changes in multiple cortical areas beyond the primary sensory and motor cortices, indicating that subcortical WM changes after SCI could also extend beyond the CST.

Fractional anisotropy (FA) and mean diffusivity (MD) are currently the most commonly used DTI metrics [Guleria et al., 2008; Hulkower et al., 2013; Wei et al., 2008], and both reflect WM integrity in various pathological conditions [Alexander et al., 2007]. FA is mostly lower and MD higher in pathological regions compared to healthy tissue. Additionally, radial diffusivity (RD), and axial diffusivity (AD) can be examined. RD is thought to be largely affected by the integrity of the myelin sheath, while changes in AD reflect the degree of axonal degeneration [Alexander et al., 2007; Song et al., 2002]. With pathological tissue, RD is usually higher in myelin degradation, while AD can be lower in axonal disruption.

In this study, we applied tract-based spatial statistics (TBSS) [Smith et al., 2006], which is a whole-brain group comparison analysis method, adapting a unique approach on whole-brain analysis by its registration and "skeletonisation" phases. Previously, only one study [Wei et al., 2008] addressed cerebral WM changes after SCI with TBSS. Contrary to the Wei group's region of interest findings, they found no structural between-group differences in their TBSS analyses.

The purpose of this study was to investigate the effects of SCI on the entire cerebral WM, detectable by DTI. We also investigated the association between cerebral DTI values and clinical SCI parameters, including injury severity, and time since injury (TSI), and applied an atlas-based analysis (ABA) method to supplement the TBSS results. We hypothesized that (i) SCI-induced WM changes would be detectible beyond the CST with TBSS and (ii) that the motor and sensory functions of chronic SCI patients would be related to brain WM integrity.

MATERIALS AND METHODS

Subjects

All consecutive patients with a chronic traumatic cervical spine injury ($n = 88$) who were admitted to either the ward or an outpatient clinic at Tampere University Hospital between 1989 and 2010 (the annual incidence rate of SCI in Finland mirrored the area of responsibility of Tampere University Hospital, leading to ~8.3 new tetraplegia patients per year [Ahoniemi et al., 2008], of which not all are sent to Tampere University Hospital) were contacted in 2011 to participate in the study. The inclusion criteria were as follows: (i) over 18 years of age, (ii) resident of the hospital district, (iii) clinically

TABLE I. Subject demographics

Group comparisons	Controls ($n = 70$)	Patients ($n = 32$)	AIS A ($n = 10$)	P (con v. pat)	P (con v. AIS A)
Age (yrs, mean ± SD)	39.5 ± 11.8	56.5 ± 14.2	51.3 ± 15.7	<0.001	0.008
Gender (male/female)	29/41	25/7	7/3	<0.001	0.089
TSI (yrs, mean ± SD)		13.8 ± 12.3	23.5 ± 13.1		
ASIA impairment scale					
AIS A		10	10		
AIS B		1			
AIS C		4			
AIS D		16			
AIS E		1			
Injury etiology					
Fall		13	3		
Transport		11	5		
Sports		6	2		
Assault		1			
Other		1			

The gender distribution between the controls and the patients was tested with a chi-squared test and the age distribution with a Mann-Whitney U test.

significant neurological findings due to a traumatic cervical SCI after 24 h of monitoring in the hospital, and (iv) TSI was greater than 1 year. The exclusion criteria were as follows: (i) known neurological illness other than SCI (including traumatic brain injury), (ii) respiratory arrest, (iii) contraindication for MRI, and (iv) refusal to participate in the study. In addition to the exclusion criteria, two subjects were dismissed due to severe microangiopathy on brain MRI. The final SCI population sample consisted of 32 patients.

The control subject sample comprised two separate groups of DTI study controls, both imaged at Tampere University Hospital using the same scanner and imaging protocol. We enrolled a total of 70 control subjects, of which 40 were orthopedically injured patients evaluated in the ED of Tampere University Hospital. This group of control subjects was categorised in an age- and gender-stratified manner, with five men and five women in the following age groups: (i) 18–30 years, (ii) 31–40 years, (iii) 41–50 years, and (iv) 51–60 years. The remaining 30 control subjects were healthy voluntary hospital staff members. Conventional MRI findings of the control subjects were interpreted as normal by a neuroradiologist (A.B.). All subjects included in this study provided written informed consent according to the Declaration of Helsinki.

Clinical Data

All patients with SCI were examined at an outpatient clinic at Tampere University Hospital. The collection of clinical data was performed by a neurologist (E.K.). The aetiology of the SCI was classified using the International SCI Core Data Set [DeVivo et al., 2006]. The International Standards for Neurological Classification of Spinal Cord Injury (ISNCSCI) were used to evaluate and classify the neurological consequence of SCI [Waring et al., 2010]. Ten of the SCI patients had complete injury [American Spinal Injury Association Impairment Scale (AIS), grade A]. See Table I for demographic information on the control and patient groups.

Imaging

A head MRI was done with a 3 Tesla MRI scanner (Siemens Trio, Siemens AG Medical Solutions, Erlangen, Germany). A 12-channel head coil and a 4-channel neck coil were used simultaneously for the SCI patients, but only the head MRI data were used in this study. The MRI protocol included sagittal T1-weighted 3D inversion recovery prepared gradient echo, axial T2 turbo spin echo, conventional axial and high-resolution sagittal FLAIR, axial T2*, axial susceptibility-weighted imaging, and diffusion-weighted imaging series.

The brain DTI data were collected by a single-shot, spin echo-based and diffusion-weighted echo planar imaging sequence. The parameters for the DTI sequence were TR 5144 ms, TE 92 ms, field of view 230 mm, matrix 128 × 128, 3 averages, slice/gap 3.0/0.9 mm, voxel dimensions of 1.8 × 1.8 × 3.0 mm, and b-factors 0 and 1000 s/mm^2 with 20 diffusion gradient orientations. Diffusion tensors were calculated from the gradient data and further derived into DTI scalars used in the analyses (FA, MD, RD, and AD).

Statistical Analysis

Whole-brain voxel-wise statistical analysis for the DTI data was carried out using TBSS [Smith et al., 2006], a part of FSL, version 5.0.6 (http://fsl.fmrib.ox.ac.uk/fsl/fslwiki/

) [Smith et al., 2004]. After pre-processing the data, a mean FA image was derived and thinned to create a mean FA skeleton. The threshold for FA values for the creation of the skeleton was chosen as $\geq$0.25. Each subject's aligned data were then projected onto this skeleton for each DTI parameter, and the resulting skeletonised data were fed into voxel-wise cross-subject statistics.

Statistical group comparison analysis was performed using FSL with TFCE [Smith and Nichols, 2009]. Nonparametric two-sample permutation test using general linear model (GLM) design was used for statistics [Winkler et al., 2014]. Inference was obtained through 50,000 permutations, testing the resulting clusters for significance at $P \leq 0.01$ (one-sided), corrected for multiple comparisons across space. The type I error caused by multiple analyses on the same dataset was potentially minimized by adopting a more conservative significance level ($P \leq 0.01$). Statistical regression was performed in a similar manner, using a GLM to check the DTI data for partial regression with clinical parameters. Effects of age and gender were controlled by adding them as covariates to the design matrices in all analyses.

Two group analyses were performed: (i) a comparison between the whole SCI group ($n = 32$) and the healthy control subjects ($n = 70$) and (ii) a comparison between patients with complete SCI (AIS grade A, $n = 10$) and healthy control subjects ($n = 70$). The clinical variables used in the partial correlation analyses were (i) the ISNCSCI-derived total motor score (TMS), (ii) motor subscore for upper extremities (UEMS), (iii) motor subscore for lower extremities, (iv) total sensory score (TSS), and (v) the TSI = time between injury and MRI. Due to the findings in stepwise linear regression analyses performed on the significant clusters in the group comparison, we decided to control TSI analysis with UEMS and motor and sensory subscores with TSI, respectively.

To further specify our findings, we utilised the JHU-ICBM-DTI-81 WM labels atlas in an ABA approach, which, in theory, should complement the TBSS results [Faria et al., 2010]. Additionally, it can help to further localize the findings. Regional DTI metric values were derived for each atlas tract by taking the arithmetic mean of the skeleton voxels inside the corresponding atlas volume. The mean values were then fed to JASP (JASP Team, 2016, Version 0.8) for statistical analysis. The group comparison was carried out using analysis of covariance (ANCOVA), controlling for age and gender, and correlation analyses by linear regression. To distinguish between the anatomical regions in general and the volume defined by the JHU atlas, the abbreviated atlas volumes will be referred to with a subscript JHU (e.g., CST_{JHU}).

RESULTS

Both group comparisons [i.e., patient group ($n = 32$) vs. control subjects ($n = 70$) and full injury patients ($n = 10$) vs. control subjects ($n = 70$)] resulted in statistically significant differences at a significance level of $P \leq 0.01$. The ABA group comparison results were mostly in concordance with the TBSS results. Most linear regression analyses did not reach statistical significance in TBSS; TSI was the only variable that produced a statistically significant correlation with DTI metrics. The ABA, however, revealed individual correlations that did not reach significance in the TBSS analysis. The complete list of results from the ABA are displayed in Table II. Detailed information on the ABA results are provided as Supporting Information.

Group Comparison

The TBSS group comparison between all SCI patients ($n = 32$) and control subjects ($n = 70$) yielded statistically significant ($P \leq 0.01$) differences in FA, MD, RD, and AD values. The FA values were found to be lower and the MD, RD, and AD values higher in the patients when compared with the control subjects.

Instead of being mainly focused on the CST as expected, the changes related to SCI were more widespread. The coverage of statistically significant voxels in FA was 30.3% of the skeleton's total volume, 32.9% in MD, 38.7% in RD, and 13.0% in AD, respectively. The areas with significantly decreased FA and increased MD can be seen in Figure 1, and the actual differences in DTI values are displayed as bar graphs in Figure 2. The significant areas with increased RD and AD are presented as Supporting Information. Due to the widespread nature of the findings, we also created images with the *P*-value threshold set to 0.002 to emphasize the areas with the most change in DTI values. The areas of FA, MD, and RD with $P \leq 0.002$ can be seen in the Supporting Information.

The significant findings were extensive, with clusters spread nearly throughout the whole cerebrum. Areas of WM affected by SCI in the group analysis included projection, commissural, and association fibres. From the projection fibres, the majority of the CST and the thalamocortical projections were affected. Between-group differences in the area of the CST extended from the cerebral peduncle (CP), through the posterior limb of internal capsule (PLIC), up to the subcortical WM underneath the primary motor and sensory cortices. The genu and the anterior part of the body of the corpus callosum (CC) were the most affected of the commissural fibres. The association fibres were widely affected, with most prominent findings in the inferior and superior longitudinal fasciculi, inferior fronto-occipital fasciculus, and uncinate fasciculus. The anterior cingulum was also affected. The findings in MD are notably similar to FA, although with slightly wider coverage.

As an addition to the TBSS analyses, we utilised the JHU-ICBM-DTI-81 WM atlas to extract parts of the skeleton and ran statistical tests on the areas' mean values. We compared the patient group with the control subjects via ANCOVA. Statistically significant ($P \leq 0.01$) lower FA

TABLE II. Atlas – based analysis results ($P \leq 0.01$)

	SCI v controls*				AIS A v controls*				TSI correlation**				UEMS**			TMS**	TSS**	
WM tract (ICBM DTI−81)	FA	MD	RD	AD	FA	MD	RD	AD	FA	MD	RD	AD	FA	MD	RD	FA	FA	MD
Anterior corona radiata L	↓	↑	↑						+		−							
Anterior corona radiata R	↓	↑	↑															
ALIC L	↓	↑	↑	↑	↓	↑	↑								−			
ALIC R	↓	↑	↑		↓	↑	↑											
Body of CC		↑		↑														
Cingulum (cingulate gyrus) L		↑	↑							−	−							
Cingulum (cingulate gyrus) R		↑	↑			↑			+									
CST R				↓														
External capsule R		↑	↑															
Fornix (column and body of fornix)				↑						−	−	−						
Fornix (cres)/Stria terminalis L	↓		↑						+		−							
Genu of CC	↓	↑	↑		↓	↑	↑											
Inferior cerebellar peduncle L	↓		↑	↓	↓		↑	↓										
Inferior cerebellar peduncle R	↓		↑	↓	↓			↓										
Medial lemniscus L								↓										
Medial lemniscus R								↓										
Middle cerebellar peduncle													+					
Posterior corona radiata L										−	−	−						
Posterior corona radiata R	↓	↑	↑		↓		↑			−		−						
Posterior limb of internal capsule L		↑	↑				↑											
Posterior thalamic radiation L[a]	↓	↑	↑		↓	↑	↑				−							
Retrolenticular part of internal capsule L					↓					−	−							
Retrolenticular part of internal capsule R																+	+	
Sagittal stratum L[b]	↓	↑	↑		↓		↑		+	−	−							
Sagittal stratum R[b]											−							
Splenium of CC									+	−	−							
Superior cerebellar peduncle L									+									
Superior cerebellar peduncle R									+				+			+		
Superior corona radiata L		↑	↑							−		−		−				
Superior corona radiata R																		−
Superior fronto−occipital fasciculus L	↓	↑	↑															
Superior fronto−occipital fasciculus R	↓	↑	↑															
Superior longitudinal fasciculus L		↑								−	−			−	−			
Tapetum L									+		−							
Tapetum R			↑			↑												
Uncinate fasciculus L	↓		↑															

*Up arrows (↑) indicate higher values, and down arrows (↓) indicate lower values in the patient group compared with the control subjects.
**Plus signs (+) indicate positive correlation, and minus signs (−) indicate negative correlation.
[a]Includes optic radiation.
[b]Includes inferior longitudinal fasciculus and inferior fronto − occipital fasciculus.

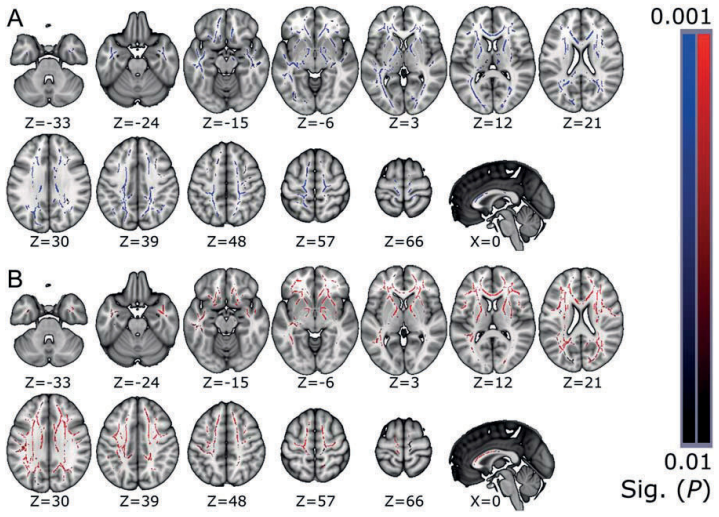

Figure 1.

Statistically significant clusters of lower FA acquired in the TBSS group comparison analysis shown in the two upper rows (**A**), with the significant clusters of higher MD shown in the two lower rows (**B**). Results are limited to *P*-values ≤ 0.01. The results are overlaid on the MNI152 standard-space template, with corresponding MNI coordinates below the slices. Neurological convention, left = left. [Color figure can be viewed at wileyonlinelibrary.com]

values were found in several locations, along with higher MD and RD values. Several atlas locations included changes in more than one DTI metric: changes in both FA and MD were found in the anterior corona radiata (CR_{JHU}), the anterior limb of internal capsule ($ALIC_{JHU}$), the genu of the CC_{JHU}, the right posterior CR_{JHU}, the left posterior thalamic radiation, the left sagittal stratum, and in the superior fronto-occipital fasciculus. According to our analysis, AD correlated positively in the left $ALIC_{JHU}$, the body of the CC_{JHU}, and in the fornix, whereas negative correlation was found in the right CST_{JHU} and in the inferior CP_{JHU}. The complete list of locations is shown in Table II.

Complete SCI

Patients with AIS grade A ($n = 10$) were compared with the healthy control subjects ($n = 70$) with TBSS. Age and gender were used as covariates in the GLM setup. The analysis resulted in statistically significant ($P \leq 0.01$) differences in FA, MD, and RD: patients had lower FA and higher MD and RD values compared with the control subjects. AD did not reach statistical significance at the 0.01 level. The results were reminiscent of the group comparison (whole SCI group and control subjects), but considerably more spatially restricted. Significant clusters covered 9.2% of the skeleton volume in FA and only 2.8% in MD, while the coverage was 10.4% in RD.

Differences in FA were somewhat asymmetric, occurring predominantly on the left side of the cerebrum. Statistically significant areas of FA and MD can be seen in Figure 3, with the absolute DTI values of the significant clusters displayed in Figure 4. The affected areas in FA were mostly in the projection fibres, including the PLIC, the anterior limb of the internal capsule, the posterior thalamic radiation, and the subcortical CST. While higher MD values were found mostly in the genu of the CC, a small, significant cluster was located near the subcortical CST. The significant clusters of RD can be seen in the Supporting Information.

Comparing the complete (AIS A) SCI patient group ($n = 10$) with the control subjects ($n = 70$) in an ABA, we found significantly lower FA and AD values and higher MD and RD values. Again, there were some locations with findings in multiple DTI metrics: FA was found lower and MD higher in the $ALIC_{JHU}$, the genu of CC_{JHU}, and in the left posterior thalamic radiation. See Table II for listing of the ABA results.

Partial Correlations with Injury Parameters

None of the sensory or motor score variables correlated significantly ($P \leq 0.01$) with the DTI metrics in our TBSS analyses. Of all the tested clinical parameters, only the TSI produced a statistically significant partial correlation with

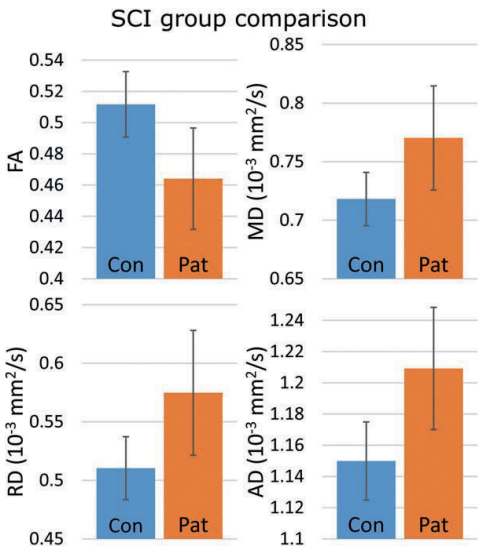

Figure 2.

The differences in absolute DTI values taken from the statistically significant clusters in the group comparison for each DTI metric ($P \leq 0.01$; FA, MD, RD, and AD). The bar graph values represent mean values of the significant voxels, with error bars showing the ± SD for the volume's mean. [Color figure can be viewed at wileyonlinelibrary.com]

the DTI metrics in the patient group. The TSI correlation analysis was conducted using age, gender, and UEMS as covariates.

The TSI correlated positively with FA and negatively with MD, RD, and AD at the 0.01 *P*-value level. Statistically significant clusters in positive correlation between FA and the TSI covered 5.0% of the skeleton volume, while coverages were 26.3% for MD, 31.5% for RD, and 2.4% for AD. Partial correlation maps for FA and MD can be seen in Figure 5. Correlation maps for RD and AD are provided as Supporting Information. Partial correlation coefficients for the significant clusters of FA, MD, RD, and AD were 0.378, −0.331, −0.328, and −0.366, respectively.

A positive correlation between the TSI and FA was spatially concentrated to the commissural fibres: virtually the whole volume of the CC was affected. No correlations were found in the caudal parts of the projection fibres. For MD, the areas with correlation were similar to the FA findings, but with additional correlation findings widely in the association fibres and subcortically in the projection fibres.

In addition to TSI, we found a correlation between DTI metrics and the UEMS motor subscore, TMS, and TSS in ABA. TSI correlated positively with FA and negatively with MD, RD, and AD in our analysis. UEMS correlated positively with FA and negatively with MD and RD. TSS correlated positively with FA and negatively with MD, and TMS correlated positively with FA. See Table II for a complete list of the ABA results.

DISCUSSION

Group Comparison

The direction of the differences found in FA and MD were in agreement with previous studies, but the spatial extent of the findings was significantly larger than has been previously reported [Guleria et al., 2008; Koskinen et al., 2014; Wrigley et al., 2009]. The results suggest degenerative-type changes in the majority of the cerebral WM, with the bulk of lower FA and higher MD extending beyond the CST. These changes could signify large-scale post-SCI secondary anterograde (Wallerian) and retrograde cerebral degeneration [Beirowski et al., 2005; Buss et al., 2004; Guleria et al., 2008].

Previous studies focusing on separate pathological conditions have hypothesized that areas of WM containing increased RD and AD values in addition to lower FA are associated with axonal degeneration [Della Nave et al., 2011; Metwalli et al., 2010; Roosendaal et al., 2009; Song et al., 2002]. In light of these previous studies, the rise in RD and AD found in our TBSS results may be associated with post-SCI axonal degeneration. However, the increase of AD beyond the spinal cord and brain stem, which include mainly coherent WM tracts, could also be a consequence of crossing WM fibres, causing fictitious change in directional diffusivities [Wheeler-Kingshott and Cercignani, 2009].

The CST_{JHU} and the inferior CP_{JHU} had significantly lower AD in contrast to the otherwise found higher AD in our ABA. This is, however, convergent with previous DTI studies of chronic SCI which have reported a reduction of AD associated with axonal degeneration in areas like CP and CST [Freund et al., 2012; Wrigley et al., 2009], as well as in the spinal cord remote from the site of injury [Cohen-Adad et al., 2011]. The inconsistency in AD results may be linked to post-SCI neuroplasticity [Nudo et al., 2001; Schallert et al., 2000] and secondary degeneration [Beirowski et al., 2005; Buss et al., 2004; Guleria et al., 2008] associated with different regions of the cerebrum. Unfortunately, this type of speculation based only on AD cannot fully be confirmed with our current results and requires further research.

AIS Grade A

The absolute differences between the groups in the AIS A analysis were slightly larger for FA and MD compared with the full-group comparison, but the lower sample size may distort the results. However, low power, along with the strict *P*-value limit, may imply an even larger effect size of the findings compared with the group comparison.

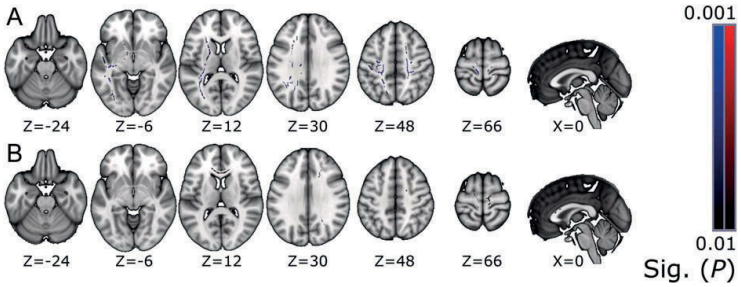

Figure 3.

Areas with statistically significant ($P \leq 0.01$) differences between patients with full injury and control subjects. Areas with lower FA values are shown above (**A**), and areas with higher MD are below (**B**). The results are overlaid on the MNI152 standard-space template, with corresponding MNI coordinates below the slices. Neurological convention, left = left. [Color figure can be viewed at wileyonlinelibrary.com]

Future studies with a larger sample of AIS grade A patients could provide interesting results.

The ABA results of AIS A seem logical due to findings in areas of the brain often associated with secondary degeneration [Beirowski et al., 2005; Buss et al., 2004]. Unfortunately, no definite conclusions can be made with the current sample size.

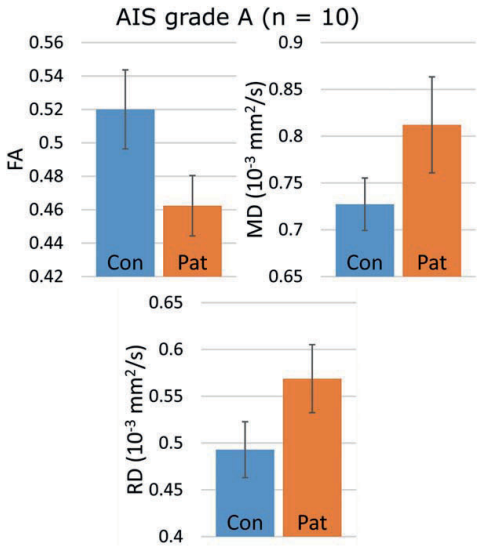

Figure 4.

The differences in absolute DTI values for the full injury group, taken from the statistically significant clusters for each significant DTI metric ($P \leq 0.01$; FA, MD, and RD). The values represent mean values of the significant voxels, with error bars showing the ± SD for the volume mean. Note the apparent increase in difference compared to the whole-group comparison. [Color figure can be viewed at wileyonlinelibrary.com]

Correlations

Contrary to previous studies with chronic SCI patients [Freund et al., 2012; Koskinen et al., 2014; Wrigley et al., 2009], we found a correlation between DTI scalars and TSI with both TBSS and ABA. However, owing to the limited sample of patients, the regression analyses could only reliably detect large effect sizes. While TSI correlations with DTI metrics have not been previously detected in the cerebrum [Freund et al., 2012; Koskinen et al., 2014; Wrigley et al., 2009], these studies have concentrated on the CST instead of the whole brain volume. It is worth noting that Guleria et al. [2008] observed increased FA and decreased MD values in the rostral part of the CST in SCI patients compared with control subjects, and this trend seemed to increase with TSI during the first 12 months after injury. According to experimental studies [Ramu et al., 2008], these types of changes have been suggested to reflect post-SCI subcortical regeneration.

Previous studies have suggested a connection between DTI scalars and neuroplasticity (axonal regeneration, glial processes, or synaptogenesis), detectible as an increase in FA and/or decrease in MD and RD [Keller and Just, 2016; Sagi et al., 2012; Steele et al., 2013]. Due to the restrictions in our study setting, it is difficult to draw a solid causal conclusion on the findings. Hypothetically, positive correlation with FA and negative with MD over time suggest axonal regeneration or other plastic mechanisms. However, it is uncertain whether post-SCI neuroplasticity could affect the brain over a decade post-injury, and whether the observed correlation is actually associated with the post-injury neurophysiology.

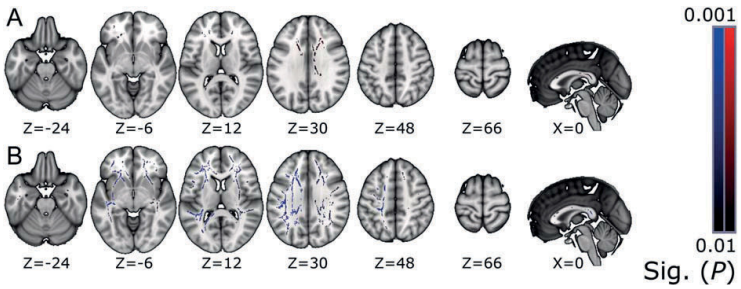

Figure 5.

Partial correlations maps ($P \leq 0.01$) for TSI obtained from TBSS analysis. FA correlated positively with TSI (above, **A**), and MD correlated negatively (below, **B**). The results are overlaid on the MNI152 standard-space template, with corresponding MNI coordinates below the slices. Neurological convention, left = left. [Color figure can be viewed at wileyonlinelibrary.com]

The directions of the correlations between UEMS, TMS, and TSS and DTI scalars in the ABA are in agreement with our previous study [Koskinen et al., 2014], where FA was found to correlate positively and MD negatively with UEMS, TMS, and TSS, suggesting that the clinical state of the patient tends to be better with higher FA and lower MD values. These findings imply that the severity and extent of SCI have an effect on the cerebral WM microstructure, detectable with DTI in the chronic phase.

Study Design and Limitations

In our study, we decided to combine two separate control groups to form a single larger pool of controls in favour of statistical power. After some consideration, we deemed the groups sufficiently homogeneous, and comparable from a pathological point of view, for them to be combined. Had we opted to create a pool of age- and gender-matched controls, the raw statistical power of our group analysis would have been lower than in our current setup. Regarding the effect of ageing on DTI scalars, previous studies have suggested that the slight quadratic trend of the relationship between age and DTI metrics can be modelled as linear with sufficient precision [Kodiweera et al., 2016; Westlye et al., 2010]. It should thus be possible to reliably control for the effect of age in a GLM. In addition, controlling for gender in the analyses is straightforward, as it is a binary categorical variable. Nevertheless, our study would have benefited from a large pool of age- and gender-matched subjects.

While our patient data were screened carefully to exclude any previous neurological diseases, including traumatic brain injury, the possibility of a concomitant mild brain injury with SCI cannot fully be ruled out [Wei et al., 2008]. However, it has been generally postulated that the traumatic brain injury mechanism affects the largest axon bundles, of which the CC is a perfect example [Hulkower et al., 2013], while our results were concentrated in areas less severely affected by brain trauma. Additionally, the different types of medication and rehabilitation methods possibly adapted to various patients in our sample could influence the magnitude of neuroplasticity [Schallert et al., 2000] and cause slight bias when not controlled for. In general, numerous physical and mental factors can affect DTI results, and while these cannot all be controlled for, several known confounding factors were used as exclusion criteria for our subject pool.

In terms of clinical relevance and rehabilitation, the acute phase is the most crucial stage of SCI, and while studies on neuroplasticity mostly focus on the acute to sub-acute phase, our study focused on the chronic phase of SCI. Another concern is the large deviation of the mean TSI of our patient population, which could distort our results.

The fundamental microstructural mechanisms of neurodegeneration and plasticity are diverse, and the changes perceived by a single imaging modality are the combined effects of these mechanisms [Zatorre et al., 2013]. DTI alone is not sufficient to fully classify the mechanisms affecting WM post-SCI, and multimodal imaging would be preferred. In addition, glial processes are likely to be present in post-SCI cerebral WM [Keyvani and Schallert, 2002], and the presence of gliosis may cause increased FA values [Budde et al., 2011]. A known limitation of DTI is the crossing fibre problem, which may lead to anomalous DTI scalars in voxels containing neural tracts of different orientations [Wheeler-Kingshott and Cercignani, 2009]. While crossing fibres may be considered as a fixed attribute of DTI, a possible solution could be acquiring the data with a high angular resolution diffusion imaging (HARDI) suited imaging sequence [Berman et al., 2013; Frank, 2001; Tuch, 2004; Tuch et al., 2002]. However, no direct replacement for DTI scalars, mainly FA, as the measure for axonal integrity currently exist for HARDI and finding such a measure may prove time-consuming.

Future Prospects

Based on the results of our group comparison, future studies of the effects of SCI on the human brain WM should be extended outside the CST. Examining brain WM outside the sensorimotor tracts may also give a more thorough outlook on the link between neural structure and clinical function in chronic SCI. Nevertheless, additional evidence, especially longitudinal studies, is needed in the future to evaluate the presumptive change in DTI metrics with time after an acute injury and the association of that change with clinical recovery. This knowledge could facilitate the prognostication of recovery and our ability to understand and monitor the changes induced by treatment and rehabilitative interventions beyond clinical disability scales and conventional MRI. However, it should be noted that group-level research results are not directly applicable to individual clinical cases.

CONCLUSION

Patients with chronic SCI were found to show changes detectable with DTI in their cerebral WM, extending widely beyond the motor cortex and sensorimotor tracts, and those changes were associated with TSI and clinical parameters indicating the severity of injury. Primarily, the changes manifested as reduction of FA and increase of MD. Furthermore, DTI-measured WM integrity of chronic SCI patients altered as time elapsed since injury.

In the future, additional evidence, especially longitudinal studies from the acute stage of SCI, is required to evaluate the presumptive change in DTI values with time after injury and the association of that change with clinical recovery. Optimistically, DTI metrics could serve as adjunct biomarkers in the evaluation of an individual patient's susceptibility to different types of rehabilitative interventions.

CONFLICT OF INTEREST

The authors declare no conflicts of interest.

REFERENCES

Ahoniemi E, Alaranta H, Hokkinen E-M, Valtonen K, Kautiainen H (2008): Incidence of traumatic spinal cord injuries in Finland over a 30-year period. Spinal Cord 46:781–784.

Alexander AL, Lee JE, Lazar M, Field AS (2007): Diffusion tensor imaging of the brain. Neurotherapeutics 4:316–329. http://www.pubmedcentral.nih.gov/articlerender.fcgi?artid=2041910&tool=pmcentrez&rendertype=abstract.

Beaulieu C (2002): The basis of anisotropic water diffusion in the nervous system - a technical review. NMR Biomed 15:435–455.

Beirowski B, Adalbert R, Wagner D, Grumme DS, Addicks K, Ribchester RR, Coleman MP (2005): The progressive nature of Wallerian degeneration in wild-type and slow Wallerian degeneration (WldS) nerves. BMC Neurosci 6:6.

Berman JI, Lanza MR, Blaskey L, Edgar JC, Roberts TPL (2013): High angular resolution diffusion imaging probabilistic tractography of the auditory radiation. Am J Neuroradiol 34:1573–1578.

Budde MD, Janes L, Gold E, Turtzo LC, Frank JA (2011): The contribution of gliosis to diffusion tensor anisotropy and tractography following traumatic brain injury: Validation in the rat using Fourier analysis of stained tissue sections. Brain 134:2248–2260.

Buss A, Brook GA, Kakulas B, Martin D, Franzen R, Schoenen J, Noth J, Schmitt AB (2004): Gradual loss of myelin and formation of an astrocytic scar during Wallerian degeneration in the human spinal cord. Brain 127:34–44.

Chang Y, Jung T-D, Yoo DS, Hyun JK (2010): Diffusion tensor imaging and fiber tractography of patients with cervical spinal cord injury. J Neurotrauma 27:2033–2040.

Cohen-Adad J, El Mendili M-M, Lehericy S, Pradat P-F, Blancho S, Rossignol S, Benali H (2011): Demyelination and degeneration in the injured human spinal cord detected with diffusion and magnetization transfer MRI. Neuroimage 55:1024–1033.

Della Nave R, Ginestroni A, Diciotti S, Salvatore E, Soricelli A, Mascalchi M (2011): Axial diffusivity is increased in the degenerating superior cerebellar peduncles of Friedreich's ataxia. Neuroradiology 53:367–372.

DeVivo M, Biering-Sørensen F, Charlifue S, Noonan V, Post M, Stripling T, Wing P (2006): International Spinal Cord Injury Core Data Set. Spinal Cord 44:535–540. http://www.ncbi.nlm.nih.gov/pubmed/16955073.

Faria AV, Zhang J, Oishi K, Li X, Jiang H, Akhter K, Hermoye L, Lee SK, Hoon A, Stashinko E, Miller MI, van Zijl PCM, Mori S (2010): Atlas-based analysis of neurodevelopment from infancy to adulthood using diffusion tensor imaging and applications for automated abnormality detection. Neuroimage 52:415–428.

Florence SL, Taub HB, Kaas Jon H, Kaas JH (1998): Large-scale sprouting of cortical connections after peripheral injury in adult macaque monkeys. Science (80-) 282:1117–1121. http://www.ncbi.nlm.nih.gov/pubmed/9804549.

Frank LR (2001): Anisotropy in high angular resolution diffusion-weighted MRI. Magn Reson Med 45:935–939. http://www.ncbi.nlm.nih.gov/pubmed/11378869%5Cnhttp://onlinelibrary.wiley.com/store/10.1002/mrm.1125/asset/1125_ftp.pdf?v=1&t=hh7uma40&s=e80eb97a04934cad9917e3ef0a6b725024ce9fe2.

Freund P, Weiskopf N, Ward NS, Hutton C, Gall A, Ciccarelli O, Craggs M, Friston K, Thompson AJ (2011): Disability, atrophy and cortical reorganization following spinal cord injury. Brain 134:1610–1622.

Freund P, Wheeler-Kingshott C, Nagy Z, Gorgoraptis N, Weiskopf N, Friston K, Thompson AJ, Hutton C (2012): Axonal integrity predicts cortical reorganisation following cervical injury. J Neurol Neurosurg Psychiatry 83:629–637. http://www.ncbi.nlm.nih.gov/pubmed/22492214/.

Guleria S, Gupta RK, Saksena S, Chandra A, Srivastava RN, Husain M, Rathore R, Narayana PA (2008): Retrograde Wallerian degeneration of cranial corticospinal tracts in cervical spinal cord injury patients using diffusion tensor imaging. J Neurosci Res 86:2271–2280.

Gustin SM, Wrigley PJ, Siddall PJ, Henderson LA (2010): Brain anatomy changes associated with persistent neuropathic pain following spinal cord injury. Cereb Cortex 20:1409–1419.

Henderson LA, Gustin SM, Macey PM, Wrigley PJ, Siddall PJ (2011): Functional Reorganization of the Brain in Humans Following Spinal Cord Injury: Evidence for Underlying Changes

in Cortical Anatomy. J Neurosci 31:2630–2637. http://www.jneurosci.org/cgi/doi/10.1523/JNEUROSCI.2717-10.2011.

Hulkower MB, Poliak DB, Rosenbaum SB, Zimmerman ME, Lipton ML (2013): A decade of DTI in traumatic brain injury: 10 years and 100 articles later. Am J Neuroradiol 34:2064–2074.

Jurkiewicz MT, Mikulis DJ, McIlroy WE, Fehlings MG, Verrier MC (2007): Sensorimotor cortical plasticity during recovery following spinal cord injury: A longitudinal fMRI study. Neurorehabil Neural Repair 21:527–538.

Keller TA, Just MA (2016): Structural and functional neuroplasticity in human learning of spatial routes. Neuroimage 125: 256–266.

Keyvani K, Schallert T (2002): Plasticity-associated molecular and structural events in the injured brain. J Neuropathol Exp Neurol 61:831–840. http://www.ncbi.nlm.nih.gov/pubmed/12387449.

Kim BG, Dai H-N, McAtee M, Vicini S, Bregman BS (2006): Remodeling of synaptic structures in the motor cortex following spinal cord injury. Exp Neurol 198:401–415.

Kodiweera C, Alexander AL, Harezlak J, McAllister TW, Wu YC (2016): Age effects and sex differences in human brain white matter of young to middle-aged adults: A DTI, NODDI, and q-space study. Neuroimage 128:180–192. https://doi.org/10.1016/j.neuroimage.2015.12.033.

Koskinen E, Brander A, Hakulinen U, Luoto T, Helminen M, Ylinen A, Ohman J (2013): Assessing the state of chronic spinal cord injury using diffusion tensor imaging. J Neurotrauma 30: 1587–1595. http://www.ncbi.nlm.nih.gov/pubmed/23758292.

Koskinen E, Hakulinen U, Brander A, Luoto TM, Ylinen A, Ohman JE (2014): Clinical correlates of cerebral diffusion tensor imaging findings in chronic traumatic spinal cord injury. Spinal Cord 1–7. http://www.ncbi.nlm.nih.gov/pubmed/24418961.

Metwalli NS, Benatar M, Nair G, Usher S, Hu X, Carew JD (2010): Utility of axial and radial diffusivity from diffusion tensor MRI as markers of neurodegeneration in amyotrophic lateral sclerosis. Brain Res 1348:156–164.

Nudo R, Plautz EJ, Frost SB (2001): Role of adaptive plasticity in recovery after damage to motor cortex. Muscle Nerve 24: 1000–1019.

Petersen J. a, Wilm BJ, von Meyenburg J, Schubert M, Seifert B, Najafi Y, Dietz V, Kollias S (2012): Chronic cervical spinal cord injury: DTI correlates with clinical and electrophysiological measures. J Neurotrauma 29:1556–1566. http://www.ncbi.nlm.nih.gov/pubmed/22150011.

Ramu J, Herrera J, Grill R, Bockhorst T, Narayana P (2008): Brain fiber tract plasticity in experimental spinal cord injury: Diffusion tensor imaging. Exp Neurol 212:100–107.

Roosendaal SD, Geurts JJG, Vrenken H, Hulst HE, Cover KS, Castelijns JA, Pouwels PJW, Barkhof F (2009): Regional DTI differences in multiple sclerosis patients. Neuroimage 44:1397–1403.

Sagi Y, Tavor I, Hofstetter S, Tzur-Moryosef S, Blumenfeld-Katzir T, Assaf Y (2012): Learning in the Fast Lane: New Insights into Neuroplasticity. Neuron 73:1195–1203. https://doi.org/10.1016/j.neuron.2012.01.025.

Schallert T, Leasure JL, Kolb B (2000): Experience-Associated Structural Events, Subependymal Cellular Proliferative Activity, and Functional Recovery After Injury to the Central Nervous System. J Cereb Blood Flow Metab 20:1513–1528. http://jcb.sagepub.com/content/20/11/1513.long.

Sen PN, Basser PJ (2005): A model for diffusion in white matter in the brain. Biophys J 89:2927–2938.

Smith S, Jenkinson M, Woolrich M, Beckmann C, Behrens T, Johansen-Berg H, Bannister P, De Luca M, Drobnjak I, Flitney D, Niazy R, Saunders J, Vickers J, Zhang Y, De Stefano N, Brady J, Matthews P (2004): Advances in functional and structural MR image analysis and implementation as FSL. Neuroimage 23 Suppl 1:S208–S219. http://www.ncbi.nlm.nih.gov/pubmed/15501092.

Smith SM, Jenkinson M, Johansen-Berg H, Rueckert D, Nichols TE, Mackay CE, Watkins KE, Ciccarelli O, Cader MZ, Matthews PM, Behrens TEJ (2006): Tract-based spatial statistics: Voxelwise analysis of multi-subject diffusion data. Neuroimage 31:1487–1505.

Smith SM, Nichols TE (2009): Threshold-free cluster enhancement: Addressing problems of smoothing, threshold dependence and localisation in cluster inference. Neuroimage 44:83–98.

Song S-K, Sun S-W, Ramsbottom MJ, Chang C, Russell J, Cross AH (2002): Dysmyelination Revealed through MRI as Increased Radial (but Unchanged Axial) Diffusion of Water. Neuroimage 17:1429–1436. http://www.sciencedirect.com/science/article/pii/S105381190291267X.

Steele CJ, Bailey JA, Zatorre RJ, Penhune VB (2013): Early musical training and white-matter plasticity in the corpus callosum: Evidence for a sensitive period. J Neurosci 33:1282–1290.

Tuch DS (2004): Q-ball imaging. Magn Reson Med 52:1358–1372.

Tuch DS, Reese TG, Wiegell MR, Makris N, Belliveau JW, Van Wedeen J (2002): High angular resolution diffusion imaging reveals intravoxel white matter fiber heterogeneity. Magn Reson Med 48:577–582.

Waring WP, Biering-Sorensen F, Burns S, Donovan W, Graves D, Jha A, Jones L, Kirshblum S, Marino R, Mulcahey MJ, Reeves R, Scelza WM, Schmidt-Read M, Stein A (2010): 2009 Review and Revisions of the International Standards for the Neurological Classification of. Spinal Cord Injury. J Spinal Cord Med 33: 346–352.

Wei CW, Tharmakulasingam J, Crawley A, Kideckel DM, Mikulis DJ, Bradbury CL, Green RE (2008): Use of Diffusion-Tensor Imaging in Traumatic Spinal Cord Injury to Identify Concomitant Traumatic Brain Injury. Arch Phys Med Rehabil 89: S85–S91. https://doi.org/10.1016/j.apmr.2008.07.005.

Westlye LT, Walhovd KB, Dale AM, Bjørnerud A, Due-Tønnessen P, Engvig A, Grydeland H, Tamnes CK, Østby Y, Fjell AM (2010): Life-span changes of the human brain white matter: Diffusion tensor imaging (DTI) and volumetry. Cereb Cortex 20:2055–2068.

Wheeler-Kingshott CAM, Cercignani M (2009): About "axial" and "radial" diffusivities. Magn Reson Med 61:1255–1260.

Winkler AM, Ridgway GR, Webster MA, Smith SM, Nichols TE (2014): Permutation inference for the general linear model. Neuroimage 92:381–397.

Wrigley PJ, Gustin SM, Macey PM, Nash PG, Gandevia SC, Macefield VG, Siddall PJ, Henderson LA (2009): Anatomical changes in human motor cortex and motor pathways following complete thoracic spinal cord injury. Cereb Cortex 19:224–232.

Yamamoto T, Yamasaki M, Imai T (1989): Retrograde pyramidal tract degeneration in a patient with cervical haematomyelia. J Neurol Neurosurg Psychiatry 52:382–386. http://www.ncbi.nlm.nih.gov/pmc/articles/PMC1032415/.

Zatorre RJ, Fields R, Johansen-Berg H (2013): Plasticity in Gray and White : Neuroimaging changes in brain structure during learning. Nat Neurosci 15:528–536.

PUBLICATION III

Automated Pipeline for Brain ROI Analysis with Results Comparable to Previous Freehand Measures in Clinical Settings

Ilvesmäki T, Hakulinen U, Eskola H.

Original publication channel (IFMBE Proceedings 65, 635-638)
Doi: 10.1007/978-981-10-5122-7_159

Automated Pipeline for Brain ROI Analysis with Results Comparable to Previous Freehand Measures in Clinical Settings

T. Ilvesmäki[1,2], U. Hakulinen[1,3,4] and H. Eskola[1,3]

[1] BioMediTech Institute and Faculty of Biomedical Sciences and Engineering, Tampere University of Technology, Tampere, Finland
[2] Department of Medical Physics, Turku University Hospital, Turku, Finland
[3] Department of Radiology, Medical Imaging Centre of the Pirkanmaa Hospital District, Tampere, Finland
[4]Department of Medical Physics, Medical Imaging Centre of the Pirkanmaa Hospital District, Tampere, Finland

Abstract—**Diffusion tensor imaging (DTI) has become a relatively common MR imaging technique in only 10 years. DTI can provide important information of brain microstructure *in vivo*. Many quantitative DTI analysis methods utilize either region of interest (ROI) or voxel-wise whole-brain methods. ROI methods do not require potentially bias-inducing image data altering, e.g., resampling and smoothing, and are the preferred method in clinical settings. We present an automated pipeline for quantitative ROI analysis of brain DTI data. The pipeline includes pre-processing, registrations, and calculation of mean (and SD) DTI scalar values from the automated ROIs. In addition to atlas regions, the pipeline accepts freehand ROIs, as long as the frame of reference is also provided. By the uniquely designed pipeline, we ensure that the results can be retrospectively compared to previously conducted manual freehand ROI measurement results, if desired. We validated the feasibility of the pipeline by comparing manual freehand ROI measurement results from 40 subjects against the results obtained from automated ROIs. A single set of freehand ROIs (drawn similarly to the original freehand manual ROIs in the population) was input to the pipeline, and the resulting scalar values from the automated ROIs were compared to the manual freehand ROIs' data. Adopting a limit for goodness of fit of z = ± 1.6 resulted in 94 % success rate for the pipeline's automated ROI registrations in the whole population. The pipeline can reduce the time taken in clinical ROI measurements.**

Keywords— **DTI, image analysis, pipeline, atlas, ROI**

I. Introduction

The amount of research focusing on the use of diffusion tensor imaging (DTI) has rapidly increased since the beginning of the 21st century. DTI has the potential to noninvasively quantify water diffusion in microscopic structures, essentially providing a method for observing changes in the neural network [1]. A potentially unlimited set of scalars can be calculated from the obtained diffusion tensor data, but currently the most used diffusion scalars are fractional anisotropy (FA) and mean diffusivity (MD), with the more recent addition of axial diffusivity (AD) and radial diffusivity (RD). These scalars can be more or less linked to certain pathologies (e.g. demyelination or axonal degeneration), but especially the interpretation of AD and RD is still slightly debatable [1, 2].

Most common methods used in quantitative analysis of diffusion images are region of interest (ROI), tractography, and voxel-wise whole-brain analysis [3]. Each method has its flaws; ROI method is susceptible to intra- and inter-observer variability, tractography is slightly unreliable and hard to delineate, whereas whole-brain methods rely on image registration and smoothing, a potential source of bias [4, 5].

Various procedures have been suggested to overcome these problems, such as atlas-based ROI analyses, and tract-based spatial statistics for whole-brain approach. Atlas-based image analysis has been successfully applied as an alternative to manual ROI studies [6–8], but the results of these analyses are not comparable to previously conducted manual ROI studies due to the shape differences of the ROIs themselves. Additionally, registration to a standard template may introduce a bias to the atlas-based ROI analyses.

The purpose of this study is to create an automated ROI analysis pipeline, which can produce quantitative ROI data comparable to previously conducted manual freehand ROI measurements. In addition, the pipeline is capable to utilize atlas-based ROIs, which can be of clinical use after a solid normal value database has been established for the atlas regions.

Additionally, we aim to validate the compatibility of the method with manual freehand ROI measurement results by comparing quantitative DTI metric values between the manual freehand and automated ROIs.

II. Materials and Methods

A. Pipeline

The pipeline created for the analysis can be fully automated from the pre-processing step to the extraction of quantitative diffusion metrics. Only minimal user involvement is required in the process, and the most important measure is to visually inspect the accuracy of the automated ROIs. The statistical analysis process can be altered, and a multitude of

analyses can be performed based on the extracted quantitative image data. The pipeline uses tools included in FSL [9, 10] for pre-processing, registration, and the extraction of quantitative metrics from the ROIs.

We executed the automated ROI analysis by using a single set of manual freehand ROIs. The manual ROIs and the FA map (frame of reference) were fed to the pipeline. We used the control subject pool (n = 40) as the data to be analyzed, and no patient subject was chosen in the analysis for the validation process.

Pre-processing: First the control subject image data were corrected for eddy currents and minor head movements, and a brain mask was created to remove any non-brain tissue from the data. After brain masking, the scalar diffusion data was calculated from the tensor data. After the pre-processing steps, the diffusion metric data (FA, MD, AD and RD maps) is ready for the analysis.

Regions of Interest: The set of ROIs used in our research were manually drawn on the JHU-DTI-SS "Eve" atlas [8] FA map, which was first resampled to the spatial resolution of the acquired control DTI data to simulate the original manual freehand ROI drawing process. The drawn manual freehand ROIs were converted back to the original space of the high resolution JHU FA map by inverse transformation. The ROIs used in the validation were: the genu of the corpus callosum (CC_g), the splenium of the corpus callosum (CC_s), the cerebral peduncle (CP), the posterior limb of internal capsule (PLIC), the corona radiata (CR), the centrum semiovale (CS), the uncinate fasciculus (UF), the forceps minor (FM), and the thalamus. Examples of the ROIs are shown in Fig. 1. Due to image slice orientations, identical ROI regions are not visible on subject 1 and the JHU FA map. Also, the atlas ROIs differ substantially from the freehand based automated ROIs.

All of the manual ROIs were drawn by the same person (U.H.) in order to minimize ROI variability.

Registration: In order to extract values from each individual subject, the manual freehand ROI set was transferred to each subject's native space. First, the frame of reference was linearly registered (FLIRT [11]) to each subject, followed by a nonlinear transformation (FNIRT [12]). The affine registration matrices and the nonlinear registration warp fields were saved for each subject, which were then applied to the ROIs. This effectively placed the ROIs in the desired locations for each individual subject.

In order to improve the ROI accuracy, trilinear interpolation was used in the transformations (instead of nearest-neighbour interpolation often used in ROI registrations). The registered ROIs were then transformed back into binary masks by thresholding them at > 0.15, which produced good results based on visual evaluation (i.e. good accuracy, no overlapping, or too small ROIs). The threshold may differ depending on the used ROIs.

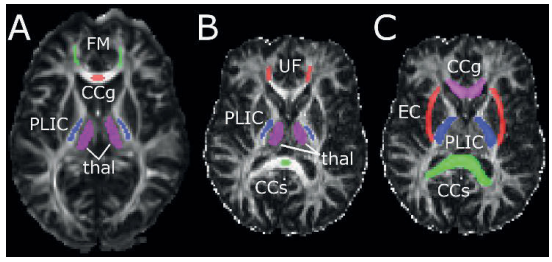

Fig. 1 A: Manual freehand ROIs drawn by U.H. on the JHU-DTI-SS FA map: FM (green), CC_g (red), PLIC (blue), thalamus (magenta). B: Corresponding slice of subject 1 with automated ROIs: UF (red), PLIC (blue), thalamus (magenta), CC_s (green). C: Same slice of subject 1 with automated atlas ROIs: CC_g (magenta), external capsule (red, EC), PLIC (blue), CC_s (green).

Quantitative Analysis: Once the ROIs were transferred to the subjects' space, quantitative DTI metrics were derived from the automated ROIs. Mean FA, MD, RD, and AD values along with standard deviations were calculated for each ROI, for each subject.

The extracted quantitative data can be fed to a statistical software of choice. For research and method validation purposes we collected FA data in a table to compare it with the freehand ROI data collected by U.H.

B. Validation

In order to validate the feasibility of the automated registration step, we compared the automated ROI data obtained through our pipeline to that of the manual freehand ROI measurements. The ROIs' congruency was validated by comparing the manual freehand ROI mean FA values against the pipeline's automated ROI mean FA values. In addition, we tested the difference between the automated ROIs and the manual freehand ROIs by z-scores and a two-tailed t-test. Assuming the ROI voxel values are normally distributed is debatable, but due to the representation of the results, a Mann-Whitney U test could not be performed. The resulting p-value from the t-test is thus only an approximate indication of the possible statistically significant difference.

C. Imaging Data

The DTI data used in the validation of our pipeline consisted of 40 control subjects imaged in the Tampere University Hospital. The subjects were originally gathered as a control group for the Tampere Traumatic Head and Brain Injury Study between August 2010 and July 2012.

Head MRI was done with a 3 Tesla MRI scanner, using a 12-channel head matrix coil. The DTI data were collected by a single-shot, spin echo-based and diffusion-weighted echo

planar imaging sequence. The parameters for the DTI sequence were TR 5144 ms, TE 92 ms, field of view 230 mm, matrix 128 × 128, 3 averages, slice/gap 3.0/0.9 mm, voxel dimension of 1.8 × 1.8 × 3.0 mm, and two b-factors: 0 and 1000 s/mm2 with 20 diffusion gradient orientations.

Conventional MRI findings of the control subjects were interpreted as normal.

III. Results

The described pipeline was applied to the control subject pool, and the utilization value of the pipeline was evaluated with respect to automated ROI compatibility with manual freehand ROI measurements. Additionally, the pipeline was executed with atlas ROIs, but the obtained quantitative data could not be plausibly validated.

A. Freehand ROI

The manual freehand ROIs drawn by U.H. to the low resolution JHU-DTI-SS FA map were transformed to the native resolution of the atlas, and the FA map and the ROIs were then used to run the described pipeline.

We visually inspected the automated ROIs and altered the pipeline parameters iteratively in order to gain adequate registration results for the current dataset. Mean and SD values were then extracted from the ROIs and saved to a table for comparison. Due to the large amount of data, we chose four example subjects to be reported in the paper. The registration validation data for FA of the four subjects is shown in Table 1.

We compared the subjects' automated ROIs' mean FA values, and used z-scores and a statistical t-test to evaluate the accuracy of the pipeline. The SD values used in the calculations were taken from the manual freehand ROIs. We adapted a z-score of 1.6 as a limit for significant difference. Z-values over 1.6 are highlighted with an asterisk in the table, along with p-values less than 0.05, but the significance of the t-test is slightly questionable. The ROIs with best correspondence were the PLIC (mean absolute difference in the population 2.9 %) and CC_s (mean absolute difference in the population 3.9 %). The ROIs with the poorest correspondence were the CP (mean absolute difference in the population 9.5 %) and the CR (mean absolute difference in the population 9.2 %). Of all the ROIs (n=360), a total of 338 had FA values within the limit of $-1.6 < z < 1.6$, which can be considered as a 94 % success rate of the registration. The mean absolute difference in FA across all ROIs and subjects was 6.6 %, and the mean absolute z-value was 0.581.

Table 1 Manual freehand ROI vs. pipeline's automated ROI comparison for FA values. Manual freehand ROI values are considered as reference.

	Subject 1	Subject 2	Subject 3	Subject 4
Age	32	56	22	39
CC genu				
Difference (rel, %)	-5,0	-2,9	-1,1	1,8
Z-value	-0,793	-0,336	-0,218	0,165
P-value	0,020*	0,544	0,534	0,513
CC splenium				
Difference (rel, %)	-2.6	2,4	-8,1	2,7
Z-value	-0,338	0,325	-1,154	0,694
P-value	0,363	0,334	0,001*	0,152
Cerebral peduncle				
Difference (rel, %)	-0,4	-11,2	-0,7	-5,1
Z-value	-0,040	-1,740*	-0,095	-0,415
P-value	0,883	0,001*	0,808	0,160
Corona radiata				
Difference (rel, %)	28,6	3,9	23,9	7,4
Z-value	1,975*	0,261	1,764*	0,387
P-value	< 0,001*	0,092	< 0,001*	0,016*
Centrum semiovale				
Difference (rel, %)	0,3	-4,8	0,1	0,5
Z-value	0,019	-0,276	0,004	0,028
P-value	0,868	0,058	0,974	0,826
Forceps minor				
Difference (rel, %)	-1,5	4,7	-20,6	6,2
Z-value	-0,081	0,233	-1,508	0,276
P-value	0,787	0,546	< 0,001*	0,331
PLIC				
Difference (rel, %)	7,6	-1,7	2,4	4,0
Z-value	0,607	-0,162	0,173	0,364
P-value	0,001*	0,375	0,320	0,053
Thalamus				
Difference (rel, %)	-1,3	-2,4	-6,0	-2,5
Z-value	-0,046	-0,089	-0,238	-0,109
P-value	0,677	0,447	0,046*	0,405
Uncinate fasciculus				
Difference (rel, %)	-14,2	6,1	2,4	-0,2
Z-value	-1,054	0,335	0,122	-0,013
P-value	< 0,001*	0,214	0,574	0,957

*) Significant difference.

B. Atlas Based

In addition to the freehand ROIs, we ran the pipeline using the ICBM-DTI-81 white matter atlas regions. While it is not possible to straightforwardly validate the registration and

DTI metric accuracy of the atlas regions, we visually verified the registration accuracy, and reviewed the standard deviation of each atlas region ROI. We compared the atlas ROIs' deviation against the manual freehand ROIs' SD. The mean SD for all the automated atlas FA ROIs was 28.1 %, whereas the automated freehand ROIs had a mean SD of 13.8 %.

IV. Discussion

Though the pipeline is configured for both manual freehand ROI and atlas usage, further validation and mirroring to previous measurements needs to be done prior to clinical use in both cases. An alternative clinical application could be use of the registration step to speed up freehand ROI drawing. Due to the accuracy of the automated ROIs with respect to the manual freehand ROIs, the registration step alone could save a considerable amount of time in clinical ROI measurements.

While the registration seems reasonably accurate, alternative methods should be studied in the future. Especially in pathologic cases, the lowered FA values may confound the registration. Tensor based registration (DTI-TK) might improve the accuracy of the pipeline with DTI data [13]. The registration accuracy should also be validated through the ROIs themselves in the future, e.g., by overlap percentage or other segmentation comparison metrics.

The high SD obtained from the atlas ROIs could indicate either low SNR, or inclusion of grey matter inside caused by bad registration. This may imply that the use of freehand ROIs in the pipeline would be more robust. Although, due to the notably larger size of the atlas ROIs, the difference in SD cannot be so straightforwardly interpreted.

In the future, we aim to create a standard value library based on a normal population. The standard values would first be collected based on the clinic specific manual freehand ROIs, but also on the ICBM-DTI-81 atlas later on. The automated freehand ROIs can be validated through previous ROI measurement results, and the possible future studies utilizing our pipeline will be comparable to previously conducted clinical ROI studies. Use of the pipeline in clinical settings at Tampere University Hospital will be researched.

V. Conclusions

We have presented and validated the accuracy of an automated pipeline for quantitative ROI analysis. What makes the pipeline unique is its compatibility to previous manual ROI analysis results within a clinic.

Acknowledgment

The authors are grateful to Juha Öhman and Teemu Luoto (Tampere University Hospital) for providing the diffusion imaging data for our research.

Funding for this work was provided by the Finnish Cultural Foundation as a personal research grant to T.I.

Conflict of Interest

The authors declare that they have no conflict of interest.

References

1. Alexander AL, Lee JE, Lazar M, Field AS (2007) Diffusion tensor imaging of the brain. Neurotherapeutics 4:316–29. doi: 10.1016/j.nurt.2007.05.011
2. Wheeler-Kingshott CAM, Cercignani M (2009) About "axial" and "radial" diffusivities. Magn Reson Med 61:1255–1260. doi: 10.1002/mrm.21965
3. Hulkower MB, Poliak DB, Rosenbaum SB, et al (2013) A decade of DTI in traumatic brain injury: 10 years and 100 articles later. Am J Neuroradiol 34:2064–2074. doi: 10.3174/ajnr.A3395
4. Hakulinen U, Brander A, Ryymin P, et al (2012) Repeatability and variation of region-of-interest methods using quantitative diffusion tensor MR imaging of the brain. BMC Med Imaging 12:30. doi: 10.1186/1471-2342-12-30
5. Farquharson S, Tournier J-D, Calamante F, et al (2013) White matter fiber tractography: why we need to move beyond DTI. J Neurosurg 118:1367–77. doi: 10.3171/2013.2.JNS121294
6. Wang Y, Gupta A, Liu Z, et al (2011) DTI registration in atlas based fiber analysis of infantile Krabbe disease. Neuroimage 55:1577–1586. doi: 10.1016/j.neuroimage.2011.01.038
7. Radoeva PD, Coman IL, Antshel KM, et al (2012) Atlas-based white matter analysis in individuals with velo-cardio-facial syndrome (22q11.2 deletion syndrome) and unaffected siblings. Behav Brain Funct 8:38. doi: 10.1186/1744-9081-8-38
8. Oishi K, Faria A, Jiang H, et al (2009) Atlas-based whole brain white matter analysis using large deformation diffeomorphic metric mapping: application to normal elderly and Alzheimer's disease participants. Neuroimage 46:486–499.
9. Woolrich MW, Jbabdi S, Patenaude B, et al (2009) Bayesian analysis of neuroimaging data in FSL. Neuroimage 45:S173-86. doi: 10.1016/j.neuroimage.2008.10.055
10. Jenkinson M, Beckmann CF, Behrens TEJ, et al (2012) FSL. Neuroimage 62:782–790. doi: 10.1016/j.neuroimage.2011.09.015
11. Jenkinson M, Bannister P, Brady M, Smith S (2002) Improved optimization for the robust and accurate linear registration and motion correction of brain images. Neuroimage 17:825–841.
12. Andersson JLR, Jenkinson M, Smith S (2007) Non-linear registration aka Spatial normalisation FMRIB Technial Report TR07JA2. In Pract 22.
13. Wang Y, Shen Y, Liu D, et al (2017) Evaluations of diffusion tensor image registration based on fiber tractography. Biomed Eng Online 16:9. doi: 10.1186/s12938-016-0299-2

Author: Tero Ilvesmäki
Institute: Tampere University of Technology
Country: Finland
Email: tero.ilvesmaki@student.tut.fi

PUBLICATION IV

A Robust Quantitative Diffusion Tensor Analysis Method: Application to Ageing and Mild Traumatic Brain Injury

Ilvesmäki T, Luoto TM, Hakulinen U, Panenka WJ, Terry DP, Iverson GL, Brander A, Öhman J, Eskola H.

Unpublished manuscript

Corresponding author: Tero Ilvesmäki

A Robust Quantitative Diffusion Tensor Analysis Method: Application to Ageing and Mild Traumatic Brain Injury

Tero Ilvesmäki

BioMediTech Institute and Faculty of Biomedical Sciences and Engineering, Tampere University of Technology, Tampere, Finland

Teemu Luoto

Department of Neurosurgery, Tampere University Hospital, Tampere, Finland

Ullamari Hakulinen

Department of Radiology, Medical Imaging Center of Pirkanmaa Hospital District

BioMediTech Institute and Faculty of Biomedical Sciences and Engineering, Tampere University of Technology, Tampere, Finland

Department of Medical Physics, Medical Imaging Center of Pirkanmaa Hospital District Tampere, Finland.

William J. Panenka

British Columbia Neuropsychiatry Program, Department of Psychiatry, University of British Columbia, Vancouver, BC, Canada

Douglas P Terry

Massachusetts General Hospital, Department of Physical Medicine and Rehabilitation, Department of Psychiatry

Corresponding author: Tero Ilvesmäki

Grant L. Iverson

Department of Physical Medicine and Rehabilitation, Harvard Medical School; & Red Sox Foundation and Massachusetts General Hospital Home Base Program, Boston, Massachusetts, USA

Antti Brander

Department of Radiology, Medical Imaging Centre of the Pirkanmaa Hospital District, Tampere, Finland

Hannu Eskola

BioMediTech Institute and Faculty of Biomedical Sciences and Engineering, Tampere University of Technology, Tampere, Finland

Department of Radiology, Medical Imaging Centre of the Pirkanmaa Hospital District, Tampere, Finland

Corresponding author: Tero Ilvesmäki, tero.ilvesmaki@student.tut.fi

Short title: Robust quantitative DTI brain analysis

Corresponding author: Tero Ilvesmäki

ACKNOWLEDGEMENTS

Partial financial support for this research was provided by a personal research grant from the Finnish Cultural Foundation to T.I. Conflict of interest: The authors declare no conflicts of interest.

Corresponding author: Tero Ilvesmäki

ABSTRACT

Freehand region of interest brain analysis is laborious and time-consuming, with limited reproducibility even with substantial expertise. We attempted to overcome the issue with an automated analysis pipeline, and by modelling normal population diffusion metrics. We describe an automated analysis method that can be used to (i) create a scanner-specific normal population model and (ii) to analyse individual diffusion data by comparing it against the model. We registered atlas-based regions of interest separately to each participant. Mean diffusion metrics of the registered regions were calculated for each participant and then used in the analysis. Our model was most successful when we applied the Johns Hopkins University probabilistic diffusion brain atlas to a normal sample of 70 participants with a mean age of 39.5 ± 11.8 years. Linear regression models between age and fractional anisotropy were statistically significant ($p < .05$) in each of the atlas brain region, and in majority of the regions between other diffusivity measures. Additionally, we analysed ten mild traumatic brain injury patients by comparing each against our normal model. Compared to freehand analysis, our automated method showed a greater number of abnormal regions in the mild traumatic brain injury patients. The automated analysis method is promising and may be applicable in clinical research with minor refinements.

Keywords: Diffusion Tensor Imaging; Neuroimaging; Image Processing, Computer-Assisted; Regression Analysis; Brain Concussion

INTRODUCTION

There is enormous interest in using diffusion tensor imaging (DTI) to draw inferences about the integrity of white matter in the human brain. Numerous published studies have examined brain microstructure using DTI in people with (i) neurological disorders and neurodegenerative diseases, such as amnestic mild cognitive impairment (Yu, Lam, & Lee, 2017), Parkinson's disease (Atkinson-Clement, Pinto, Eusebio, & Coulon, 2017), and traumatic brain injuries (TBI) (Wallace, Mathias, & Ward, 2018); (ii) neurodevelopmental conditions, such as attention-deficit/hyperactivity disorder (ADHD) (Aoki, Cortese, & Castellanos, 2018), dyslexia (Moreau, Stonyer, McKay, & Waldie, 2018), and autism spectrum disorder (Di, Azeez, Li, Haque, & Biswal, 2018); (iii) general medical conditions such as hypertension (Power et al., 2017), metabolic syndrome (Alfaro et al., 2018), and HIV infection (O'Connor, Jaillard, Renard, & Zeffiro, 2017); and (iv) psychiatric disorders such as depression (Jiang et al., 2017; Kambeitz et al., 2017) and posttraumatic stress disorder (Siehl, King, Burgess, Flor, & Nees, 2018).

DTI metrics quantify the directional coherence of water diffusion in tissue using magnetic resonance imaging (MRI) sequences. DTI metrics commonly reported in the literature include fractional anisotropy (FA), mean diffusivity (MD), radial diffusivity (RD), and axial diffusivity (AD). FA is a measure of the diffusion anisotropy and AD can be considered as a measure of diffusion along the main fibre axis. RD is believed to reflect the total diffusion perpendicular to the main fibre axis. RD and AD are thus orthogonal metrics. MD is a measure of total diffusion in all directions. FA and MD are composite metrics that are derived from combinations of RD and AD, and MD will increase if either RD or AD increase.

Image registration is an essential part of most standard DTI brain analysis pipelines. In this post-processing step, scans acquired in one space (e.g., individual patient space) are converted to a different space (e.g., a common atlas space) through a series of transformations. Image registration process can introduce bias to the results through imperfect registration or possibly even due to

excessive blurring caused by over smoothing. Some investigators will examine DTI metrics of the brain inside specific structures, regions of interest (ROI). Manually performed ROI measurements in native space obviate the need for image registration, but the process can be laborious, time-consuming, and have low inter-rater reproducibility (Hakulinen et al., 2012). Various different approaches have been suggested to reduce or eliminate the bias introduced by image data registration. While most attempts to reduce the registration bias have focused on enhancing the registration methods (De Groot et al., 2013; Newlander, Chu, Sinha, Lu, & Bartzokis, 2014; Schwarz et al., 2014; Wang et al., 2011, 2017), there are also those who approach the problem differently. Suri et al. (2015) used a participant-based registration approach where all the control participants were registered to the patient instead of to a common template. Radoeva et al. (Radoeva et al., 2012) studied velo-cardio-facial syndrome by successfully applying a method where they registered ROIs to the study participants, instead of registering the participants' image data to a ROI template. Applying the registration matrices to the atlas ROIs instead of the participant image data eliminates bias associated with image registrations and may be a better approach.

To create an objective and reproducible method for quantitative human brain DTI analysis, we chose to pursue a method that would require minimal end-user interaction. In addition, because we intend for the method to be robust to a wide range of clinical scenarios, we strived to create a method independent of the initial chosen ROI set. Our method transfers the chosen ROI set to the current participant's native space, leaving the participant's brain data spatially unmodified. In theory, any quantitative diffusion measures can be used for the required analyses. The mean DTI scalar value is calculated if the ROI volume is deterministic, or a weighted average of the DTI scalar value is calculated if the ROI is probabilistic. This type of approach allows the user to rapidly compare an individual participant's diffusion metrics against normal population DTI metrics in order to infer pathology.

Reference values are essential for testing of pathologies, and therefore it is compulsory to create a normal value model to compare the patient's DTI values against. A large sample of control

participants is required for accurate age-dependent reference value ranges, and should be collected for possible diagnostic purposes. Cox et al. (Cox et al., 2016) studied the ageing human brain and attempted to create quantitative models relative to brain WM microstructure. They used a pool of 3513 participants from the UK biobank resource, which allowed them to derive accurate and statistically powerful models of the associations between demographical factors and DTI metrics. We compared our results to the findings of Cox et al. in attempt to further validate our findings.

The purpose of this study was to (i) partially replicate the recent findings of Cox et al. (Cox et al., 2016) of white matter (WM) age associations, (ii) create a preliminary age-dependant human brain WM DTI model that is applicable applied in native participant space, and (iii) test the model's diagnostic accuracy in a small sample of people who have sustained mild TBIs. There are dozens of published studies relating to DTI findings following MTBI in athletes, civilians, active duty service members, and veterans (Asken, DeKosky, Clugston, Jaffee, & Bauer, 2018; Oehr & Anderson, 2017; Wallace et al., 2018). Moreover, there is considerable interest in techniques that would allow researchers or clinicians to examine DTI metrics in individual participants and determine if those participants show evidence of possible hetero-spatial changes in brain microstructure.

MATERIALS AND METHODS

Participants

The control participants were 70 people originally from two separate groups of DTI study controls, imaged at the Tampere University Hospital (age M = 39.5, SD = 11.8, Range = 18 – 60; 58.6% women). Forty were orthopedically injured patients evaluated in the emergency department of the Tampere University Hospital and were used in our previous study (Ilvesmäki et al., 2014). The other 30 control participants consisted of volunteer hospital staff members. The combined group of 70 control participants was also used in a previous study (Ilvesmäki et al., 2017). All control participants completed a structured health questionnaire and they did not report a chronic neurological or psychiatric disease. All participants were scanned using the same scanner and

imaging protocol. Conventional MRI findings of the control participants were interpreted as normal by a neuroradiologist (A.B.). All participants included in this study provided written informed consent according to the Declaration of Helsinki. To compare our automated algorithm against a ROI method, we selected 10 patients with mTBIs including five complicated and five uncomplicated cases from the pool of mTBI patients used in one of our previous studies (Ilvesmäki et al., 2014). Patients with a complicated mTBI were defined as having traumatic lesions on conventional brain MRI. Demographics for the participant groups used in this study are presented in Table 1.

Imaging

Brain MRI images were acquired using a 3 Tesla MRI scanner (Siemens Trio, Siemens AG Medical Solutions, Erlangen, Germany). The MRI protocol included sagittal T1- weighted 3D inversion recovery prepared gradient echo, axial T2 turbo spin echo, conventional axial and high-resolution sagittal FLAIR, axial T2*, axial SWI (susceptibility weighted imaging), and DWI (diffusion weighted imaging) series. The DTI data were collected by a single-shot, spin echo-based and diffusion-weighted echo planar imaging sequence. The parameters of the DTI sequence were TR 5144 ms, TE 92 ms, FOV (field of view) 230 mm, matrix 128 × 128, 3 averages, slice/gap 3.0/0.9 mm, and voxel dimension of 1.8 × 1.8 × 3.0 mm. Two diffusion weightings were used; b-value 0 and 1000 s/mm^2, with 20 diffusion gradient orientations. A 12-channel head matrix coil was used.

Image Processing and Analysis

The acquired image data was converted to the Neuroimaging Informatics Technology Initiative (Nifti) format for the analysis using MRIConvert 2.0.7. The data was corrected for eddy currents and possible motion artefacts. Diffusion tensor data, including FA, MD, AD, and RD, were derived from the original diffusion gradient images. No further modifications were made to the participant MR images. Image manipulations were executed entirely with tools included in FSL (v5.0.10) (Jenkinson, Beckmann, Behrens, Woolrich, & Smith, 2012), allowing us to create a simple and relatively easy implementation of the process.

In addition to the acquired imaging data, we used two probabilistic adult human brain WM atlases in our analysis: the Johns Hopkins University (JHU) DTI atlases (Hua et al., 2008; Oishi et al., 2008) and the Illinois Institute of Technology (IIT) Human Brain atlas (v. 4.1) (Zhang & Arfanakis, 2018). Specifically, we used the JHU WM tractography atlas (20 ROIs) in conjunction with the 1 mm isotropic mean FA map, including the following ROIs: anterior thalamic radiation (left and right hemispheres), corticospinal tract [CST; Left (L) & Right (R)], cingulate gyrus (L & R), hippocampal portion of the cingulum (L & R), forceps major, forceps minor, inferior fronto-occipital fasciculus (IFOF; L & R), inferior longitudinal fasciculus (ILF; L & R), superior longitudinal fasciculus (SLF; L & R), uncinate fasciculus (UF; L & R), and temporal part of the SLF (L & R). We used the IIT major fibre-bundles (17 ROIs) with the IIT mean FA map as the base, including the following ROIs: forceps major, forceps minor, fornix, cingulate gyrus (L & R), hippocampal portion of the cingulum (L & R), CST (L & R), IFOF (L & R), ILF (L & R), SLF (L & R), and UF (L & R).

The atlas ROI volumes were transferred to the participant's native space via affine and deformable transformations. The high-resolution base image of the ROIs, i.e., the underlying standard FA map, was first linearly transformed (affine; 12 DOF), then nonlinearly transformed (cubic B-spline) to the participant's low-resolution FA map, saving the linear transformation matrix and the warp field coefficients separately. These linear and nonlinear transformations were then applied to each ROI volume, using nearest neighbour interpolation in order to preserve the probabilistic or binary values of the ROIs. Examples of the registered probabilistic tracts in participant native space are shown in Figure 1.

The quantitative values obtained from the ROIs of the normal sample (N = 70) were used to create a normal population linear regression model, along with the training and test sets for specificity analysis. The values obtained from the mTBI participants were used to identify abnormalities by comparing them against the predicted normal population DTI metrics from the normal model. The analysis pipeline is visualized as a flow chart in Figure 2.

Statistics

Statistical analyses were performed with JASP (JASP Team, Version 0.8.5.1). To obtain normal values for a chosen ROI template set, the linear relationship between age and DTI scalars was modelled for each ROI using linear regression. This resulted in an age-dependent model for mean values, and a root-mean-square error (RMSE) for each ROI.

To test the specificity of our method, we first created a trial with 65 control participants as the training set, and the remaining five participants as a test set. The five control participants for the test set were chosen pseudo-randomly (i.e., the five participants who were born closest to the 1st of their respective birth month). For the training set participants, the mean DTI values of the specific regions and the ages of the participants were entered into the linear regression. The method was repeated for each ROI for each DTI metric (FA, MD, RD, and AD). This produced a simple model for the DTI scalar's age dependence inside the specific region, along with a p-value for possible statistical significance of the model, and the RMSE of the linear fit.

We then compared the test participants' ROI mean values against the model's predicted values using the parameter Z_r (named here as the regression standard score),

$$Z_r = \frac{M_s - M_m}{RMSE_{ROI}},$$

where M_s is the participant's ROI mean, M_m is the model's predicted ROI mean, adjusted for age, and $RMSE_{ROI}$ is the ROI dependent root-mean-square error of the model. The regression standard score acts as an indicator of deviation from the model, and a limit of acceptance for the specificity analysis was chosen at $|Z_r| < 1.645$ (similar to the 90% confidence level). For the specificity analysis, we included only the ROIs with statistically significant linear regression models in the training set. Additionally, we compared our model to the regression models obtained by Cox et al (Cox et al., 2016). Because Cox et al. combined left and right hemisphere ROIs, we similarly averaged those ROIs with bilateral representation into single ROIs. Due to the much larger participant pool and a slightly different data reporting method of Cox et al., we decided to compare only the significance and direction of the associations inside the tract regions.

To test the method against freehand ROI measurements, we compared 10 patients who had

sustained an mTBI against a normal value model created from the entire normal sample (N = 70). The limit for abnormal findings was chosen at $|Z_r| \geq 2$ for each ROI. Methods similar to those in the specificity analysis were used in this mTBI analysis. Each of the 10 patients with mTBIs were compared against the model created using the 70 controls. The patients with mTBIs were also assessed by U.H. with the freehand ROI DTI analysis procedure used in Tampere University Hospital. Several freehand ROIs were drawn to the patient FA maps (i.e., genu and splenium of the corpus callosum, thalamus, forceps minor, uncinate fasciculus, centrum semiovale, posterior corona radiata, and posterior limb of the internal capsule). Left and right hemispheric regions were measured separately for each ROI, apart from the corpus callosum. Then, the ROI values were compared against mean values calculated from a carefully selected control sample (N = 40, the orthopedically injured patients) with a criterion of abnormal findings defined as $|Z| > 2$ for each ROI. The control sample for the freehand ROI analysis is smaller than the one used in the linear regression model (40 participants) due to a compatibility issue caused by an update to the hospital's DTI software.

RESULTS

Registrations of the WM tract ROIs were successful, and the registered probabilistic ROI regions were representative of the tracts in the participants' native anatomical spaces according to visual inspection. The registration accuracy was deemed adequate for clinical use by a neuroradiologist (A.B.) and a neurosurgeon (T.L). In the following sections we will report the statistical significance of the models in each ROI, and carry out a brief comparison between our results and the results obtained by Cox et al. We then present the results of the specificity test, and finally the results of the mTBI analysis in comparison to the manual ROI measurements.

Normal Sample Linear Model

We created an age-based normal sample model with both IIT and JHU probabilistic WM atlases using the amalgamated sample set of all controls (N = 70). Implementation with the JHU atlas was considerably more successful than the IIT atlas, with all of the 20 ROIs showing a statistically

significant ($p < .05$) linear regression between age and FA. The percentage of ROIs with statistically significant linear models for MD, RD, and AD, was 85%, 95%, and 40%, respectively, out of a total of 20. For the IIT atlas the percentage of ROIs with statistically significant linear models for FA, MD, RD, and AD were 80%, 35%, 80%, and 30%, respectively, out of a total of 17 ROIs. The correlations between age and FA were negative in all significant ROIs, and positive for MD and RD in all significant ROIs for both atlases. AD correlated positively in all significant ROIs except for the left and right CST in the JHU atlas, and the correlation was negative for all significant ROIs except for the fornix in the IIT atlas. Details of the JHU atlas age-based FA model is shown in Table 2. Representative examples of age association graphs for the JHU atlas are shown in Figure 3, with full details of all metrics for both atlases and other graphs available as supplementary material.

Specificity

Linear regression models for the training set were similar to the ones created from the total combined control sample, with only minor differences. Details of the specificity models are shown in the supplementary material. Specificities of the model per DTI metric were defined as the percentages of the ROIs with $|Z_r| < 1.645$ out of the cumulative total amount of ROIs of the five test participants. However, only the ROIs with statistically significant linear regression models in the training set were included in the comparison. For the JHU atlas, the specificity of the FA model was 78.9%, of a total of 95 ROIs with statistically significant linear model in the training set. The specificity of MD, RD, and AD models were 95% of a total of 80 ROIs, 89.5% of 95 ROIs, and 91.1% of 45 ROIs, respectively. For the IIT atlas, the corresponding figures were 78.3% of 60 ROIs, 90% of 20 ROIs, 83.3% of 60 ROIs, and 100% of 30 ROIs, for FA, MD, RD, and AD, respectively.

Mild Traumatic Brain Injury

The freehand ROI measurements performed on the selected mTBI sample (N = 10) revealed abnormal FA ($|Z| \geq 2$) in the corpus callosum for three patients and in the forceps minor for two patients. One patient had abnormal MD in in the corpus callosum, and one in the posterior internal

capsule. Abnormal AD and RD values were found in the corpus callosum, forceps minor, UF, centrum semiovale, and posterior corona radiata. Most of the abnormalities were found in patients with complicated mTBI: 75% of the patients with abnormal FA were participants with complicated mTBI, while the numbers for MD, RD, and AD were 50%, 67%, and 60%, respectively. Data from the mTBI ROI comparison is shown in Table 3.

ROIs with non-significant linear regression model were discarded from the automated analysis. Examining the mTBI sample with the JHU atlas, abnormal FA values were found in the temporal portion of the left SLF, right CST, left and right cingulate gyrus, left and right UF, and forceps minor. Differences in MD were found in the right ILF, temporal part of the left and right SLF, right SLF, right hippocampal cingulum, right cingulate gyrus, and left UF. Abnormal RD values were found in right cingulate gyrus, right CST, temporal part of the left and right SLF, right SLF, and left UF. Abnormal AD values were found in the right CST and left UF. A majority of the abnormalities were again found in patients with complicated mTBI: 80% of the patients with abnormal FA were participants with complicated mTBI, while the number for MD, RD, and AD was 60%, 60%, and 50%. Details of the analysis for the JHU atlas are shown in Table 4. A quick comparison between the results of the ROI measurements and the automated analysis using JHU atlas is shown in Table 5. Apart from AD, the automated analysis identified a larger number of patients with abnormal DTI metrics. Patient 10 was an exception, showing abnormalities in FA, RD, and AD in the freehand measurement, but none in the automated analysis.

Using the IIT atlas, abnormal FA values in the patients with mTBIs were found in the left superior longitudinal fasciculus, left IFOF, and fornix. Differences in MD were found in the left superior longitudinal fasciculus, right IFOF, and fornix. Abnormal RD values were found in the left superior longitudinal fasciculus, right hippocampal cingulum, and fornix. Abnormal RD values were found in the forceps minor, left and right CST, and fornix.

DISCUSSION

Registration

Image registration is a crucial step in the DTI post-processing pipeline. After several iterations, we feel that we have substantially improved the registration of high resolution standard FA maps to the participant's lower resolution image. The use of FA images as the source of the linear registration coefficients and the warp field was obvious due to the clear delineation of brain white and grey matter. Also, traditional structural images may not always depict the small underlying variances in neural tract structures, which are essential when using WM tract-based regions of interest.

Our current registration methods allow any combination of ROIs to be used in the analysis, as long as the ROIs are provided with the underlying FA image. This is an advantage from a clinical perspective as different ROI may be desirable for studying different pathologies. In theory one could also use hand drawn ROIs in the analysis, but the results would not be directly comparable to previously made freehand ROI measurements due to differences in MRI slice positioning and the effects of 3D registration to the ROI volumes. Because they are not comparable, the choice of using manually drawn ROIs in the analysis pipeline, e.g., a set of clinically used ROIs, will not grant any additional benefits and is thus unadvisable.

Age Effects

For the limited participant sample available for the study, linear regression is a sufficient approximation of the correlation between age and DTI metrics (Kodiweera, Alexander, Harezlak, McAllister, & Wu, 2016; Westlye et al., 2010). Several publications describe a linear correlation between age and WM diffusion (Cox et al., 2016; Kodiweera et al., 2016; Westlye et al., 2010); more precisely, a negative correlation between age and FA, and a positive correlation between age and MD/RD. However, AD has been shown to both correlate negatively and positively with age. Although axial and radial diffusivities have often been of less interest, they include valuable information which can complement FA and MD analyses to further specify the cause of abnormal diffusion values in the

brain (Alexander et al., 2011). Our method fared quite well for FA, MD and RD, and we were able to derive age-dependent models for the JHU atlas. On the other hand, the results examining AD were heterogeneous and did not reveal a specific pattern. Similar heterogeneity has been observed in previous studies (Bennett, Madden, Vaidya, Howard, & Howard, 2010; Burzynska et al., 2010), and the phenomenon could be explained by the specific effects that various age-related pathologic mechanisms have on AD, e.g., demyelination, Wallerian degeneration, fibre degeneration and fibre structural reorganization (plasticity) (Madden et al., 2012). For younger individuals with developing brains, age may show opposite correlations of FA, MD and RD as compared to the aged brain, perhaps justifying a separate linear model for people below the age of approximately 25 (Lebel & Beaulieu, 2011; Westlye et al., 2010). Therefore, a possible future implementation would be a parabolic or two-part regression model.

Similar to our results, Cox et al. reported a negative correlation between FA and age, and a positive correlation between MD/RD/AD and age in all of the tested regions with significant regression ($p < .001$). In fact, with a more liberal P-value (e.g. $p < .01$), both positive and negative correlations between age and AD would have emerged, identical to our findings. Regions with non-significant correlation ($p > .001$) in the study by Cox et al. included the parahippocampal cingulum (FA), cingulate gyrus (AD), superior thalamic radiation (FA), acoustic radiation (FA, AD), middle cerebellar peduncle (FA), medial lemniscus (FA, RD), forceps major (RD), and forceps minor (RD). While our comparison with the results obtained by Cox et al. was far from comprehensive, the direction of correlation was in perfect agreement for FA, MD and RD in across all ROIs. The only differences were with respect to AD, which correlates positively with age in most of Cox et al.'s study, but in our sample several regions had negative correlation between AD and age. The difference may be attributed to the different age distribution of the samples, or from the difference in sample sizes. The only significant region (at $p < .05$) in our atlases that was non-significant in Cox et al.'s study was the cingulum; however, this region was not statistically significant when we used the same stricter requirement for statistical threshold as Cox et al. ($p < .001$). Overall, there were

more areas with non-significant differences in our study, which is at least partially attributable to the lower sample size.

Deviations from the Linear Model

A smaller number of ROIs reached statistical significance in the linear model fit for the IIT atlas compared to the JHU atlas; while regression models of FA and RD were statistically significant for most ROIs, MD models were mostly non-significant. This could be a consequence of the ROI sizes. The IIT atlas contains smaller regions than the JHU atlas, and ageing has been shown to cause global change in the entire WM area (Hsu et al., 2008; Salat et al., 2005; Sexton et al., 2014). It may also be possible that the IIT atlas is more suited for accurate analysis but is hindered by the low statistical power of our analysis. The use of IIT atlas in the model should be revisited in the future with a larger normal participant pool.

The specificity analysis resulted in a satisfactory percentage of true negatives, but the specificity would most likely have been better with a multiple regression model. However, the purpose of the analysis was not initially to be a standalone clinical method, but to serve as a supporting method for clinicians in assessing possible changes in WM integrity due to brain insult or disease. As a standalone method, our analysis would require higher specificity, but for a supporting method the most important aspect would be sensitivity, which is already acceptable, and can likely be further improved by increasing the statistical power by adding to the number of controls.

Study Design and Limitations

For consistency, we used the same protocol to compare the freehand measurements against our automated model, comparing the freehand ROI data against 40 control participants instead of all the controls (N = 70) used in this study. The smaller control group for the freehand measurements is due to an update on the DTI processing software which occurred in the timeframe between the collections of our two control groups. The smaller control group may relatively disadvantage the

freehand ROI method but using the complete control participant pool would have deviated from the original freehand ROI procedure.

Furthermore, most of the freehand ROIs do not correspond to the atlas ROIs, additionally frustrating comparison efforts. We can, however, make general claims about the sensitivity of our normal model analysis based on the detection of abnormalities on a patient level. The automated analysis found abnormalities in more patients than the freehand ROI measurement in FA (5 vs. 4), MD (5 vs. 2) and RD (5 vs. 3) measures, while for AD, freehand ROI measurements indicated abnormalities in five and automated analysis in two patients. Therefore, the sensitivity may be slightly higher in the automated analysis than in the freehand measurement. The larger number of ROIs in the automated analysis also contributes to a higher sensitivity.

There are important limitations to consider when interpreting our data. Although our chosen registration process is sufficient for our study goals, other methods of registration may be more accurate under certain conditions. Common registration methods work well with normal population, but a tensor-based registration could yield greater registration accuracy especially on patients with large neuroanatomical abnormalities. Patients with mTBI patients seldom have such severe lesions, so it is unclear how our method may function in more neuroanatomically compromised populations. We do not perform a separate WM segmentation on our DTI data. The use of WM segmentation before calculating the ROI mean values might be a beneficial addition to the analysis pipeline and is a prospect that should be studied and tested if the pipeline is to be used clinically. Another limitation is related to the size of our normal sample. Gender was not used as a covariate because of this. However, in our previous research, there were no statistically significant differences were found between male and female participants using TBSS analyses with the same sample. Another limitation is that simple one predictor linear model is not an efficient way to model the population's DTI metrics, and multiple linear regression should be used with a larger participant pool. For a viable regression model, a sample of at least 300 participants should be used with multiple predictor variables (Knofczynski & Mundfrom, 2007). Another potential limitation is that the specificity test

was performed by creating a test set pseudo-randomly. While unlikely, it is a potential source of bias. However, the results of the specificity test's results seem sensible, without exaggerations in terms of excessively high or low sensitivity.

One important factor to discuss about our current method is the analysis method itself and the characteristics of the results produced by the analysis. Most of the existing DTI analyses produce voxelwise results, where the abnormalities can in principal be pinpointed with the accuracy of a single voxel. Our analysis, however, can be considered to yield results that are similar to those of ROI measurements. This causes a possible loss of sensitivity due to averaging of the DTI values inside the analysed region. The WM abnormalities may also lie between the chosen analysis regions, which causes a loss of sensitivity and can lead to false negative findings. The problem can be partly countered by utilizing smaller ROIs in the pipeline. However, due to the methodology of our analysis, the possible decrease in sensitivity is a permanent component of the method, analogously to ROI analysis.

A final limitation is related to choosing mTBI as the initial clinical disorder to test. While mTBI patients may not be an optimal choice due to their lack of large-scale pathology, it is one of the most important and relevant clinical entities to study. Because the most prominent traumatic changes induced by mTBI are diffuse axonal injuries, the exact locations of the ROIs are not as crucial. Comparisons between our method and the freehand ROI measurements is challenging, due to the discrepancies between the atlas-defined regions and freehand regions, as well as the fundamental differences in the approaches. Both of the methods should at least be able to distinguish a clinically significant mTBI case with a diffuse axonal injury from a control participant.

CONCLUSION

We created a quantitative brain analysis pipeline that can be used in conjunction with various ROI datasets. The analysis is simple to conduct due to its dependence only on a single software package for image processing. Despite the small sample size, our regression model for the normal population was successful in confirming age-DTI scalar correlations, notably with FA. Further

work to enhance the utility and accuracy of the automated analysis is needed before our algorithms can be useful for clinical purposes.

The results of our normal sample regression model were largely similar to the regression presented by Cox et al. (Cox et al., 2016), and thus can be considered a successful partial replication of the study. In addition, we applied our analysis method to mTBI patients with results comparable to commonly utilised freehand ROI measurements. With increased statistical power, further validation of the analysis method, and the additional prospect of combining machine learning and custom deep-learning algorithms with our models, this method may possess the potential to complement or replace freehand ROI measurement as the gold standard brain DTI analysis method in the near future.

REFERENCES

Alexander, A. L., Hurley, S. A., Samsonov, A. A., Adluru, N., Hosseinbor, A. P., Mossahebi, P., … Field, A. S. (2011). Characterization of Cerebral White Matter Properties Using Quantitative Magnetic Resonance Imaging Stains. *Brain Connectivity*, *1*(6), 423–446. https://doi.org/10.1089/brain.2011.0071

Alfaro, F. J., Gavrieli, A., Saade-Lemus, P., Lioutas, V.-A., Upadhyay, J., & Novak, V. (2018). White matter microstructure and cognitive decline in metabolic syndrome: a review of diffusion tensor imaging. *Metabolism: Clinical and Experimental*, *78*, 52–68. https://doi.org/10.1016/j.metabol.2017.08.009

Aoki, Y., Cortese, S., & Castellanos, F. X. (2018). Research Review: Diffusion tensor imaging studies of attention-deficit/hyperactivity disorder: meta-analyses and reflections on head motion. *Journal of Child Psychology and Psychiatry, and Allied Disciplines*, *59*(3), 193–202. https://doi.org/10.1111/jcpp.12778

Asken, B. M., DeKosky, S. T., Clugston, J. R., Jaffee, M. S., & Bauer, R. M. (2018). Diffusion tensor imaging (DTI) findings in adult civilian, military, and sport-related mild traumatic brain injury (mTBI): a systematic critical review. *Brain Imaging and Behavior*, *12*(2), 585–612. https://doi.org/10.1007/s11682-017-9708-9

Atkinson-Clement, C., Pinto, S., Eusebio, A., & Coulon, O. (2017). Diffusion tensor imaging in Parkinson's disease: Review and meta-analysis. *NeuroImage. Clinical*, *16*, 98–110. https://doi.org/10.1016/j.nicl.2017.07.011

Bennett, I. J., Madden, D. J., Vaidya, C. J., Howard, D. V., & Howard, J. H. (2010). Age-related differences in multiple measures of white matter integrity: A diffusion tensor imaging study of healthy aging. *Human Brain Mapping*, *31*(3), 378–390. https://doi.org/10.1002/hbm.20872

Burzynska, A. Z., Preuschhof, C., Bäckman, L., Nyberg, L., Li, S. C., Lindenberger, U., & Heekeren, H. R. (2010). Age-related differences in white matter microstructure: Region-specific patterns of diffusivity. *NeuroImage*, *49*(3), 2104–2112. https://doi.org/10.1016/j.neuroimage.2009.09.041

Cox, S. R., Ritchie, S. J., Tucker-Drob, E. M., Liewald, D. C., Hagenaars, S. P., Davies, G., … Deary, I. J. (2016). Ageing and brain white matter structure in 3,513 UK Biobank participants. *Nature Communications*, *7*. https://doi.org/10.1038/ncomms13629

De Groot, M., Vernooij, M. W., Klein, S., Ikram, M. A., Vos, F. M., Smith, S. M., … Andersson, J. L. R. (2013). Improving alignment in Tract-based spatial statistics: Evaluation and optimization of image registration. *NeuroImage*, *76*, 400–411. https://doi.org/10.1016/j.neuroimage.2013.03.015

Di, X., Azeez, A., Li, X., Haque, E., & Biswal, B. B. (2018). Disrupted focal white matter integrity in autism spectrum disorder: A voxel-based meta-analysis of diffusion tensor imaging studies. *Progress in Neuro-Psychopharmacology & Biological Psychiatry*, *82*, 242–248. https://doi.org/10.1016/j.pnpbp.2017.11.007

Hakulinen, U., Brander, A., Ryymin, P., Öhman, J., Soimakallio, S., Helminen, M., … Eskola, H. (2012). Repeatability and variation of region-of-interest methods using quantitative diffusion tensor MR imaging of the brain. *BMC Medical Imaging*, *12*, 30. https://doi.org/10.1186/1471-2342-12-30

Hsu, J. L., Leemans, A., Bai, C. H., Lee, C. H., Tsai, Y. F., Chiu, H. C., & Chen, W. H. (2008). Gender differences and age-related white matter changes of the human brain: A diffusion tensor imaging study. *NeuroImage*, *39*(2), 566–577. https://doi.org/10.1016/j.neuroimage.2007.09.017

Hua, K., Zhang, J., Wakana, S., Jiang, H., Li, X., Reich, D. S., … Mori, S. (2008). Tract probability maps in stereotaxic spaces: analyses of white matter anatomy and tract-specific quantification. *NeuroImage*, *39*(1), 336–347. https://doi.org/10.1016/j.neuroimage.2007.07.053

Ilvesmäki, T., Koskinen, E., Brander, A., Luoto, T., Ohman, J., & Eskola, H. (2017). Spinal Cord Injury Induces Widespread Chronic Changes in Cerebral White Matter. *Human Brain Mapping*, *38*(7), 3637–3647. https://doi.org/10.1002/hbm.23619

Ilvesmäki, T., Luoto, T. M., Hakulinen, U., Brander, A., Ryymin, P., Eskola, H., … Ohman, J. (2014).

Acute mild traumatic brain injury is not associated with white matter change on diffusion tensor imaging. *Brain*, *137*(Pt 7), 1876–1882. https://doi.org/10.1093/brain/awu095

Jenkinson, M., Beckmann, C. F., Behrens, T. E. J., Woolrich, M. W., & Smith, S. M. (2012). FSL. *NeuroImage*, *62*(2), 782–790. https://doi.org/10.1016/j.neuroimage.2011.09.015

Jiang, J., Zhao, Y.-J., Hu, X.-Y., Du, M.-Y., Chen, Z.-Q., Wu, M., … Gong, Q.-Y. (2017). Microstructural brain abnormalities in medication-free patients with major depressive disorder: a systematic review and meta-analysis of diffusion tensor imaging. *Journal of Psychiatry & Neuroscience : JPN*, *42*(3), 150–163.

Kambeitz, J., Cabral, C., Sacchet, M. D., Gotlib, I. H., Zahn, R., Serpa, M. H., … Koutsouleris, N. (2017). Detecting Neuroimaging Biomarkers for Depression: A Meta-analysis of Multivariate Pattern Recognition Studies. *Biological Psychiatry*, *82*(5), 330–338. https://doi.org/10.1016/j.biopsych.2016.10.028

Knofczynski, G. T., & Mundfrom, D. (2007). Sample Sizes When Using Multiple Linear Regression for Prediction. *Educational and Psychological Measurement*, *68*(3), 431–442. https://doi.org/10.1177/0013164407310131

Kodiweera, C., Alexander, A. L., Harezlak, J., McAllister, T. W., & Wu, Y. C. (2016). Age effects and sex differences in human brain white matter of young to middle-aged adults: A DTI, NODDI, and q-space study. *NeuroImage*, *128*, 180–192. https://doi.org/10.1016/j.neuroimage.2015.12.033

Lebel, C., & Beaulieu, C. (2011). Longitudinal Development of Human Brain Wiring Continues from Childhood into Adulthood. *Journal of Neuroscience*, *31*(30), 10937–10947. https://doi.org/10.1523/JNEUROSCI.5302-10.2011

Madden, D. J., Bennett, I. J., Burzynska, A., Potter, G. G., Chen, N., & Song, A. W. (2012). Diffusion Tensor Imaging of Cerebral White Matter Integrity in Cognitive Aging. *Biochim Biophys Acta*, *1822*(3), 386–400. https://doi.org/10.1016/j.bbadis.2011.08.003.Diffusion

Moreau, D., Stonyer, J. E., McKay, N. S., & Waldie, K. E. (2018). No evidence for systematic white matter correlates of dyslexia: An Activation Likelihood Estimation meta-analysis. *Brain*

Research, *1683*, 36–47. https://doi.org/10.1016/j.brainres.2018.01.014

Newlander, S. M., Chu, A., Sinha, U. S., Lu, P. H., & Bartzokis, G. (2014). METHODOLOGICAL IMPROVEMENTS IN VOXEL BASED ANALYSIS OF DIFFUSION TENSOR IMAGES: APPLICATIONS TO STUDY THE IMPACT OF APOE ON WHITE MATTER INTEGRITY. *Journal of Magnetic Resonance Imaging : JMRI*, *39*(2), 387–397. https://doi.org/10.1002/jmri.24157

O'Connor, E. E., Jaillard, A., Renard, F., & Zeffiro, T. A. (2017). Reliability of White Matter Microstructural Changes in HIV Infection: Meta-Analysis and Confirmation. *AJNR. American Journal of Neuroradiology*, *38*(8), 1510–1519. https://doi.org/10.3174/ajnr.A5229

Oehr, L., & Anderson, J. (2017). Diffusion-Tensor Imaging Findings and Cognitive Function Following Hospitalized Mixed-Mechanism Mild Traumatic Brain Injury: A Systematic Review and Meta-Analysis. *Archives of Physical Medicine and Rehabilitation*. https://doi.org/10.1016/j.apmr.2017.03.019

Oishi, K., Zilles, K., Amunts, K., Faria, A., Jiang, H., Li, X., … Mori, S. (2008). Human brain white matter atlas: identification and assignment of common anatomical structures in superficial white matter. *NeuroImage*, *43*(3), 447–457. https://doi.org/10.1016/j.neuroimage.2008.07.009

Power, M. C., Tingle, J. V, Reid, R. I., Huang, J., Sharrett, A. R., Coresh, J., … Mosley, T. H. (2017). Midlife and Late-Life Vascular Risk Factors and White Matter Microstructural Integrity: The Atherosclerosis Risk in Communities Neurocognitive Study. *Journal of the American Heart Association: Cardiovascular and Cerebrovascular Disease*, *6*(5), e005608. https://doi.org/10.1161/JAHA.117.005608

Radoeva, P. D., Coman, I. L., Antshel, K. M., Fremont, W., McCarthy, C. S., Kotkar, A., … Kates, W. R. (2012). Atlas-based white matter analysis in individuals with velo-cardio-facial syndrome (22q11.2 deletion syndrome) and unaffected siblings. *Behavioral and Brain Functions : BBF*, *8*, 38. https://doi.org/10.1186/1744-9081-8-38

Salat, D. H., Tuch, D. S., Greve, D. N., Van Der Kouwe, A. J. W., Hevelone, N. D., Zaleta, A. K., … Dale, A. M. (2005). Age-related alterations in white matter microstructure measured by diffusion

tensor imaging. *Neurobiology of Aging*, *26*(8), 1215–1227. https://doi.org/10.1016/j.neurobiolaging.2004.09.017

Schwarz, C. G., Reid, R. I., Gunter, J. L., Senjem, M. L., Przybelski, S. A., Zuk, S. M., … Initiative, the A. D. N. (2014). Improved DTI registration allows voxel-based analysis that outperforms Tract-Based Spatial Statistics. *NeuroImage*, *94*, 65–78. https://doi.org/10.1016/j.neuroimage.2014.03.026

Sexton, C. E., Walhovd, K. B., Storsve, A. B., Tamnes, C. K., Westlye, L. T., Johansen-Berg, H., & Fjell, A. M. (2014). Accelerated Changes in White Matter Microstructure during Aging: A Longitudinal Diffusion Tensor Imaging Study. *Journal of Neuroscience*, *34*(46), 15425–15436. https://doi.org/10.1523/JNEUROSCI.0203-14.2014

Siehl, S., King, J. A., Burgess, N., Flor, H., & Nees, F. (2018). Structural white matter changes in adults and children with posttraumatic stress disorder: A systematic review and meta-analysis. *NeuroImage. Clinical*, *19*, 581–598. https://doi.org/10.1016/j.nicl.2018.05.013

Suri, A. K., Fleysher, R., & Lipton, M. L. (2015). Subject based registration for individualized analysis of diffusion tensor MRI. *PLoS ONE*, *10*(11), 1–17. https://doi.org/10.1371/journal.pone.0142288

Wallace, E. J., Mathias, J. L., & Ward, L. (2018). Diffusion tensor imaging changes following mild, moderate and severe adult traumatic brain injury: a meta-analysis. *Brain Imaging and Behavior*, *0*(0), 1–15. https://doi.org/10.1007/s11682-018-9823-2

Wang, Y., Gupta, A., Liu, Z., Zhang, H., Escolar, M. L., Gilmore, J. H., … Styner, M. (2011). DTI registration in atlas based fiber analysis of infantile Krabbe disease. *NeuroImage*, *55*(4), 1577–1586. https://doi.org/10.1016/j.neuroimage.2011.01.038

Wang, Y., Shen, Y., Liu, D., Li, G., Guo, Z., Fan, Y., & Niu, Y. (2017). Evaluations of diffusion tensor image registration based on fiber tractography. *BioMedical Engineering OnLine*, *16*(1), 9. https://doi.org/10.1186/s12938-016-0299-2

Westlye, L. T., Walhovd, K. B., Dale, A. M., Bjørnerud, A., Due-Tønnessen, P., Engvig, A., … Fjell, A. M.

(2010). Life-span changes of the human brain white matter: Diffusion tensor imaging (DTI) and volumetry. *Cerebral Cortex*, *20*(9), 2055–2068. https://doi.org/10.1093/cercor/bhp280

Yu, J., Lam, C. L. M., & Lee, T. M. C. (2017). White matter microstructural abnormalities in amnestic mild cognitive impairment: A meta-analysis of whole-brain and ROI-based studies. *Neuroscience and Biobehavioral Reviews*, *83*, 405–416. https://doi.org/10.1016/j.neubiorev.2017.10.026

Zhang, S., & Arfanakis, K. (2018). Evaluation of standardized and study-specific diffusion tensor imaging templates of the adult human brain: Template characteristics, spatial normalization accuracy, and detection of small inter-group FA differences. *NeuroImage*, *172*, 40–50. https://doi.org/10.1016/j.neuroimage.2018.01.046

Corresponding author: Tero Ilvesmäki

TABLES

Table 1. Demographics of the control participants and patients with complicated and uncomplicated mild traumatic brain injury.

	Age (yrs, mean ± SD)	Gender (male / female)	LOC (min)	PTA (h)	Traumatic findings on conventional brain MRI	MRI imaging delay from trauma (days)
Normal data (N = 70)	39.5 ± 11.8	29 / 41	-	-	-	-
Training dataset (N = 65)	39.8 ± 11.7	39 / 26	-	-	-	-
Test dataset (N = 5)	34.4 ± 11.6	2 / 3	-	-	-	-
Patient 1†	22	male	5	.083	Contusion, SDH	5
Patient 2†	29	male	15	1	DAI	6
Patient 3†	49	male	5	.083	DAI	2
Patient 4†	28	male	2	6.5	DAI	5
Patient 5†	33	male	0.5	2.5	DAI	6
Patient 6	38	male	0	3	No lesions	3
Patient 7	19	male	0	.033	No lesions	10
Patient 8	28	male	0	.017	No lesions	5
Patient 9	48	male	0	.5	No lesions	7
Patient 10	26	male	0	0	No lesions	3

LOC = loss of consciousness, PTA = post-traumatic amnesia, SDH = subdural hematoma, DAI = diffuse axonal injury.

†) Patients with complicated mTBI

Table 2. Details of the FA normal value model for the JHU white matter probabilistic atlas.

Region	FA regression function	p	RMSE
Anterior thalamic radiation L	.4216953 - .0007476 × age	< .001	0.0200335
Anterior thalamic radiation R	.4000638 - .0008487 × age	< .001	0.0202835
Cingulate gyrus L	.4067053 - .000975 × age	< .001	0.026084
Cingulate gyrus R	.3960036 - .0009912 × age	< .001	0.0274607
Hippocampal portion of the cingulum L	.3197929 - .0007011 × age	.0042055	0.0232557
Hippocampal portion of the cingulum R	.3432481 - .0006444 × age	.0184947	0.0262355
Corticospinal tract (CST) L	.5673051 - .001023 × age	< .001	0.0202251
Corticospinal tract (CST) R	.5544531 - .0009758 × age	< .001	0.020501
Forceps major	.5256287 - .0009244 × age	.0018824	0.0280815
Forceps minor	.4904246 - .0013848 × age	< .001	0.022653
Inferior fronto-occipital fasciculus (IFOF) L	.4555804 - .0012634 × age	< .001	0.0174475
Inferior fronto-occipital fasciculus R (IFOF R)	.4473206 - .0010437 × age	< .001	0.0165715
Inferior longitudinal fasciculus (ILF) L	.4245957 - .0009795 × age	< .001	0.0203935
Inferior longitudinal fasciculus (ILF) R	.4194901 - .0008494 × age	< .001	0.0182781
Temporal part of the superior longitudinal fasciculus (SLF) L	.4615694 - .0010949 × age	< .001	0.0203335
Temporal part of the superior longitudinal fasciculus (SLF) R	.447034 - .0011284 × age	< .001	0.0184707
Superior longitudinal fasciculus (SLF) L	.4116664 - .0010241 × age	< .001	0.0187179
superior longitudinal fasciculus (SLF) R	.4034946 - .0011602 × age	< .001	0.0170947
Uncinate fasciculus (UF) L	.421141 - .0010389 × age	< .001	0.0212249
Uncinate fasciculus (UF) R	.3983145 - .0007049 × age	.0010712	0.020269

FA = fractional anisotropy, RMSE = root-mean-square error, L = left, R = right.

Table 3. Results of the freehand ROI analysis of 10 patients with mild traumatic brain injuries. Z-values and the corresponding patient is shown in the table, if $|Z| \geq 2$, when compared against a control group of 40 selected normal participants.

Region	**FA**	**MD**	**RD**	**AD**
Posterior internal capsule R		Patient 6: -2.027		
Posterior corona radiata L				Patient 2†: +2.643
Centrum semiovale R				Patient 6: -2.118
Uncinate fasciculus R				Patient 3†: -2.265
Forceps minor L	Patient 2†: +2.273 Patient 10: +2.424		Patient 2†: -2.043	Patient 10: +2.440
Corpus callosum G	Patient 10: -3.038	Patient 5†: +2.576	Patient 10: -3.062	Patient 5†: +2.135 Patient 10: -3.062
Corpus callosum S	Patient 3†: -2.195 Patient 4†: -2.603		Patient 4†: +2.215	Patient 2†: -2.272

FA = fractional anisotropy, MD/RD/AD = mean/radial/axial diffusivity, L = left, R = right, G = genu, S = splenium.

†) Patients with complicated mild traumatic brain injury.

Table 4. Normal value model analysis results of from the 10 patients with mTBIs. The JHU atlas was used for the analysis, where participants with mTBIs were compared against predicted values obtained from the linear model created with 70 normal participants. Table values are presented as Z_r, i.e., difference from the model predicted value as multiples of the model's root-mean-square error. The difference was considered significant if $|Z_r| > 2$.

Region	FA	MD	RD	AD
Cingulate gyrus L	Patient 5†: -2.175			
Cingulate gyrus R	Patient 5†: -2.416	Patient 5†: +2.623 Patient 6: -2.139	Patient 5†: +2.758	
Hippocampal portion of the cingulum R		Patient 2†: +2.031		
corticospinal tract (CST) R	Patient 3†: +2.064		Patient 3†: -2.177 Patient 6: -3.178	Patient 6: -4.205
Forceps minor	Patient 2†: +2.198			
Inferior fronto-occipital fasciculus (IFOF) R		Patient 4†: +2.081		
Temporal part of the superior longitudinal fasciculus (SLF) L	Patient 4†: -2.086 Patient 5†: -2.353	Patient 5†: +2.099	Patient 5†: +2.306	
Temporal part of the superior longitudinal fasciculus (SLF) R		Patient 4†: +2.222	Patient 4†: +2.282	
Superior longitudinal fasciculus (SLF) R		Patient 4†: +2.078	Patient 4†: +2.185	
Uncinate fasciculus (UF) L	Patient 7: -2.911	Patient 7: +3.074	Patient 7: +3.385	Patient 1†: +2.449
Uncinate fasciculus (UF) R	Patient 5†: -2.258			

FA = fractional anisotropy, MD/RD/AD = mean/radial/axial diffusivity, L = left, R = right.

†) Patients with complicated mild traumatic brain injury.

Table 5. Comparison of the abnormal findings between the freehand ROI measurement and the automated analysis with JHU atlas. Plus and minus signs signify whether the abnormal findings are larger or smaller than the normal sample predicted value.

	FA		MD		RD		AD	
Patient	ROI	Autom	ROI	Autom	ROI	Autom	ROI	Autom
1†								+
2†	+	+		+	-		+/-	
3†	-	+				-	-	
4†	-	-		+	+	+		
5†		-	+	+		+	+	
6			-	-		-	-	-
7		-		+		+		
8								
9								
10	+				-		+/-	

FA = fractional anisotropy, MD/RD/AD = mean/radial/axial diffusivity.

†) Patients with complicated mild traumatic brain injury.

FIGURES

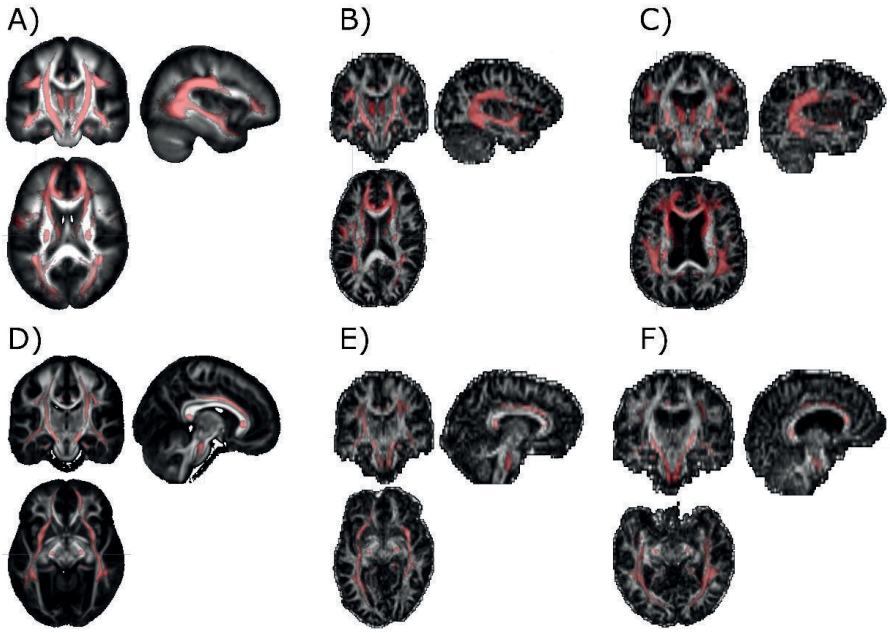

Figure 1. Two example participants with probabilistic DTI atlases shown on top of their FA maps as red. A) The original JHU probabilistic atlas on top of the JHU mean FA map, B) the JHU atlas registered to control X, C) the JHU atlas registered to control Y, D) the original IIT probabilistic atlas on top the IIT mean FA map, E) the IIT atlas registered to control X, F) the IIT atlas registered to control Y. The probabilistic atlases' ROI areas are limited to probabilities > 10% for visualization purposes. Neurological convention; left = left.

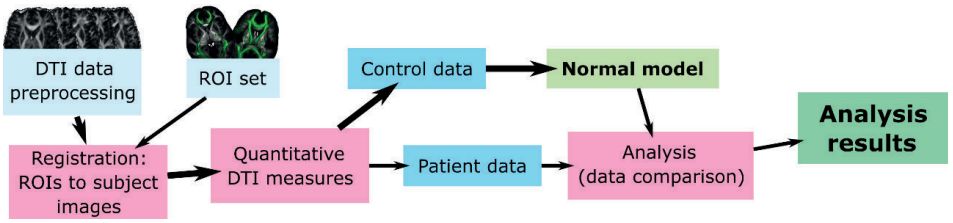

Figure 2. The quantitative brain analysis presented as a flow chart. Following the bolded arrows, the statistical power and accuracy of the normal model can be improved by adding more control participants. Blue rectangles present data, pink rectangles present work phases, and green indicates results.

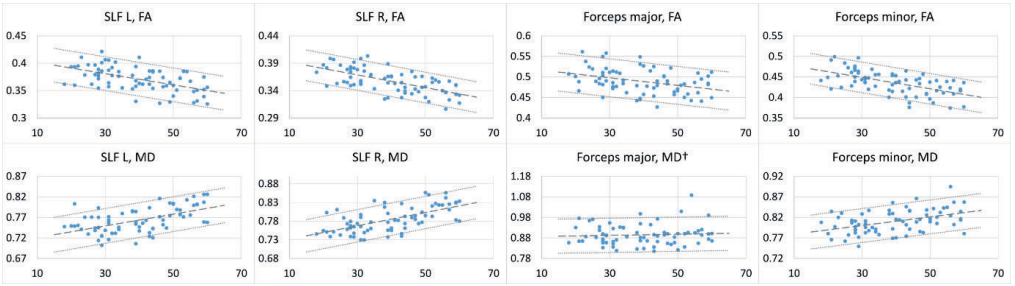

Figure 3. Age associations of the left and right SLF and forceps major and minor for FA and MD in the JHU atlas. The linear regression model is plotted as dashed line, and ± 1.645 RMSE values are plotted as dotted lines above and below the model line. The horizontal axis in the graphs represents age in years, while the vertical axis is dimensionless for FA and of units 10^{-3} mm^2/s for MD. SLF = superior longitudinal fasciculus, L = left, R = right.

†) Not a statistically significant regression.